

Alma Mater Studiorum – Università di Bologna

**DOTTORATO DI RICERCA IN**

**CHIMICA**

Ciclo XXVIII

**Settore Concorsuale di afferenza: 03/A2**

**Settore Scientifico disciplinare: CHIM/02**

**CONFORMATIONAL EQUILIBRIA, NON-BONDING INTERACTIONS AND  
CHIRALITY FROM ROTATIONAL SPECTROSCOPY**

**Presentata da: LORENZO SPADA**

**Coordinatore Dottorato**

**Prof. ALDO RODA**

**Relatore**

**Prof. WALTHER CAMINATI**

**Correlatore**

**D. ssa ASSIMO MARIS**

**Esame finale anno 2016**

# CONTENTS

PREFACE.....	4
CHAPTER 1. FUNDAMENTAL THEORY AND NON-BONDING INTERACTIONS.....	6
1.1 THE RIGID ROTOR.....	6
1.2 THE DISTORTABLE ROTOR.....	9
1.3 EFFECT OF VIBRATIONS.....	10
1.4 SELECTION RULES.....	11
1.5 POPULATION OF THE ENERGY LEVELS.....	12
1.6 NUCLEAR QUADRUPOLE COUPLING.....	13
1.7 INTERNAL ROTATION.....	15
1.8 MOLECULAR STRUCTURE DETERMINATION.....	18
1.8.1 <i>Equilibrium Structure</i> .....	19
1.8.2 <i>Single Substitution Structure</i> .....	19
1.8.3 <i>Effective Structure</i> .....	19
1.9 CONFORMATIONAL AND TAUTOMERIC EQUILIBRIA.....	20
1.10 DISSOCIATION ENERGY.....	21
1.11 NON-BONDING INTERACTIONS.....	21
1.12 CHIRALITY.....	22
1.13 REFERENCES.....	23
CHAPTER 2. EXPERIMENTAL AND COMPUTATIONAL METHODS.....	26
2.1 SUPERSONIC FREE JETS.....	26
2.2 MICROWAVE SPECTROMETERS.....	28
2.2.1 <i>Coaxially Oriented Beam Resonator Arrangement Pulsed Jet Fourier Transform MicroWave Spectrometers</i> .....	29
2.2.2 <i>Chirped Pulse Fourier Transform MicroWave Spectrometers</i> .....	32
2.3 COMPUTATIONAL METHODS.....	34
2.4 REFERENCES.....	35
CHAPTER 3. MOLECULAR ADDUCTS AND ISOLATED MOLECULES: RESULTS.....	38
3.1 HYDROGEN BONDING.....	38
3.1.1 <i>Pyridine – Formic Acid</i> .....	38
3.1.2 <i>2-Fluoropyridine – Water</i> .....	43
3.1.3 <i>3-Fluoropyridine – Water</i> .....	48
3.1.4 <i>Trifluoroanisole – Water</i> .....	54
3.1.5 <i>Conclusions</i> .....	59
3.2 WEAK HYDROGEN BONDING.....	60
3.2.1 <i>Difluoromethane – Dichloromethane</i> .....	60
3.2.2 <i>Difluoromethane – Chlorofluoromethane</i> .....	65
3.2.3 <i>Pyridine – Methane</i> .....	71
3.2.4 <i>Pyridine – Fluoromethane</i> .....	77
3.2.5 <i>Pyridine – Difluoromethane</i> .....	82
3.2.6 <i>Indane – Trifluoromethane</i> .....	85
3.2.7 <i>Conclusions</i> .....	89
3.3 HALOGEN BONDING.....	91
3.3.1 <i>Chlorotrifluoromethane - Fluoromethane</i> .....	91
3.3.2 <i>Chlorotrifluoromethane – Formaldehyde</i> .....	95
3.3.3 <i>Conclusions</i> .....	99

3.4 LONE PAIR ··· $\Pi$ INTERACTION.....	101
3.4.1 Chlorotrifluoroethylene – Ammonia.....	101
3.4.2 Chlorotrifluoroethylene – Dimethylether .....	106
3.4.3 Conclusions .....	111
3.5 ISOLATED MOLECULES .....	112
3.5.1 Fluoroxene .....	112
3.5.2 Methyl $\beta$ -D-Ribofuranoside .....	117
3.5.3 Purine.....	121
3.5.4 Conclusions .....	126
3.6 REFERENCES .....	127
ACKNOWLEDGEMENTS .....	133

# PREFACE

The fascinating ways, in which nature shows its magnificence, are governed by fine mechanisms which are led by a multitude of interactions, whose features are of crucial importance to understand the macroscopic behaviors.

In this respect, whilst the covalent bonds provide the basic structures and energies of molecules, non-bonding interactions are responsible of their specific features, playing a role in conformational preferences, in molecular recognition mechanisms, in solvation processes, in catalysis and in many other fields.

Non-covalent interactions have a common electrostatic nature. They can be non-specific, as van der Waals interaction, or they can involve specific sites of the molecules of interest. In this case, chemists like to label these interactions as “hydrogen, weak hydrogen and halogen bonds” as well as the “lone-pair $\cdots\pi$  interaction”. The involved energies can vary from few to tens of  $\text{kJ}\cdot\text{mol}^{-1}$ , with respect to the hundreds of  $\text{kJ}\cdot\text{mol}^{-1}$  for the covalent bonds.

In this context, rotational spectroscopy in supersonic expansion is a suitable technique to investigate the genuine nature of the non-bonding interactions because no solvent and no matrix effects are encountered.

Thanks to this, in the pyridine-formic acid adduct the proton transfer process is described, together with the effect of the H $\rightarrow$ D substitution in the O-H $\cdots$ N interaction, analyzing, also, the synergy between hydrogen and weak hydrogen bonds.

Following the same kind of interactions, microsolvation processes are described in the case of 2-fluoropyridine, 3-fluoropyridine and trifluoroanisole, focusing the attention on the effects of the fluorine substitution and on the possible dynamics of water.

Weak hydrogen bond features are described in the second paragraph where the C-H $\cdots$ F-C, C-H $\cdots$ Cl-C, C-H $\cdots$ N, C-H $\cdots\pi$  contacts are characterized, together with the internal dynamics and dissociation energies, for the dichloromethane-difluoromethane, chlorofluoromethane-difluoromethane, pyridine with methane, fluoromethane, difluoromethane and indane-trifluoromethane complexes.

The F $\cdots$ Cl and the O $\cdots$ Cl halogen bonds are the interactions linking the molecular subunits fluoromethane and formaldehyde with chlorotrifluoromethane. In these complexes internal rotation of the CF<sub>3</sub> group causes the experimental *A* rotational constants of the ground state ( $v=0$ ,  $\sigma==$ , *A*-species) to be almost one order of magnitude larger than their “rigid” values.

The Bürgi-Dunitz interaction links together the two subunits of the molecular complexes ammonia-chlorotrifluoroethylene and dimethylether-chlorotrifluoroethylene, characterized by N- and O-lone-

pair $\cdots\pi$  interactions, respectively. The lone-pair $\cdots\pi$  interaction is preferred to the halogen bond in perhalogenated olefins.

Finally, three molecules of biological interest have been investigated. The conformational equilibrium has been described for a  $\beta$ -ribofuranoside, a sugar with a five membered ring structure while in the case of the anesthetic fluoroxene a single conformer was found. The tautomeric equilibrium of purine, a molecule which constitutes the mainframe of adenosine and guanine, has been studied by Fourier transform MW spectroscopy combined with laser ablation: the N(9)H  $\rightleftharpoons$  N(7)H equilibrium is strongly in favour of the N(9)H species.

# CHAPTER 1:

## Fundamental Theory and Non-Bonding Interactions

### 1.1 The Rigid Rotor

The angular momentum of a rigid system of particles, rotating at the angular velocity  $\omega$  with respect to a Cartesian coordinate system  $(x, y, z)$  fixed in the body and whose origin is at the center of gravity of the body, with  $I$  the real, hermitian moment of inertia tensor, is defined as<sup>1</sup>:

$$P = I \cdot \omega \quad (1.1)$$

The moment of inertia tensor elements are:

$$\begin{vmatrix} I_{xx} & I_{xy} & I_{xz} \\ I_{yx} & I_{yy} & I_{yz} \\ I_{zx} & I_{zy} & I_{zz} \end{vmatrix} \quad (1.2)$$

Where:

$$I_{xx} = \sum_i m_i (y_i^2 + z_i^2); \quad I_{yy} = \sum_i m_i (x_i^2 + z_i^2); \quad I_{zz} = \sum_i m_i (x_i^2 + y_i^2); \quad I_{xy} = I_{yx} = -\sum_i m_i x_i y_i;$$
$$I_{xz} = I_{zx} = -\sum_i m_i x_i z_i; \quad I_{yz} = I_{zy} = -\sum_i m_i y_i z_i.$$

It is always possible to rotate the coordinate axes system in such a way that all the products of inertia vanish. This corresponds, within the linear algebra field, to a similarity transformation of the moment of inertia matrix by changing the basis. The three roots ( $I$ ) of the secular determinant (see 1.3) resulting are the so-called principal moments of inertia ( $I_a, I_b, I_c$ ), where the subscripts  $a, b, c$  represents the principal axes system.

$$\begin{vmatrix} I_{xx} - I & I_{xy} & I_{xz} \\ I_{yx} & I_{yy} - I & I_{yz} \\ I_{zx} & I_{zy} & I_{zz} - I \end{vmatrix} = 0 \quad (1.3)$$

The principal moments of inertia undergo the convention for which  $I_a \leq I_b \leq I_c$  by with different kinds of rotor can be derive as reported in Table 1.

Rotor type	Principal moments of inertia
Diatomic and Linear	$I_b = I_c \neq I_a = 0$
Spherical	$I_a = I_b = I_c$
Symmetric Oblate	$I_a = I_b < I_c$
Symmetric Prolate	$I_a < I_b = I_c$
Asymmetric	$I_a \neq I_b \neq I_c$

**Table 1.** Classification of the rigid rotors according to their principal moments of inertia values.

The rotational kinetic energy for a generic rigid rotor is defined as:

$$K = \frac{1}{2} \omega \cdot I \cdot \omega \quad (1.4)$$

It follows that, substituting equation (1.1) in (1.4), the rotational kinetic energy in the principal axes system yields:

$$K = \frac{1}{2} \left( \frac{P_a^2}{I_a} \right) + \frac{1}{2} \left( \frac{P_b^2}{I_b} \right) + \frac{1}{2} \left( \frac{P_c^2}{I_c} \right) \quad (1.5)$$

It can be proven that, if no torque is applied, the energy of equation (1.5) is constant.

According to the relations between the principal moments of inertia as reported in Table 1, the rotational kinetic energy results in different equations. In going from Classical to Quantum Mechanics, their relative Hamiltonian operators, taking into the account their conjugate angular momentum operators<sup>2</sup>, have to be considered.

Solving the relative Schrödinger equations, it is possible to determine the respective rotational energy eigenvalues. This is allowable for diatomic, linear, spherical and symmetric rotors.

Because in my PhD work I studied only molecules and adducts which are asymmetric rotors, I am going to derive the rotational energy levels of those ones with a brief description of those for the symmetric rotors. For these latter, the eigenvalues of energy  $E_{J,K,M}$  for the angular momentum operators  $\hat{P}^2$ ,  $\hat{P}_z$  and  $\hat{P}_Z$  (where  $z$  is the axis of symmetry of the  $x, y, z$  body-fixed system and  $Z$  is a specific axis of the  $X, Y, Z$  space-fixed axes), with  $\psi_{J,K,M}$  the symmetric top eigenfunctions, are calculated be:

$$\hat{P}^2 \psi_{J,K,M} = \hbar J(J+1) \psi_{J,K,M} \quad (1.6)$$

$$\hat{P}_z \psi_{J,K,M} = \hbar K \psi_{J,K,M} \quad (1.7)$$

$$\hat{P}_Z \psi_{J,K,M} = \hbar M \psi_{J,K,M} \quad (1.8)$$

Where  $J = 0, 1, \dots$ ;  $K = 0, \pm 1, \dots, \pm J$ ;  $M = 0, \pm 1, \dots, \pm J$ .

If no fields perturbs the system, the rotational energies are independent from the quantum number  $M$ , and, then, the resulting energies for the prolate and oblate symmetric rotors are defined as, respectively:

$$E_{J,K} = h[BJ(J+1) + (A-B)K^2] \quad (1.9)$$

$$E_{J,K} = h[BJ(J+1) + (C-B)K^2] \quad (1.10)$$

Where  $A = \frac{h}{8\pi^2 I_a}$ ,  $B = \frac{h}{8\pi^2 I_b}$ ,  $C = \frac{h}{8\pi^2 I_c}$  are the rotational constants in frequency units with  $h$  the Planck constant (for a generic rotational constant ( $X$ ), the conversion factor is  $X(\text{MHz}) = \frac{505376}{I_x(\text{amu}\cdot\text{\AA}^2)}$ ).

The asymmetric rotor is, unlike the previous case, more complex since there is not an internal axis for which the angular momentum component is a constant of the motion and approximate methods are used to derive rotational energy levels. In order to calculate the rotational energy levels, since a close wave functions expression is not achievable, can be used a linear combination of the wave functions for the symmetric rotor<sup>1</sup> ( $A_{J_{K_{-1}K_1}M} = \sum_{K,\gamma} a_{K\gamma}^{J_{K_{-1}K_1}M} S_{JKM\gamma}$ ). Hence,  $J$  and  $M$  are still constants of the motion, and a generic rotational energy level is defined as  $J_{K_{-1}K_1}$  where  $J$  is the rotational quantum number,  $K_{-1}$  (or  $K_a$ ) and  $K_1$  (or  $K_c$ ) are the pseudo quantum numbers indicating the energy level of the considered asymmetric rotor in the prolate and oblate limit, respectively.

The Hamiltonian operator ( $\hat{H}$ ) is

$$\hat{H} = h(A\hat{P}_a^2 + B\hat{P}_b^2 + C\hat{P}_c^2) \quad (1.11)$$

As developed by Ray<sup>3</sup>, equation (1.11) can be rearranged in a way in which only the so-called ‘‘Reduced Hamiltonian’’ ( $\hat{H}(\kappa) = \hat{P}_a^2 + \kappa\hat{P}_b^2 - \hat{P}_c^2$ ) is function of the inertial asymmetry parameter ( $\kappa$ ):

$$\frac{\hat{H}}{h} = \frac{1}{2}(A+C)\hat{P}^2 + \frac{1}{2}(A-C)\hat{H}(\kappa) \quad (1.12)$$

Where  $\hat{P}^2 = \hat{P}_a^2 + \hat{P}_b^2 + \hat{P}_c^2$ .

As to the Ray’s parameter ( $\kappa$ ), this is defined as:



$$\kappa = \frac{2B - A - C}{A - C} \quad (1.13)$$

According to equation (1.13) it can be distinguished 3 types of rotors:

- 1) symmetric prolate rotor ( $\kappa=-1$ )
- 2) symmetric oblate rotor ( $\kappa=1$ )
- 3) asymmetric rotor ( $-1 < \kappa < 1$  with, for  $\kappa=0$ , the most asymmetric rotor).

The obtained rotational energy for a specific level of an asymmetric rotor is given by:

$$E = \frac{1}{2}(A + C)J(J + 1) + \frac{1}{2}(A - C)E_{J_{K-1, K_1}}(\kappa) \quad (1.14)$$

In the case of near – prolate (1.15) (the most typical kind of rotor in nature) and near – oblate (1.16) asymmetric rotors, the energies can be written as, respectively<sup>4</sup>:

$$\frac{E}{h} = \frac{B + C}{2}J(J + 1) + \left(A - \frac{B + C}{2}\right)\omega_p \quad (1.15)$$

$$\frac{E}{h} = \frac{A + B}{2}J(J + 1) + \left(C - \frac{A + B}{2}\right)\omega_o \quad (1.16)$$

Where  $\omega_p = K^2 + c_1 b_p + c_1 b_p^2$  etc. (with  $b_p = \frac{C-B}{2A-B-C}$ ) and  $\omega_o = K^2 + c_1 b_o + c_1 b_o^2$  etc. (with  $b_o = \frac{A-B}{2C-A-B}$ ).

## 1.2 The Distortable Rotor

A molecule in rotation undergoes to a change of its rigid configuration, the equilibrium geometry, to a distorted one, affected by the centrifugal distortion, which gives a small contribution to the rotational energy. The Hamiltonian operator for a semirigid nonvibrating asymmetric rotor, in the harmonic approximation, is<sup>1</sup>:

$$\hat{H} = \frac{1}{2} \sum_{\alpha, \beta} \mu_{\alpha\beta}^e \hat{P}_\alpha \hat{P}_\beta + \frac{1}{4} \sum_{\alpha, \beta, \gamma, \delta} \tau_{\alpha\beta\gamma\delta} \hat{P}_\alpha \hat{P}_\beta \hat{P}_\gamma \hat{P}_\delta \quad (1.17)$$

Where  $\tau_{\alpha\beta\gamma\delta} = -\frac{1}{2}\sum_{ij}\mu_{\alpha\beta}^{(i)}(f^{-1})_{ij}\mu_{\gamma\delta}^{(j)}$ , the distortion constants with  $\mu_{\alpha\beta}$  an element of the inverse moment of inertia tensor ( $\mu_{\alpha\beta}^e$  is at the equilibrium value),  $\mu_{\alpha\beta}^{(i)} = \left(\frac{\partial\mu_{\alpha\beta}}{\partial R_i}\right)_e$ ,  $(f^{-1})_{ij}$  an element of the tensor inverse to the matrix of force constants and  $\alpha, \beta, \gamma, \delta = x, y$  or  $z$ .

The Hamiltonian (1.17) can be reduced according to symmetry considerations and equivalence of the distortion constants making further simplifications by using the commutation rules for the angular momentum components. Watson proposed two different types of reduction<sup>5</sup> by with the possible 81 distortion constants have been reduced to 5 linearly independent: the Symmetric (S) and the Asymmetric (A) one. Their respectively Hamiltonian operators are:

$$\hat{H}^S = \hat{H}_r + \hat{H}_d^{S(4)} \quad (1.18)$$

$$\hat{H}^A = \hat{H}_r + \hat{H}_d^{A(4)} \quad (1.19)$$

Where the Symmetric and Asymmetric Reduced Hamiltonian ( $\hat{H}^S$ ) are composed by a rotational term<sup>2</sup> ( $\hat{H}_r$ ) plus a centrifugal distortion one ( $\hat{H}_d^{(4)}$ ) which depends on the quartic power of the angular momentum operators and result be:

$$\hat{H}_d^{S(4)} = D_J\hat{P}^4 - D_{JK}\hat{P}^2\hat{P}_z^2 - D_K\hat{P}_z^4 + d_1\hat{P}^2(\hat{P}_+^2 - \hat{P}_-^2) + d_2(\hat{P}_+^4 + \hat{P}_-^4) \quad (1.20)$$

$$\hat{H}_d^{A(4)} = \Delta_J\hat{P}^4 - \Delta_{JK}\hat{P}^2\hat{P}_z^2 - \Delta_K\hat{P}_z^4 - 2\delta_J\hat{P}^2(\hat{P}_x^2 - \hat{P}_y^2) - \delta_K[P_z^2(P_x^2 - P_y^2) + (P_x^2 - P_y^2)P_z^2] \quad (1.21)$$

Where  $\hat{P}_\pm = (\hat{P}_x \pm i\hat{P}_y)$ .

### 1.3 Effect of Vibrations

Rotational and centrifugal distortion constants are affected by vibrational averaging effects not taken into the account in the description of the rigid rotor. The effective constants (with the subscript  $v$ ), which are obtained fitting the observed rotational transition frequencies, are related with the equilibrium ones (with the subscript  $e$ ) according to:

$$A_v = A_e - \sum_i \alpha_i^a \left( \nu_i + \frac{d_i}{2} \right) \quad (1.22)$$

$$B_v = B_e - \sum_i \alpha_i^b \left( \nu_i + \frac{d_i}{2} \right) \quad (1.23)$$

$$C_v = C_e - \sum_i \alpha_i^c \left( \nu_i + \frac{d_i}{2} \right) \quad (1.24)$$

And taken into the account a generic centrifugal distortion constant:

$$D_v = D_e - \sum_i \beta_i \left( v_i + \frac{d_i}{2} \right) \quad (1.25)$$

Where  $i$  is the  $i^{\text{th}}$  normal mode of vibration,  $d_i$  is its degeneracy,  $v_i$  represents its  $v^{\text{th}}$  vibrational state and  $\alpha_i$ ,  $\beta_i$  are represents the contributions (harmonic, anharmonic, Coriolis) with respect to the equilibrium values which due to the  $i^{\text{th}}$  normal mode of vibration.

## 1.4 Selection Rules

Permitted rotational transitions between two rotational levels, which satisfy the Bohr frequency condition, interacting with a microwave radiation fixed in space (space fixes axis  $F=X,Y,Z$ ), are derivable from the dipole matrix elements (1.26) according to two conditions:

- 1) The presence of, at least, a non zero dipole moment component along  $a, b, c$ .
- 2) The integrand of the dipole matrix elements (1.26) transforms according to the totally symmetric representation  $A$  of the inertia ellipsoid for an asymmetric rotor. Every asymmetric rotor wave function<sup>2</sup> and dipole moment component in fact, can be classified according to the Character table of Group  $V$  (Four-group operations:  $E, C_2^a, C_2^b, C_2^c$ ).

Integral (1.26) is defined as<sup>1</sup>:

$$\int A_{J_{K_{-1}K_1}} \mu_F A_{J'_{K'_{-1}K'_1}} \delta\tau \quad (1.26)$$

Where  $\mu_F = \sum_g \cos(Fg)\mu_g$  with  $\mu_g$  components of the permanent molecular dipole moment along  $g = a, b, c$  and  $\cos(Fg)$  the director cosines (which underlying the symmetry properties of Group  $V$ ) between the space fixes axis  $F=X,Y,Z$  and the principal axes of inertia.

Transitions caused by interaction of  $\mu_a$ ,  $\mu_b$  or  $\mu_c$  dipole moment component with the electromagnetic radiation along the external axis give rise to the so-called “ $\mu_a$ ,  $\mu_b$  or  $\mu_c$  type transition”.

From symmetry considerations, the permitted transitions result be those for which, the parity of  $K_a$  or  $K_c$  or the parity product  $K_a K_c$  of both the two rotational levels involved, remain invariant for the  $\mu_a$ ,  $\mu_c$  or  $\mu_b$  type transition, respectively with  $\Delta J = 0, \pm 1$ . Selection rules can, thus, summarized as:

$$\Delta J = -1, 0, 1 \text{ (designated as the } P, Q, R \text{ branches)} \quad (1.27)$$

$$(\mu_a) \rightarrow \Delta K_{-1} = 0, \pm 2 \dots \quad \Delta K_1 = \pm 1, \pm 3 \dots \quad (1.28)$$

$$(\mu_b) \rightarrow \Delta K_{-1} = \pm 1, \pm 3 \dots \quad \Delta K_1 = \pm 1, \pm 3 \dots \quad (1.29)$$

$$(\mu_c) \rightarrow \Delta K_{-1} = \pm 1, \pm 3 \dots \quad \Delta K_1 = 0, \pm 2 \dots \quad (1.30)$$

Up to now, it was just considered the rotational wave function. However, the total wave function for a molecule, is defined, in the Born-Oppenheimer approximation, as:

$$\psi_T = \psi_e \psi_v \psi_r \psi_s \quad (1.31)$$

Where  $\psi_e$ ,  $\psi_v$ ,  $\psi_r$ ,  $\psi_s$  are, respectively, the electronic, vibrational, rotational and spin nuclear wave functions, whose symmetries have to satisfy the point number 2 of this paragraph to make possible a microwave transition. It follows that, tunnelling effects connected with symmetry operations, such as the exchange of identical nuclei affect the total wave function symmetry giving rise to different parity selection rules and statistical weights depending on the fermion or boson nature of the nuclei.

## 1.5 Population of the Energy Levels

In a canonical ensemble at thermal equilibrium at the temperature ( $T$ ), the number of particles per unit volume in the  $i^{\text{th}}$  quantum energy level ( $N_i$ ) with degeneracy  $g_i$ , whose difference in energy with respect to that of the ground state is  $\Delta E_i$ , is described by the Boltzmann distribution according to the equation:

$$N_i = N_0 g_i e^{-\frac{\Delta E_i}{kT}} \quad (1.32)$$

Where  $N_0$  is the number of particles in the ground state per unit volume.

Taking into the account the total number of particles per unit volume ( $N$ ), the previous equation results be:

$$N_i = \frac{N g_i e^{-\frac{\Delta E_i}{kT}}}{Q} \quad (1.33)$$

Where  $Q$  is the partition function. This is defined as:

$$Q = \sum_j g_j e^{-\frac{\Delta E_j}{kT}} \quad (1.34)$$

Where the subscript  $j$  is a particular quantum energy level.

In the case of free gaseous molecules and in the Born–Oppenheimer approximation, the partition function can be written as:

$$Q = Q_e Q_v Q_r Q_n \quad (1.35)$$

Where  $Q_e, Q_v, Q_r, Q_n$  are, respectively, the electronic, vibrational, rotational and nuclear spin states partition functions.

Focus the attention only on rotational partition function for an asymmetric rotor, its expression can be approximate as:

$$Q_r = \frac{5.34 \cdot 10^6}{\sigma} \left( \frac{T^3}{A \cdot B \cdot C} \right)^{\frac{1}{2}} \quad (1.36)$$

Where is shown the linear and cubic dependence of the rotational partition function with respect to, respectively, the rotational constants and the temperature. The symmetry number ( $\sigma$ ) result be one in the case of an asymmetric rotor when no symmetry operation, exchanging identical nuclei, are possible.

## 1.6 Nuclear Quadrupole Coupling

When a non spherical distribution of nuclear charge (nuclear spin  $I > 1/2$ ), which results in the nuclear quadrupole moment, interacts with the non spherical distribution of electronic charge about the nucleus, which depends on the molecular rotational angular momentum  $J$ , gives rise to the nuclear quadrupole coupling.

Because of this, the presence in the molecular structure of isotopes with nuclear spin  $I > 1/2$ , gives rise to this phenomenon, as for  $^{35}\text{Cl}$  ( $I = 3/2$ ),  $^{37}\text{Cl}$  ( $I = 3/2$ ),  $^{14}\text{N}$  ( $I = 1$ ).

The energy of the quadrupole interaction is expressed classically as:

$$E_Q = \frac{1}{4} \left( \frac{\partial^2 V}{\partial z^2} \right)_{z=0} \int \rho_n (3z_n^2 - r_n^2) d\tau_n \quad (1.37)$$

Where  $\left( \frac{\partial^2 V}{\partial z^2} \right)_{z=0}$  is the electric field at the nucleus center,  $\rho_n$  is the density of the nuclear charge and the term  $3z_n^2 - r_n^2$  is the deviation from spherical symmetry of the nuclear shape in the  $x, y, z$  body-fixed principal axes system with  $z$  along the nuclear spin axis and origin at the center of the nucleus. A general equation for the quadrupole coupling energy can be derived from the corresponding Hamiltonian as<sup>1</sup>:

$$E_Q = \sum_{g=a,b,c} \chi_{gg}(J, i, M_J = J | \Phi_{zg}^2 | J, i, M_J = J) \left[ \frac{0.75 \cdot C(C+1) - J(J+1)I(I+1)}{2J(2J-1)I(2I-1)} \right] \quad (1.38)$$

Where the quadrupole coupling constants are  $\chi_{gg} = eQq_{gg}$  ( $g=a, b$  or  $c$ ) with  $Q$  the nuclear electric quadrupole moment,  $e$  the elementary charge,  $q_J$  the electric field gradient at the nucleus center,  $C = F(F + 1) - J(J + 1) - I(I + 1)$  and  $(J, i, M_J = J | \Phi_{zg}^2 | J, i, M_J = J) \equiv \int \psi_{J,i,M_J=J}^* \Phi_{zg}^2 \psi_{J,i,M_J=J} \delta\tau$ .

In the case of an asymmetric rotor, the quadrupolar energy results be<sup>1</sup>:

$$E_Q = \frac{1}{J(J+1)} \left\{ \chi_{aa} \left[ J(J+1) + E(\kappa) - (\kappa+1) \frac{\delta E(\kappa)}{\delta \kappa} \right] + 2\chi_{bb} \frac{\delta E(\kappa)}{\delta \kappa} + \chi_{cc} \left[ J(J+1) + E(\kappa) + (\kappa+1) \frac{\delta E(\kappa)}{\delta \kappa} \right] \right\} \quad (1.39)$$

Where the three quadrupole coupling constants are connected according to the relation  $\chi_{aa} + \chi_{bb} + \chi_{cc} = 0$ .

Two new angular momentum quantum numbers ( $F$  and  $M_F$ ) describing the quadrupole coupling are<sup>1</sup>:

$$F = J + I, J + I - 1, \dots, |J - I| \quad (1.40)$$

$$M_F = F, F - 1, \dots, -F \quad (1.41)$$

Selection rules are  $\Delta F = 0, \pm 1$  and  $\Delta I = 0$  in addition to those for the rigid asymmetric rotor.

The nuclear quadrupole coupling has a consequence on the rotational spectrum because it causes the splitting of each microwave transition frequency in several components which are differently separated from each other, depending on the type of nucleus and the molecule of which is part of. However, chemical and electronic structure information are derivable from the knowledge of the molecular field gradients obtainable by fitting the experimental hyperfine structure of rotational transitions. In fact, equation (1.42), in which  $\rho = a, b$  or  $c$ , connects the quadrupole coupling constants ( $\chi_{xx}, \chi_{yy}, \chi_{zz}$ ) in the  $x, y, z$  body-fixed principal axes with the origin at the center of the nucleus, with the molecular quadrupole constants  $\chi_{\rho\rho}$  (physical quantity deriving from the rotational spectrum fitting) according to:

$$\chi_{\rho\rho} = \chi_x \cos^2 \theta_{x\rho} + \chi_y \cos^2 \theta_{y\rho} + \chi_z \cos^2 \theta_{z\rho} \quad (1.42)$$

Furthermore, it is possible to determine the quadrupole asymmetry parameter ( $\eta = \frac{(\chi_{xx} - \chi_{yy})}{\chi_{zz}}$ ) which describes the quadrupole tensor deviation from the cylindrical symmetry around the  $z$  axis, the one chosen close to R-Y chemical bond, where Y is a quadrupolar nucleus.

## 1.7 Internal Rotation

Internal rotation is a large amplitude motion between two rotating groups around a single bond which describes a potential energy curve whose barriers are presumably caused by the interactions of two groups of electrons and nuclei<sup>6</sup>. A more recent study of ethane rotational barrier<sup>7</sup> states that its torsional potential barrier is mainly due to steric effects with a one third contribution to the barrier coming from hyperconjugation interactions  $\sigma_{C-H} \rightarrow \sigma_{C-H}^*$ , between vicinal C-H bonds.

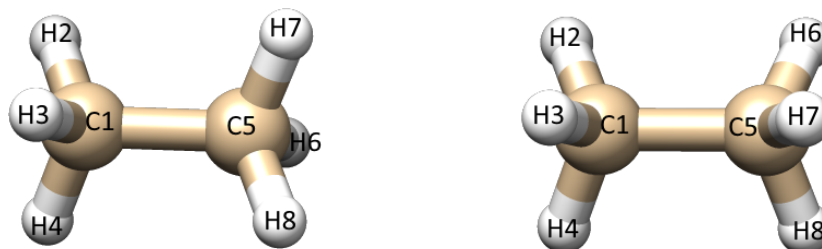
Defining a torsional angle ( $\alpha$ ) that, in the case of the ethane (see Figure 1), can be the H2C1-C5H6 dihedral angle, is possible to depict a potential function for a  $N$ -fold symmetry barrier as<sup>1</sup>:

$$V(\alpha) = \frac{V_N}{2}(1 - \cos N\alpha) + \frac{V_{2N}}{2}(1 - \cos 2N\alpha) + \dots \quad (1.43)$$

In the case of 3-fold symmetry, as in the case of ethane, truncating the Fourier series expansion up to the first term, the potential function (1.43) becomes:

$$V(\alpha) = \frac{V_3}{2}(1 - \cos 3\alpha) \quad (1.44)$$

Where the minima are for  $\alpha = 0, \pm\frac{2\pi}{3}, \pm\frac{4\pi}{3}$  etc. and the maxima for  $\alpha = \pm\frac{\pi}{3}, \pm\pi$ , etc.



**Figure 1.** Staggered and Eclipsed (from left to right) ethane conformations with atom numbering.

Solving the wave function equation for the internal rotation of a 3-fold symmetry barrier with respect to torsional energy eigenvalues  $E_{v\sigma}$  and eigenfunctions  $U_{v\sigma}(\alpha)$ , means to write:

$$-F \frac{d^2 U_{v\sigma}(\alpha)}{d\alpha^2} + \left[ \frac{V_3}{2}(1 - \cos 3\alpha) - E_{v\sigma} \right] U_{v\sigma}(\alpha) = 0 \quad (1.45)$$

Where  $F = \frac{\hbar^2}{2I_r}$ , with  $I_r$  the reduced moment of inertia.

A periodic wave functions solution of equation (1.45), can be written as:

$$U_{\nu\sigma}(\alpha) = \sum_{k=-\infty}^{+\infty} A_k^{(\nu)} e^{i(3k+\sigma)\alpha} \quad (1.46)$$

Where  $\sigma$  is an integer giving the symmetry of the torsional wave functions (for a 3-fold symmetry barrier  $\sigma = 0, \pm 1$ ) and  $\nu$  the principal torsional quantum number with  $k$  an integer.

If a classification of the wave functions  $U_{\nu\sigma}(\alpha)$  is made upon the symmetry operations within the character table<sup>1</sup> for the group  $C_3^a$ , results that for  $\sigma = 0$ ,  $U_{\nu\sigma}(\alpha)$  belongs to the non-degenerate symmetry species  $A$ , while there are, for  $\sigma = \pm 1$ , two degenerate  $U_{\nu\sigma}(\alpha)$  wave functions belonging to the  $E$  symmetry species.

Two possible  $V_3$  barrier extremes are, first of all, analyzed:

1.  $V_3 \rightarrow \infty$ .
2.  $V_3 = 0$ .

In the former case, solving equation (1.45), the torsional eigenvalues are found be<sup>1</sup>:

$$E_\nu = 3(V_3F)^{1/2} \left( \nu + \frac{1}{2} \right) \quad (1.47)$$

On the other hand, in the case of free internal rotation, the torsional eigenvalues are<sup>1</sup>:

$$E_{\nu\sigma} = F(3k + \sigma)^2 \quad (1.48)$$

One can see that in equation (1.47) the energies are independent from  $\sigma$ , which means that in the limit of high barrier the three torsional sublevels defining by  $\sigma = 0, \pm 1$  are degenerate while for  $V_3 = 0$ , the degeneration of the levels described by the same  $\nu$  quantum number is removed. Because of this, two different torsional levels (for  $\sigma = 0$  and for  $\sigma = \pm 1$ ) are split. In particular, in going from an high barrier to a free rotation case, the energy splitting between the torsional levels increase reaching the maximum difference for  $V_3 = 0$ .

Since  $(3k + \sigma)$  can have any integer value, choosing  $k = 0$  and substituting  $\sigma$  with  $m$ , equation (1.48) can be written as<sup>1</sup>:

$$E_{\nu m} = Fm^2 \quad (1.49)$$

The Combined Axis Method, on which the XIAM program<sup>8</sup> is based, uses the Hamiltonian matrix for the asymmetric rotor ( $\hat{H}_r$ ) set up in the principal axes system (PAS) while the Hamiltonian ( $\hat{H}_{ir}$ ) relative to each symmetric top (as the methyl group) is defined along its own internal axes system (the rho system (RAS)). Two Euler angles (beta and gamma angles, between the RAS and PAS)



transform  $\hat{H}_{ir}$  into the principal axes system. The total Hamiltonian, in the case of one symmetric top, is:

$$\hat{H} = \hat{H}_{rr} + \hat{H}_{cd} + \hat{H}_i \quad (1.50)$$

Where  $\hat{H}_{rr}, \hat{H}_{cd}, \hat{H}_i$  are the Hamiltonian operators terms for the asymmetric rigid rotor, the centrifugal distortion, the internal rotation of the top in the RAS. A further terms, such as the internal rotation overall - rotation distortion operator ( $\hat{H}_{ird}$ ), the top-top coupling one ( $\hat{H}_{ii}$ ), and the nuclear quadrupole coupling one ( $\hat{H}_Q$ ) of only one weakly interacting quadrupolar nucleus, can be taken into the account.

In particular, the Hamiltonian operator of the third term in equation (1.50) for one symmetric top and  $V_3$  barrier is<sup>1</sup>:

$$\hat{H}_i = F(\hat{p} - \hat{\rho})^2 + \frac{V_3}{2}(1 - \cos 3\alpha) \quad (1.51)$$

where  $F = \frac{\hbar^2}{2rI_\alpha}$  with  $I_\alpha$  is the moment of inertia of the top about its symmetry axis,  $r = 1 - \sum_g \frac{\lambda_g^2 I_\alpha}{I_g}$  (with  $g = a, b, c$  and  $\lambda$  the direction cosines between the symmetry axis of the top and the principal axes of whole molecule),  $\hat{p}$  the total angular momentum of the internal rotor, the reduced angular momentum  $\hat{\rho} = \sum_g \rho_g \hat{P}_g$  where  $\rho_g = \frac{\lambda_g I_\alpha}{I_g}$  and  $\hat{P}_g$  the total angular momentum operator of the entire molecule. In the case of an asymmetric rotor containing two symmetric top rotors, the internal rotation Hamiltonian of the second top and, eventually, the top-top Hamiltonian interaction and a second  $\hat{H}_{ird}$  term, have to be added to equation (1.50).

From this latter equation is possible to determine the magnitude of the  $V_3$  barrier by fitting the transition frequencies of both the  $A$  and  $E$  components lines for a rotor containing one symmetric top internal rotation.

The  $V_3$  barrier can be evaluate, also, from the effective rotational constants<sup>9</sup> for the  $v=0$  and  $\sigma=0$  level, in the case of one top symmetric rotor, as:

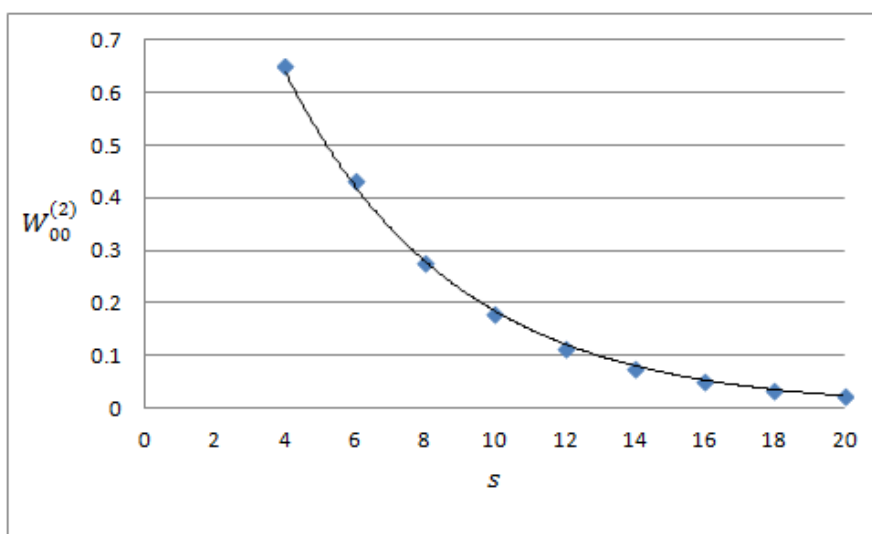
$$A_{00} = A_r + W_{00}^{(2)} F \rho_a^2 \quad (1.52)$$

$$B_{00} = B_r + W_{00}^{(2)} F \rho_b^2 \quad (1.53)$$

$$C_{00} = C_r + W_{00}^{(2)} F \rho_c^2 \quad (1.54)$$

Where  $A_r, B_r, C_r$  and  $A_{00}, B_{00}, C_{00}$  are the rigid rotor and the  $v=0$  and  $\sigma=0$  level rotational constants, respectively, with  $W_{00}^{(2)}$  the Herschbach's barrier dependent perturbation sums at the

second order for the  $\nu=0$  and  $\sigma=0$  level, which are connected to the reduced barrier  $s$  according to the exponential regression function (see Figure 2), considering  $s$  terms from 4 to 20.



**Figure 2.** The exponential regression function ( $y = 1.4646e^{-0.207x}$ ,  $R^2 = 0.9993$ , for  $s$  from 4 to 20) describing the relationship between the Herschbach's barrier dependent perturbation sums at the second order ( $W_{00}^{(2)}$ ) and the reduced barrier ( $s$ ).

The knowledge of  $s$  from solution of  $W_{00}^{(2)}$  solving the equations (1.52)  $\rightarrow$  (1.54), allows us to determine the correspondent  $V_3$  barrier as:

$$V_3 = 0.215sF \quad (1.55)$$

## 1.8 Molecular Structure Determination

Rotational spectroscopy is strictly in relation with the determination of molecular structures since rotational constants, which are reciprocals of the moments of inertia, determine the position of the microwave transition frequencies.

Three different methods<sup>1</sup> for the evaluation of molecular geometries, depending on the concept of on which are based on, have been used in this thesis, defining three possible structures:

1. The equilibrium structure ( $r_e$ ).
2. The effective structure ( $r_0$ ).
3. The substitution structure from single isotopic substitution ( $r_s$ ).

### 1.8.1 Equilibrium Structure

The equilibrium structure is that one in which the geometrical parameters, provided from *ab initio* calculations (see Chapter 2), are related to the hypothetical vibrationless state derivable by evaluating the contributions of vibrations according to equations (1.22), (1.23), (1.24).

### 1.8.2 Single Substitution Structure

Based on the Kraitchman's equations<sup>10</sup>, the single isotopic substitution method allows to locate the position of atoms for which two isotopes are available and their respective rotational spectra are observable, along the *a, b, c* axes system of the molecular structure. Because of this, the geometrical parameters, involving the aforementioned atom types, are obtainable taking the molecule as rigid upon isotopic substitution.

The Kraitchman's equations are:

$$I'_a = I_a + \mu(b^2 + c^2) \quad (1.56)$$

$$I'_b = I_b + \mu(a^2 + c^2) \quad (1.57)$$

$$I'_c = I_c + \mu(a^2 + b^2) \quad (1.58)$$

Where  $I_a, I_b, I_c$  and  $I'_a, I'_b, I'_c$  are the principal moments of inertia of the most abundant isotopologue species molecule and of the single isotopically substituted one, respectively.  $\mu = \frac{M\Delta m}{M+\Delta m}$  is the reduced mass of isotopic substitution, where  $M$  and  $\Delta m$  are the molecular weight of the most abundant isotopologue species and the variation of mass in going from this latter to the other isotopologue.

Zero-point vibration effects can greatly affect the determination of the coordinates (they can result in imaginary values) of an atom along the *a, b, c* axes system when it is close to the molecular center of mass.

### 1.8.3 Effective Structure

In the paragraph 1.3 has been introduced the concept of effective rotational constants by considering the contribution of the vibrations in a particular vibrational state  $\nu$ , on the rotational constants relative to the hypothetical vibrationless state. Hence, the effective structure is calculated by fitting, according to the linear least-square method, the geometrical parameters of the equilibrium structure in order to reproduce the experimental rotational constants. It follows that:

$$I_i = I_i^0 + \sum_j \frac{\partial I_i}{\partial p_j} \Delta p_j \quad (1.59)$$

Where  $I_i$  is the experimental founded  $i^{\text{th}}$  moment of inertia,  $I_i^0$  the  $i^{\text{th}}$  *ab initio* one and  $p_j$  the  $j^{\text{th}}$  structural parameters.

## 1.9 Conformational and Tautomeric Equilibria

Analysis of conformers and tautomers populations of molecules in their genuine nature or in micro-solvated environments make it possible a better understanding of their chemical behavior. In this respect, rotational spectroscopy in supersonic expansion can provide the relative concentrations of the isomers of a molecule in the gas phase as the fractions prior to the expansion<sup>11</sup> (this assumption could not be the real distribution in supersonic expansion conditions).

Hence, an estimation of the relative energies between the  $i^{\text{th}}$  and  $j^{\text{th}}$  conformers or tautomers, in their respectively rotational and vibrational ground states, can be obtained from intensity measurement of nearby transitions, assuming a Boltzmann distribution, according to :

$$\Delta E_{0,0} = kT \ln \left[ \frac{(I_j \Delta \nu_j \mu_{g,i}^x \gamma_i \nu_i^2)}{(I_i \Delta \nu_i \mu_{g,j}^x \gamma_j \nu_j^2)} \right] \quad (1.60)$$

Where  $T$ ,  $I_i$ ,  $\Delta \nu_i$ ,  $\mu_{g,i}^x$ ,  $\gamma_i$  and  $\nu_i$  are, respectively, the temperature prior to the expansion, the peak height, the half height width, the dipole moment component ( $g = a, b, c$ ) where  $x$  depending on the spectrometer used ( $x=1$  in the case of the “ $\pi/2$  pulse” for the PJ-FTMW spectrometer and  $x=2$  for the CP-FTMW one, see Chapter 2), the line strength and transition frequency for a given transition of  $i^{\text{th}}$  conformer or tautomer.

Even when the equilibrium condition prior to the expansion suggests the simultaneously presence of different conformations, in seeded supersonic jets (see Chapter 2), signals belonging to higher energies conformers can be missing. This can be due, as reported in a previous study<sup>12</sup> describing also the influence of different monoatomic gas carriers, to conformational relaxation to lower energy states during supersonic expansion, occurring when barrier interconnecting different conformers are of the same order or smaller than  $2kT$  ( $T$  is the temperature before the expansion).

In the case of tautomerism this is generally not observed, since the respectively interconversion barriers are even as large as, for example, 146 - 159  $\text{kJ}\cdot\text{mol}^{-1}$  in 2-pyridone/2-hydropyridine<sup>13</sup> or 250 - 300  $\text{kJ}\cdot\text{mol}^{-1}$  in 9(H)-/7(H)-Purine<sup>14</sup>, which, however, can be reduced by environment effects<sup>14,15</sup>.

## 1.10 Dissociation Energy

Rotational spectroscopy provides a method to estimate the dissociation energy relative to a dimer, if the intermolecular stretching motion connecting the two subunits, within the pseudo-diatomic approximation<sup>16</sup>, is parallel (or almost parallel) to the  $a$ -axis. The corresponding force constant ( $k_s$ ) results be:

$$k_s = 16\pi^4(\mu_D R_{CM})^2[4B^4 + 4C^4 - (B - C)^2 \cdot (B + C)^2]/hD_J \quad (1.61)$$

Where  $\mu_D$ ,  $R_{CM}$ ,  $h$  are, respectively, the pseudo diatomic reduced mass, the distance between the centers of the mass of the two subunits and the Planck's constant.  $B$ ,  $C$  and  $D_J$  are the rotational and the centrifugal distortion constants of the adduct. According to the Lennard-Jones potential, the dissociation energy ( $E_D$ ) is calculated as<sup>17</sup>:

$$E_D = \frac{k_s R_{CM}^2}{72} \quad (1.62)$$

## 1.11 Non-Bonding Interactions

Molecular recognition processes, conformational preferences, structure/activity properties, solvation mechanisms, membrane transport and much more involve non-bonding interactions, whose nature and number play a fundamental role in the resulting macroscopic behavior. Unlike covalent bonds, which are characterized by high dissociation energy ( $\sim 100$  kcal/mol), short range (typically  $\leq 2$  Å), the aforementioned interactions take place at longer distances (even  $10$  Å)<sup>18</sup> with bonding energies at least weaker from an order of magnitude to two than those ones in the covalent bonds. While these latter originate by sharing a pair of electrons between the involved atoms, the balancing among the attractive and repulsive forces terms between permanent and/or transient electric multipoles, results in the establishment of the inter- or intra-molecular non-bonding interactions, on the other<sup>18</sup>.

Four types of non-boding interactions have been encountered in the molecular system studies I am describing:

- 1) Hydrogen Bonding (hereafter HB).
- 2) Weak Hydrogen Bonding (WHB).
- 3) Halogen Bonding (HaB).
- 4) Lone Pair $\cdots\pi$  interaction (lp $\cdots\pi$ ).

In the former case, according to the IUPAC recommendations<sup>19</sup>, the HB is defined as:” an attractive interaction between a hydrogen atom from a molecule or a molecular fragment X–H in which X is more electronegative than H, and an atom or a group of atoms in the same or a different molecule, in which there is evidence of bond formation.”

It is possible to distinguish between the hydrogen bond donor X–H and the acceptor one Y, where Y is an electron rich region of an atom (Y) or a molecule (Y-Z), involving electrostatic, charge transfer and dispersion forces.

Typical HB interactions are the O–H···O, O–H···N, O–H···S, N–H···O ones, whose dissociation energy values are in the 15-25 kJ·mol<sup>-1</sup> range<sup>20</sup>, which are also characterized by high directionality (typical X–H···Y angle are close to 180°, “preferably” >110°)<sup>19</sup>.

The similar directional properties are encountered in WHB for which, however, the bonding energies are only of few kJ·mol<sup>-1</sup> and, with respect to HB, blue shifting of stretching frequencies of the hydrogen bond donor are found<sup>21</sup>. Typical WHBs are the C–H··· $\pi$ , C–H···F, C–H···Cl, C–H···O, C–H···S, C–H···N, O–H··· $\pi$ , O–H···Halogen, N–H··· $\pi$  contacts<sup>20</sup>.

When “there is evidence of a net attractive interaction between an electrophilic region associated with a halogen atom in a molecular entity and a nucleophilic region in another, or the same, molecular entity” an HaB is established<sup>22</sup>. Most of the features<sup>23</sup> are similar with the aforementioned ones in the HB case such as the directionality while the forces involved in the bonding are primarily electrostatic with important contributions coming from polarization, charge transfer, and dispersion ones.

Finally, the lp··· $\pi$  interaction occurs between a lone pair of an electronegative atom, such as oxygen or nitrogen, and an antibonding  $\pi^*$  orbital of a region with positive electrostatic potential ( $\pi$ -hole). The main driving force governing the establishment of this weak interaction (< 1 kcal·mol<sup>-1</sup>)<sup>24</sup>, following geometries which are similar to those of the Bürgi-Dunitz trajectory, is the electrostatic one<sup>25</sup>.

## 1.12 Chirality

Several efforts have been made in the last years to the differentiation of enantiomers, resulting from a chiral molecule, using triple resonant experiment via rotational spectroscopy.

In 2013, Patterson et al.<sup>26</sup> based on the theoretical approach developed by Hirota<sup>27</sup>, “producing a definitive signature of chirality”<sup>26</sup> since the opposite sign of the product  $\mu_a \cdot \mu_b \cdot \mu_c$  between the two enantiomers, results in a phase displacement ( $\pi$ ) of the two molecular signals.

An experiment to indirectly measure the enantiomeric excess of a solid sample through the enantiomeric excess of a smaller molecule that interacts with the sample has been performed during my stay in the Pate's group, which is still under progress as well as the developing of a method allowing the absolute phase calibration of the three wave mixing rotational spectroscopy signal of a chiral molecule.

Apart from the enantiomer specific detection which required a more elaborate setting of the experimental apparatus<sup>26,28</sup>, rotational spectroscopy is, also, an efficient tool for the differentiation between diastereoisomers. These latter, in fact, can be distinguished using "standard" microwave spectrometers since the set of rotational constants of each diastereoisomer is different. For the same reason, within each diastereoisomer, different conformational structures can be separately characterized.

### 1.13 References

1. Gordy, W.; Cook, R. L.. *Microwave Molecular Spectra*, John Wiley & Sons, New York, (1984).
2. Mulliken, R. S. Species Classification and Rotational Energy Level Patterns of Non-Linear Triatomic Molecules. *Phys. Rev.* **59**, 873 (1941).
3. Ray, B. S. Über die Eigenwerte des asymmetrischen Kreisels. *Z. Physik.* **78**, 74 (1932).
4. Townes, C. H.; Schawlow, A. L. *Microwave Spectroscopy*, McGraw-Hill Book Company, New York (1955).
5. Watson, J. K. G. Aspects of Quartic and Sextic Centrifugal Effects on Rotational Energy Levels. In *Vibrational Spectra and Structure* Vol. 6, J. R. Durig, Ed., Marcel Dekker, New York, (1977).
6. Lin, C. C.; Swalen, J. D. Internal Rotation and Microwave Spectroscopy. *Rev. Mod. Phys.* **31**, 841 (1959).
7. Mo, Y.; Wu, W.; Song, L.; Lin, M.; Zhang, Q.; Gao, J. The Magnitude of Hyperconjugation in Ethane: A Perspective from Ab Initio Valence Bond Theory. *Angew. Chem. Int. Ed.* **43**, 1986 (2004).
8. Hartwig, H.; Dreizler, H. The Microwave Spectrum of trans-2,3-Dimethyloxirane in Torsional Excited States. *Z. Naturforsch., A: Phys. Sci.* **51a**, 923 (1996).
9. Herschbach, D. R. Calculation of Energy Levels for Internal Torsion and Over-All Rotation. III. *J. Chem. Phys.* **31**, 91 (1959).
10. Kraitchman, J. Determination of Molecular Structure from Microwave Spectroscopic Data. *Am. J. Phys.* **21**, 17 (1953).

11. Mata, S.; Cortijo, V.; Caminati, W.; Alonso, J. L.; Sanz, M. E.; López, J. C.; Blanco, S. Tautomerism and Microsolvation in 2-Hydroxypyridine/2-Pyridone. *J. Phys. Chem. A* **114**, 11393 (2010).
12. Ruoff, R. S.; Klots, T. D.; Emilson, T.; Gutowski, H. S. Relaxation of conformers and isomers in seeded supersonic jets of inert gases. *J. Chem. Phys.* **93**, 3142 (1990).
13. Moreno, M.; Miller, W. H. On the tautomerization reaction 2-pyridone  $\rightleftharpoons$  2hydroxypyridine: an ab initio study. *Chem. Phys. Lett.* **171**, 475 (1990).
14. Doo-Sik, A.; Sungyul, L.; Bongsoo, K. Solvent-mediated tautomerization of purine: single to quadruple proton transfer. *Chem. Phys. Lett.* **390**, 384 (2004).
15. Barone, V.; Adamo, C. Density Functional Study of Intrinsic and Environmental Effects in the Tautomeric Equilibrium of 2-Pyridone. *J. Phys. Chem.* **99**, 15062 (1995).
16. Millen, D. J. Determination of Stretching Force Constants of Weakly Bound Dimers from Centrifugal Distortion Constants. *Can. J. Chem.* **63**, 1477 (1985).
17. Novick, S. E.; Harris, S. J.; Janda, K. C.; Klemperer, W. Structure and Bonding of KrClF: Intermolecular Force Fields in van der Waals Molecules. *Can. J. Phys.* **53**, 2007 (1975).
18. Müller-Dethlefs, K.; Hobza, P. Noncovalent Interactions: A Challenge for Experiment and Theory. *Chem. Rev.* **100**, 143 (2000).
19. Arunan, E.; Desiraju, G. R.; Klein, R. A.; Sadlej, J.; Scheiner, S.; Alkorta, I.; Clary, D. C.; Crabtree, R. H.; Dannenberg, J. J.; Hobza, P.; Kjaergaard, H. G.; Legon, A. C.; Mennucci, B.; Nesbitt, D. J. Definition of the Hydrogen Bond. *Pure Appl. Chem.* **83**, 1637 (2011). ©IUPAC.
20. Caminati, W.; Grabow, J.-U. Microwave Spectroscopy: Molecular Systems. In *Frontiers of Molecular Spectroscopy*. Edited by Jaan Laane, Elsevier, Amsterdam (2009).
21. Desiraju, G.R.; Steiner, T. *The weak hydrogen bond in structural chemistry and biology*, Vol. IX, IUCr monographys on crystallography, Oxford University Press, Oxford, 2001.
22. Desiraju, G. R.; Shing Ho, P.; Kloo, L.; Legon, A. C.; Marquardt, R.; Metrangolo, P.; Politzer, P.; Resnati, G.; Rissanen, K. Definition of the halogen bond. *Pure Appl. Chem.*, **85**, 1711 (2013). ©IUPAC.
23. Legon, A. C. The halogen bond: an interim perspective. *Phys. Chem. Chem. Phys.* **12**, 77 (2010).
24. Singh, S. K.; Mishra, K. K.; Sharma, N.; Das, A. Direct Spectroscopic Evidence for an  $n \rightarrow \pi^*$  Interaction. *Angew. Chem. Int. Ed.* **55**, 1 (2016).
25. Murray, J. S.; Lane, P.; Clark, T.; Riley, K. E.; Politzer, P.  $\sigma$ -Holes,  $\pi$ -Holes and Electrostatically - Driven Interactions. *J. Mol. Model.* **18**, 541 (2012).



26. Patterson, D.; Schnell, M.; Doyle, J. M. Enantiomer-specific detection of chiral molecules via microwave spectroscopy. *Nature* **497**, 475 (2013).
27. Hirota, E. Triple resonance for a three-level system of a chiral molecule. *Proc. Jpn. Acad., Ser. B* **88**, 120 (2012).
28. Lobsiger, S.; Perez, C.; Evangelisti, L.; Lehmann, K. K.; Pate, B. H. Molecular Structure and Chirality Detection by Fourier Transform Microwave Spectroscopy. *J. Phys. Chem. Lett.* **6**, 196 (2015).

# CHAPTER 2

## Experimental and Computational Methods

### 2.1 Supersonic Free Jets

A supersonic free jet is the result of a pure or mixed gas rapid expansion from a source at high pressure ( $P_0 = 0.1 - 100$  bars)<sup>1</sup> to a high vacuum chamber ( $P_1 = 10^{-7} - 10^{-10}$  bars) through an orifice which, in the spectrometers I am going to describe, is a nozzle of 0.5 – 2.0 mm diameter range, 2 mm length with conical shape wide up to 4 mm.<sup>2</sup>

The expansion process, characterized by a nonequilibrium condition, can be described by distinguishing three different zones:

- 1) The pre-expansion zone.
- 2) The source exit.
- 3) The post-expansion zone.

In the zone prior to the expansion, velocity distribution of the gas at pressure  $P_0$  and temperature  $T_0$  follows the usual Maxwell Boltzmann distribution function. In going from this stagnation state (Mach number ( $M$ ) much more less than 1) to the post-expansion zone at background pressure  $P_1$ , the gas accelerates up to  $M = 1$  at the source exit, reaching the condition<sup>3</sup>:

$$\frac{P_0}{P_1} > G \equiv \left(\frac{\gamma + 1}{2}\right)^{\frac{\gamma}{\gamma-1}} \quad (2.1)$$

Where  $G$  is a critical value which is less than 2.1 for all gases, and  $\gamma = \frac{c_p}{c_v}$ .

After this point, a rapid core isentropic supersonic expansion takes place with a continuous increasing of the velocity, reaching  $M \gg 1$  in the so-called “zone of silence” (the zone of interest for rotational spectroscopy), since its supersonic character makes it “insensitive” to  $P_1$ . This region is limited by the shock wave regions: the small thicknesses barrel and the Mach disk ( $M_d$ ) shocks at the sides and downstream, respectively. Mach disk position ( $x_{M_d}$ ), in nozzle diameter unit ( $d$ ), can be calculated, in particular, according to the following equation<sup>1</sup>:

$$x_{M_d}/d = 1.5 \sqrt{\left(\frac{P_0}{P_1}\right)} \quad (2.2)$$

From thermodynamics considerations, assuming  $\gamma$  constant during the expansion, physical properties such as temperature ( $T$ ), velocity ( $v$ ), pressure ( $P$ ) and density ( $\rho$ ) of the jet can be determined, at distances  $x_{M_d}/d$ , as<sup>3</sup>:

$$T = T_0 \left(1 + \frac{\gamma - 1}{2} M^2\right)^{-1} \quad (2.3)$$

$$v = v_0 \sqrt{\left(\frac{M^2}{1 + \frac{\gamma - 1}{2} M^2}\right)} \quad (2.4)$$

$$P = P_0 \left(\frac{T}{T_0}\right)^{\frac{\gamma}{\gamma - 1}} \quad (2.5)$$

$$\rho = \rho_0 \left(\frac{T}{T_0}\right)^{\frac{1}{\gamma - 1}} \quad (2.6)$$

Where the subscript zero is referred to the stagnation state condition.

From these equations is clear that the aforementioned physical properties, at a given  $x_{M_d}/d$ , depending on:

- 1) Their stagnation values.
- 2)  $\gamma$ , which is assumed be constant.
- 3) The Mach number.

Monoatomic gases, which have  $\gamma = 5/3$  (i.e., instead of  $7/5$  of a diatomic gas), achieve the highest Mach numbers in the jet causing the narrowest velocity distribution close to the terminal velocity ( $v_\infty$ ). If we consider a diluted mixture (0.1 - 2 %) of gas molecules of interest in a carrier gas (e.g. Helium, as made generally in my experimental studies), which is supersonically expanded, its terminal velocity is<sup>3</sup>:

$$v_\infty \cong \sqrt{\frac{2R}{\bar{W}} \left(\frac{\gamma}{\gamma - 1}\right) T_0} \quad (2.7)$$

Where  $\bar{W}$  is the molar average molecular weight assuming an ideal gas mixture.

Low translational temperatures (<1 K) are achievable in the jets where, during the initial stages of the expansion, cooling of rotational (rotational temperature 1-10 K) and vibrational modes occur, because of kinetic rotational and vibrational relaxation processes. Their cooling efficiency depends on the energy level gaps and on the number of binary collisions.

After this, the gas mixture travels in a directional flow without collisions (their number is close to zero) in, thus, a “freeze” condition. Hence, it is possible in this zone, to study molecular systems linked by weak interactions and, more in general, molecules have higher populated low rotational and vibrational energy levels than at the equilibrium condition, allowing higher intensity signals and simplifying spectra.

## 2.2 Microwave Spectrometers

Microwave spectrometers described here combine the advantages deriving from pulsed jets with the properties of the Fabry-Perot resonant cavity in the more sensitive time-domain spectroscopy than in the frequency-domain one.

Both type of rotational spectrometers used (Chirped Pulse Fourier Transform MicroWave (CP-FTMW) and Coaxially Oriented Beam Resonator Arrangement (COBRA) Pulsed Jet Fourier Transform MicroWave (PJ-FTMW)) are based on two transient processes that cause a macroscopic polarisation of the molecular ensemble followed by a spontaneous coherent emission<sup>4</sup>.

In fact, after the pulsed supersonic expansion of the molecular system (pulse duration  $\sim 500\mu\text{s}$ ) into the Fabry-Perot cavity using a solenoid pulsed valve, a shorter microwave pulse ( $\tau_p$  typical of  $1\mu\text{s}$ ) than the relaxation processes times ( $T_1$  and  $T_2$  comparing with NMR. Usually  $T_1$  is negligible and values of  $T_2 \sim 10\mu\text{s}$  such as for the 7.5–18.5 GHz CP-FTMW<sup>5</sup> and  $T_2 \sim 100\mu\text{s}$  in the case of 6.5–18.5 GHz Bologna PJ-FTMW can be determined) is applied. The transient absorption of the radiation by considering two levels system, cause a macroscopic polarization of the ensemble in a nonequilibrium population difference, from the initial negligible polarization and equilibrium population difference condition<sup>2,4</sup>.

Then, a spontaneous coherent molecular emission is released and collected for a suitable time (for example  $20\mu\text{s}$  or  $40\mu\text{s}$  for, respectively, the 6–18 GHz or 2–8 GHz CP-FTMW<sup>6</sup>) after which the Fourier transform is applied to obtain the microwave spectrum in the frequency domain. Repetition rates  $\leq 10$  Hz are typically achievable and the accumulation of FID transient emissions allow to increase the signal to noise ratio. This latter, in particular, is proportional to the root of the number of the acquisitions.

For both types of spectrometers, the Fabry-Perot cavity is evacuated by a set of one diffusion and two mechanical pumps allowing the aforementioned low background pressure.

## 2.2.1 Coaxially Oriented Beam Resonator Arrangement Pulsed Jet Fourier Transform MicroWave Spectrometers

In the case of the PJ-FTMW spectrometer, a microwave radiation of frequency  $\nu$  is generated by a synthesizer and the FID emission is collected over the full frequency range in small frequency steps of about 0.5 MHz, tuning to the resonance the cavity for a given  $\nu$  frequency. This is achievable by moving the mobile spherical mirror with respect to the other one in which is inserted the nozzle injecting the gas sample. The aluminium mirrors are in near-confocal arrangement and, for both, one L-shape antenna is fasten.

The FID emission signal amplitude ( $|S_{ab}|$ ) depends on<sup>2</sup>:

$$|S_{ab}| \propto \sqrt{\frac{\pi W_0^2 \omega_{ab} \kappa_p \Delta N_{ab} \mu_{ab}}{4 \omega_0 \delta \nu_\infty^2 \tau_M \tau_E}} \sin(x \tau_p) \times \cos(k \nu_\infty t) e^{i(\omega_{ab} t + \theta_{ab})} \quad (2.10)$$

Where, among other parameters which are related to the expansion in the Fabry-Perot cavity, the molecular signal is proportional to the two-level population difference ( $\Delta N_{ab}$ ), the first power of the electric dipole matrix elements ( $\mu_{ab}$ ), the transition frequency ( $\omega_{ab}$ ) and the Rabi flip angle ( $x \tau_p$  where  $x = \frac{\mu_{ab} \epsilon}{\hbar}$  is the Rabi angular frequency with  $\epsilon$  the electric field strength, and  $\tau_p$  the excitation pulse duration). From (2.10), the larger value of  $|S_{ab}|$  is obtainable at the Rabi flip angle of  $\pi/2$ .

The Doppler effect, taking place in this type spectrometer due to the coaxial arrangement of the supersonic jet and the resonator, splitting each rotational transition frequency into two components. Hence, the arithmetic mean of the two component transition frequencies provides the line position frequency. The accuracy of the frequency measurements is about 3 kHz and frequency lines separated by more than 10 kHz are resolvable.

Two different designs of the PJ-FTMW are present at the University of Bologna (Caminati's group, see Figure 1 and 2) and at the University of Basque Country<sup>7</sup>.

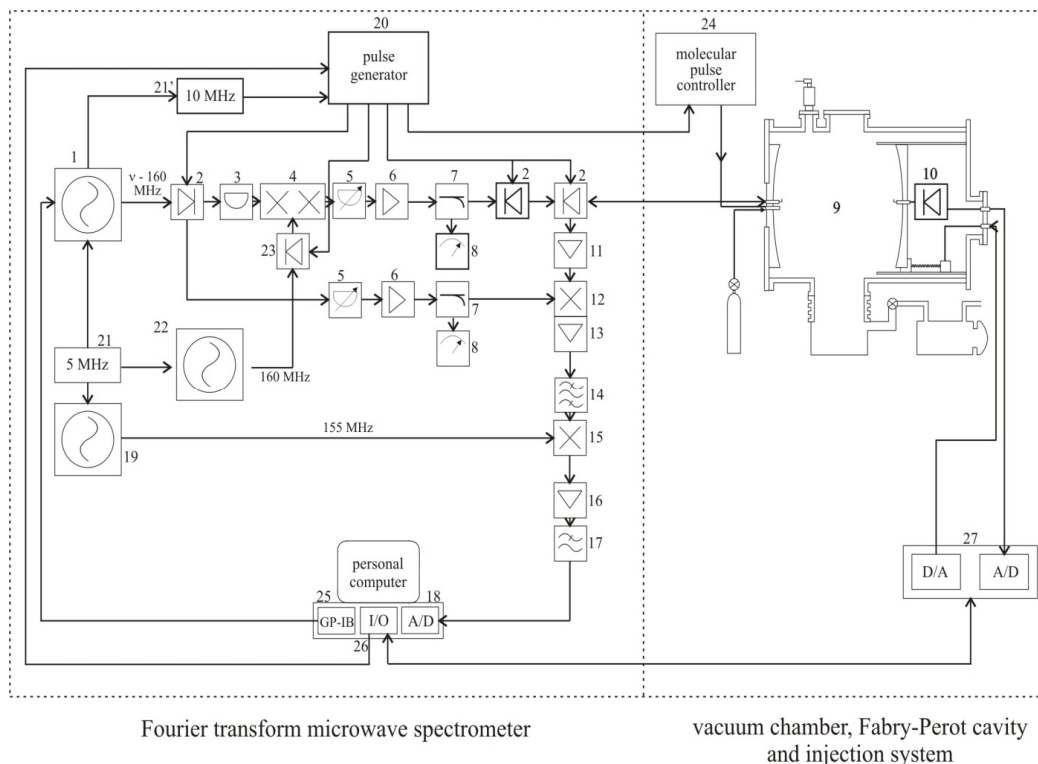
In the former case, a shifted microwave radiation (with the microwave at frequency  $\nu$  generated by the microwave synthesizer) at  $\nu + 160$  MHz is generated in a single side band modulator by mixing the synthesizer  $\nu$  microwave frequency with 160 MHz from a radiofrequency synthesizer. The obtain  $\nu + 160$  MHz is sent out, thought a MW switch SPDT bidirectional commuter, into the cavity only after passing through the amplification up to 100 mW and the pulsed modulation processes. The bidirectional commuter is the gate which divides the electronic circuit from the

cavity. The timing of the entire pulse process, the mirror positioning, governed by the computer software using a PXI system, allows to the shifted microwave radiation to enter into the cavity and to the FID signal to be collected only when the input signal is removed (or at least is far off resonance). The output signal from the cavity (*CS*) is first amplified by using a low-noise amplifier and, then, downconverted in the image-rejection mixer and, successively, in the radio-frequency mixer where the *CS* is mixed with, respectively, the  $\nu$  synthesized frequency and a 155 MHz radio frequency. All the frequencies are referenced to the Rb signal oscillator at 5 MHz.

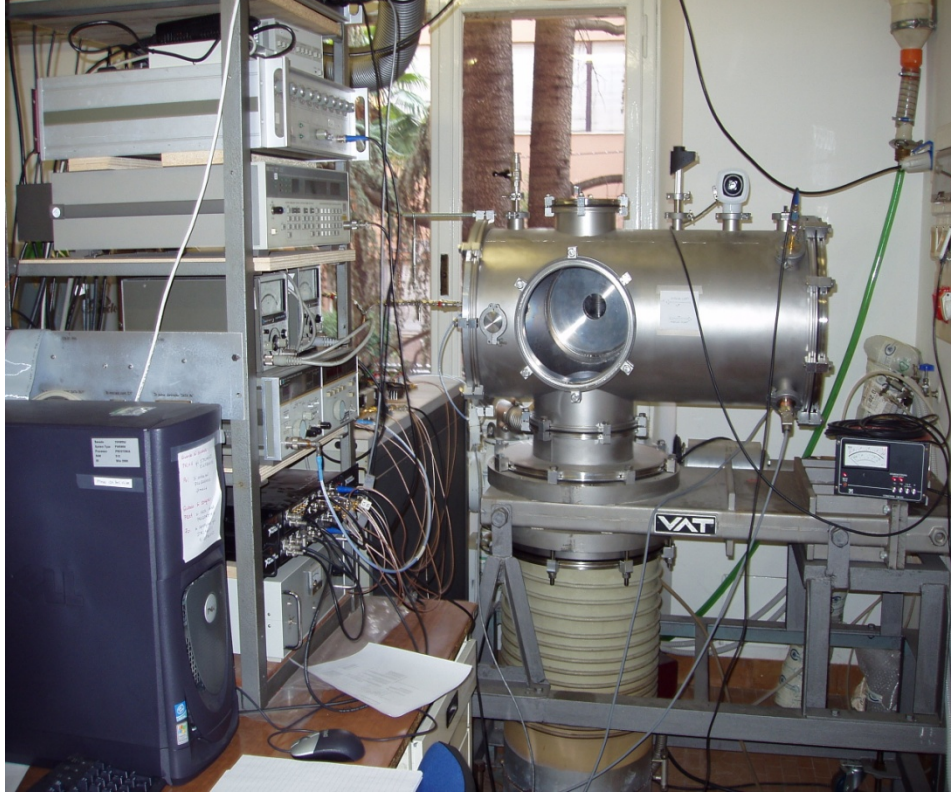
On the other hand, in the Bilbao PJ-FTMW a shifted microwave radiation at  $\nu + 30$  MHz is generated in a single side band modulator by mixing the synthesized  $\nu$  microwave frequency with 30 MHz from a radiofrequency synthesizer. Microwave radiation entry, amplified up to 150 mW, and output cavity signal exit, are located at the opposite sites on the two different mirrors. The downconversion process of the molecular emission signal  $\nu + 30$  MHz is performed in two stages, after low-noise amplification, by mixing it, at the first step with  $\nu$  synthesized frequency and in the second one with 27.5 MHz. All the frequencies are referenced to the Rb signal oscillator at 10 MHz. PXI system carries out the same functions as in the Bologna PJ-FTMW .

The laser ablation technique is associated with the Bilbao PJ-FTMW, allowing to vaporize solid samples, with really low vapour pressure or having decomposition issues by heating, which compromise the recording of the rotational spectrum.

A solid rod of cylindrical shape is prepared adding to  $\sim 0.8$  g of sample few drops of a binder and, the resulting mixture is ground and dried. The rod is pasted on a motorized micrometer which circularly moves up and down the sample in the ablation nozzle where a ps-pulsed Nd:YAG laser vaporized the rod using the third harmonic (355 nm). A scheme of the laser ablation system can be founded elsewhere.<sup>8</sup>



**Figure 1.** The 6.5-18.5 GHz Bologna COBRA-PJ-FTMW Spectrometer scheme. (MW = Micro Wave; RF = Radio Frequency; P = output power, IF = intermediate frequency, IL = insertion losses, G = gain, NF = noise figure, IS = isolation, IR = image rejection). 1. MW synthesizer, HP 8672 A. 2. MW switch SPDT, SMT SFD0526-001S. 3. Fixed attenuator MCL BW-S3W2. 4. Single side band modulator, MITEQ MN0226LC1C. 5. Variable attenuator, NARDA 4798. 6. MW amplifier ALC Microwave ALS0618-30-20. 7. Directional coupler NARDA 4203-16. 8. Power meter, HP 435 B + Power sensor 8485A. 9. Fabry-Pérot resonator. 10. MW crystal detector HP8470B. 11. MW low noise amplifier, MITEQ JSD4-0600-1800-16-8P. 12. Image rejection mixer, MITEQ IR0226LC1C. 13. 160 MHz RF amplifier, MITEQ AU-1466-140. 14. Bandpass filter, TTE KC6-160M-20M. 15. RF mixer, HP 10514A. 16. RF amplifier, MCL MAN 1LN. 17. Lowpass Filter, TTE LC5-25M-50-7135. 18. Transient recorder, SPECTRUM PAD 82A, modified following the design of the Kiel University. 19. RF synthesizer, PTS 160-M7020. 20. Pulse Sequencer TTL, made at the University of Valladolid, based on a PCB card from the University of Kiel. 21. Reference signal, Rb oscillator 5 MHz, Ball-Efraton FRK-LLN. 22. RF synthesizer, MARCONI 2019A. 23. RF switch MCL 7MSW-1111. 24. Pulse controller General Valve IOTA ONE. 25. IEEE 488 interface, NI GP-IB-488 PCII. 26. I/O card, NI PC-DIO-96. 27. A/D and D/A converter for Stepper motor control. Made in Valladolid.



**Figure 2.** The 6.5-18.5 GHz Bologna COBRA-PJ-FTMW Spectrometer.

## 2.2.2 Chirped Pulse Fourier Transform MicroWave Spectrometers

In the case of CP-FTMW spectrometer (see Figure 3), for each molecular pulse, usually 10 chirped pulses are used, consisting in a linear frequency sweep covering the full frequency range. The sweep range linearly (linear sweep rate  $\alpha$ ) depends on the excitation pulse duration ( $\tau_p$ )<sup>5</sup>:

$$\Delta\omega = \alpha\tau_p \quad (2.8)$$

The instantaneous frequency ( $\omega_i$ ) is given by<sup>5</sup>:

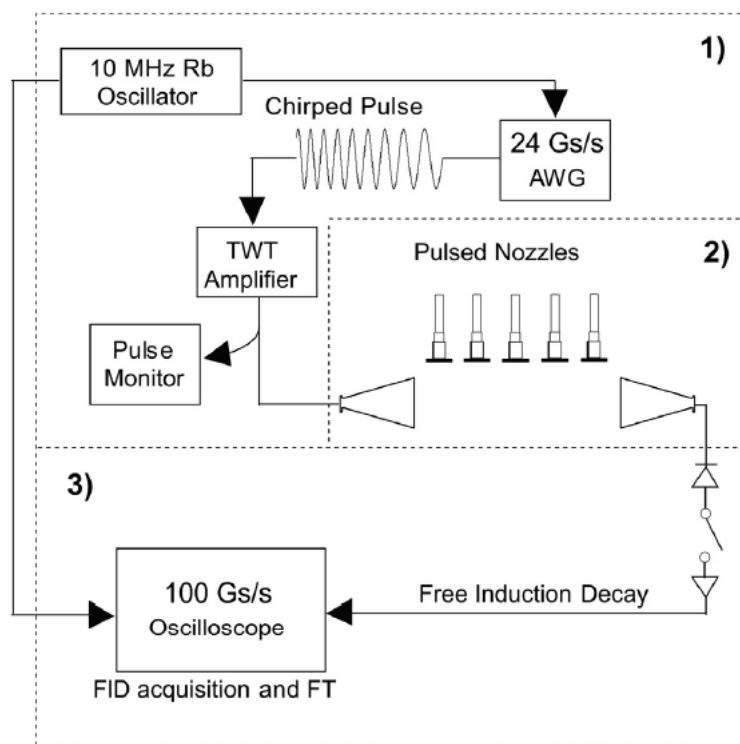
$$\omega_i = \frac{d(\omega_0 t + \frac{1}{2}\alpha t^2)}{dt} = \omega_0 + \alpha t \quad (2.9)$$

The molecular signal ( $S$ ) is proportional to<sup>5</sup>:

$$S \propto \omega \cdot \mu^2 \cdot E_{pulse} \cdot \Delta N_0 \cdot \sqrt{\frac{\pi}{\alpha}} \quad (2.10)$$



Where  $\omega$  is the frequency,  $\mu$  is the transition dipole moment,  $E_{pulse}$  is the electric field strength, and  $\Delta N_0$  the population difference at the equilibrium.



**Figure 3.** The 2-8 GHz Pate's CP-FTMW Spectrometer scheme (Reprinted from *Chem. Phys. Lett.*, 571, C. Pérez, S; Lobsiger; Seifert, N. A.; Zaleski, D. P.; Temelso, B.; Shields, G. C.; Kisiel, Z.; Pate, B. H., Broadband Fourier transform rotational spectroscopy for structure determination: The water heptamer., 1-15, Copyright (2013), with permission from Elsevier).

The microwave pulse is generated by using an arbitrary waveform generator (AWG) and then amplified thanks to a pulsed traveling wave tube amplifier (TWTA) having peak powers of 600 W (as in the 2-8 GHz microwave spectrum range)<sup>9</sup> or 250-300 W (as in the 6-18 GHz microwave spectrum range)<sup>9,10</sup>. Then, the signal is broadcasted, by a microwave horn antenna, into the Fabry-Perot cavity. After removing the microwave radiation, the FID emission is collected by a second horn antenna whose molecular signal is amplified by a low-noise amplifier and then digitized using an up to 100 Gs/s oscilloscope. A high-power pin diode and a single pole switch before the low noise amplifier is inserted to protect the detection system from the high power TWTA. A 10 MHz Rubidium crystal oscillator is used to phase-lock all the frequency signals. The 6-18 GHz range CP-FTMW is achievable by using frequency multipliers circuit receiving the 2-8 GHz AWG pulse<sup>9</sup>. Different microwave elements such as the amplifiers have to be changed to cover the wanted different frequency range.

In this type of spectrometer, the nozzles are perpendicular with respect to the microwave radiation direction. Higher sensitivity and less time and sample consuming are achievable by using a multi-nozzle setting and by recording a multi-FIDs (typically 10) for each molecular pulse. Compared with the 2-8 GHz CP-FTMW spectrometer design of figure 5, the Bilbao CP-FTMW<sup>10</sup> uses a microwave circuit to extend the smaller bandwidth generated by their AWG pulse 6 – 18 GHz following the original architecture by Pate<sup>5</sup>.

## 2.3 Computational Methods

The knowledge of the calculated rotational parameters, such as rotational and quadrupole coupling constants as well as the relative energies among different conformers, is of great importance to reduce the time consuming in collecting the rotational spectra and making it easier the assignments. On the other hand, experimental results constitute the benchmarks to validate the predicted values coming from different methods of calculations and basis sets.

In this respect, *ab initio* (MP2<sup>11</sup>) and density functional theory (B3LYP<sup>12</sup>, M06-2X<sup>13</sup>) methods have been running at, in the most of cases, 6-311++G(d,p) level, but even up to the correlation consistent basis set aug-cc-pVDZ one, using Gaussian03 and Gaussian09 packages<sup>14,15</sup>.

In several studies, a previous screening of possible isomers have been performed using molecular mechanics allowing to optimized, with the aforementioned methods, a smaller number of molecular structures whose relative energies are calculated be in a window range to below 20 kJ·mol<sup>-1</sup>.

Furthermore, frequency calculations of the optimized structure geometries have been run, within the harmonic approximation, in order to confirm their minimum potential energy point nature.

As to the case of molecular adducts, the basis set superposition error (BSSE)<sup>16</sup> corrections have been also taken into the account to evaluate the dissociation energies of different isomers.

In order to fit the transition frequencies different programs have been used:

- XIAM<sup>17</sup>
- SPFIT<sup>18</sup>.

For the former program, the Halmitonian, on which the program is based on, has been already described in Chapter 1 , where has been introduced the theory of the internal rotation.

The SPFIT program includes the operators relative to the rotational Hamiltonian, the centrifugal distorsion one in Watson *A* or *S* reduction using either *I*<sup>r</sup> (prolate basis) or *III*<sup>l</sup> (oblate basis) representation as well as the operators for quadrupolar (several nuclei, with also different interaction strength), the vibration-rotation, spin-rotation and spin-spin interaction<sup>18</sup>.

## 2.4 References

1. Jost, R. The Cooling of Internal Degrees of Freedom of Polyatomic Molecules in Supersonic Free Jets. In *Low Temperature Molecular Spectroscopy*, Edited by R. Fausto, NATO ASI Series, Series C: Mathematical and Physical Sciences, Kluwer Academic Publishers, Vol. 483 (1996).
2. Grabow, J.-U.; Caminati, W. Microwave Spectroscopy: Experimental Techniques. In *Frontiers of Molecular Spectroscopy*. Edited by Jaan Laane, Elsevier, Amsterdam (2009).
3. Miller, D. R. Free Jet Sources. In *Atomic and Molecular Beam Methods*, Edited by G. Scoles, Oxford University Press, Vol. 1, New York (1988).
4. Flygare, W. H.; Schmalz, T. G. Transient Experiments and Relaxation Processes Involving Rotational States. *Acc. Chem. Res.* **9**, 385 (1976).
5. Brown, G. G.; Dian, B. C.; Douglass, K. O., Geyer, S. M.; Shipman, S. T.; Pate, B. H. A Broadband Fourier Transform Microwave Spectrometer Based on Chirped Pulse Excitation. *Rev. Sci. Instrum.* **79**, 053103 (2008).
6. Evangelisti, L.; Perez, C.; Seifert, N. A.; Pate, B. H.; Deghany, M.; Moazzen-Ahmadi, N.; McKellar, A. R. W. Theory vs. Experiment for Molecular Clusters: Spectra of OCS trimers and tetramers. *J. Chem. Phys.* **142**, 104309 (2015).
7. Cocinero, E. J.; Lesarri, A.; Écija, P.; Grabow, J.-U.; Fernández, J. A.; F. Castaño. Conformational Equilibria in Vanillin and Ethylvanillin. *Phys. Chem. Chem. Phys.* **12**, 12486 (2010).
8. Alonso, J. L.; Cocinero, E. J.; Lesarri, A.; Sanz, M. E.; López, J. C. The Glycine–Water Complex. *Angew. Chem. Int. Ed.* **45**, 3471 (2006).
9. Pérez, C.; Lobsiger, S.; Seifert, N. A.; Zaleski, D. P.; Temelso, B.; Shields, G. C.; Kisiel, Z.; Pate, B. H. Broadband Fourier transform rotational spectroscopy for structure determination: The water heptamer. *Chem. Phys. Lett.* **571**, 1 (2013).
10. Uriarte, I.; Écija, P.; Spada, L.; Zabalza, E.; Lesarri, A.; Basterretxea, F. J.; Fernández, J. A.; Caminati, W.; Cocinero, E. J. Potential energy surface of fluoroxene: experiment and theory. *Phys. Chem. Chem. Phys.* **18**, 3966 (2016).
11. Møller, C.; Plesset, M. S. Note on an Approximation Treatment for Many-Electron Systems. *Phys. Rev.* **46**, 618 (1934).
12. Gill, P. M.W.; Johnson, B. G.; Pople, J. A.; Frisch, M. J. The performance of the Becke-Lee-Yang-Parr (B-LYP) density functional theory with various basis sets. *Chem. Phys. Lett.* **197**, 499 (1992).

13. Zhao, Y.; Truhlar, D. G. The M06 suite of density functionals for main group thermochemistry, thermochemical kinetics, noncovalent interactions, excited states, and transition elements: two new functionals and systematic testing of four M06-class functionals and 12 other functional. *Theor. Chem. Acc.* **120**, 215 (2008).
14. M. J. Frisch, G. W. Trucks, H. B. Schlegel, G. E. Scuseria, M. A. Robb, J. R. Cheeseman, J. A. Montgomery, Jr., T. Vreven, K. N. Kudin, J. C. Burant, J. M. Millam, S. S. Iyengar, J. Tomasi, V. Barone, B. Mennucci, M. Cossi, G. Scalmani, N. Rega, G. A. Petersson, H. Nakatsuji, M. Hada, M. Ehara, K. Toyota, R. Fukuda, J. Hasegawa, M. Ishida, T. Nakajima, Y. Honda, O. Kitao, H. Nakai, M. Klene, X. Li, J. E. Knox, H. P. Hratchian, J. B. Cross, C. Adamo, J. Jaramillo, R. Gomperts, R. E. Stratmann, O. Yazyev, A. J. Austin, R. Cammi, C. Pomelli, J. W. Ochterski, P. Y. Ayala, K. Morokuma, G. A. Voth, P. Salvador, J. J. Dannenberg, V. G. Zakrzewski, S. Dapprich, A. D. Daniels, M. C. Strain, Ö. Farkas, D. K. Malick, A. D. Rabuck, K. Raghavachari, J. B. Foresman, J. V. Ortiz, Q. Cui, A. G. Baboul, S. Clifford, J. Cioslowski, B. B. Stefanov, G. Liu, A. Liashenko, P. Piskorz, I. Komaromi, R. L. Martin, D. J. Fox, T. Keith, M. A. Al-Laham, C. Y. Peng, A. Nanayakkara, M. Challacombe, P. M. W. Gill, B. Johnson, W. Chen, M. W. Wong, C. Gonzalez and J. A. Pople, *Gaussian 03*, Revision B.01, Gaussian, Inc., Pittsburgh PA, 2003.
15. M. J. Frisch, G. W. Trucks, H. B. Schlegel, G. E. Scuseria, M. A. Robb, J. R. Cheeseman, G. Scalmani, V. Barone, B. Mennucci, G. A. Petersson, H. Nakatsuji, M. Caricato, X. Li, H. P. Hratchian, A. F. Izmaylov, J. Bloino, G. Zheng, J. L. Sonnenberg, M. Hada, M. Ehara, K. Toyota, R. Fukuda, J. Hasegawa, M. Ishida, T. Nakajima, Y. Honda, O. Kitao, H. Nakai, T. Vreven, J. A. Montgomery, Jr., J. E. Peralta, F. Ogliaro, M. Bearpark, J. J. Heyd, E. Brothers, K. N. Kudin, V. N. Staroverov, R. Kobayashi, J. Normand, K. Raghavachari, A. Rendell, J. C. Burant, S. S. Iyengar, J. Tomasi, M. Cossi, N. Rega, J. M. Millam, M. Klene, J. E. Knox, J. B. Cross, V. Bakken, C. Adamo, J. Jaramillo, R. Gomperts, R. E. Stratmann, O. Yazyev, A. J. Austin, R. Cammi, C. Pomelli, J. W. Ochterski, R. L. Martin, K. Morokuma, V. G. Zakrzewski, G. A. Voth, P. Salvador, J. J. Dannenberg, S. Dapprich, A. D. Daniels, Ö. Farkas, J. B. Foresman, J. V. Ortiz, J. Cioslowski and D. J. Fox, *Gaussian 09*, Gaussian, Inc., Wallingford CT, 2009.
16. Boys, S. F.; Bernardi, F. The calculation of small molecular interactions by the differences of separate total energies. Some procedures with reduced errors. *Mol. Phys.* **19**, 553 (1970).
17. Hartwig, H.; Dreizler, H. The Microwave Spectrum of trans-2,3-Dimethyloxirane in Torsional Excited States. *Z. Naturforsch., A: Phys. Sci.* **51a**, 923 (1996).

18. Pickett, M. H. The fitting and prediction of vibration-rotation spectra with spin interactions.  
*J. Mol. Spectrosc.* **148**, 371 (1991).

# CHAPTER 3

## Molecular Adducts and Isolated Molecules: Results

### 3.1 HYDROGEN BONDING

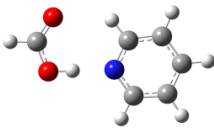
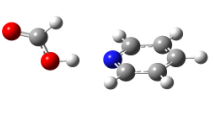
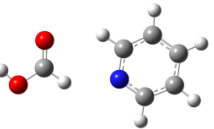
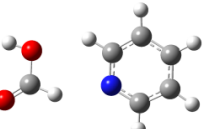
#### 3.1.1 Pyridine – Formic Acid

##### Introduction

Pyridine (hereafter PYR) and Formic acid (HCOOH) are the prototype molecules to study which is the preferred form (ionic form or non-bonding adduct) between organic acids and bases in the gas phase, following the previous characterisations for PYR-HF<sup>1</sup>, PYR-HCl<sup>2</sup>, PYR-HBr<sup>3</sup> by means of rotational spectroscopy. Among the possible intermolecular interactions, the O-H...N hydrogen bond (HB) draws the attention for the plausible proton transfer occurring as well as for the observation either the “normal”<sup>4</sup> or reverse<sup>5</sup> Ubbelohde effect upon deuteration. In this respect, the presence of the <sup>14</sup>N atom, with the relative quadrupole coupling, plays a benchmark role.

##### Theoretical calculations

The molecular structures of the four most stable isomers have been optimized by running MP2/6-311++G(d,p) calculations. Their respectively rotational parameters have been determined together with their energies at the equilibrium and at the zero point, allowing the determination of the isomer dissociation energies by including also the BSSE corrections. All the data are reported in Table 1.

	I	II	III	IV
				
$A / \text{MHz}$	4013	4804	4341	4280
$B / \text{MHz}$	805	613	613	614
$C / \text{MHz}$	671	569	537	540
$\chi_{aa} / \text{MHz}$	-3.73	-4.10	-3.82	-3.96
$\chi_{bb}-\chi_{cc} / \text{MHz}$	-2.12	-1.21	-2.83	-2.66
$\chi_{ab} / \text{MHz}$	-1.75	0.00	2.28	2.15
$\chi_{ac} / \text{MHz}$	0.00	1.37	0.08	-0.01
$\chi_{bc} / \text{MHz}$	0.00	0.00	-0.04	0.17
$\mu_a / \text{D}$	-4.16	8.45	-1.96	-3.54
$\mu_b / \text{D}$	0.51	0.00	-0.18	1.82
$\mu_c / \text{D}$	0.00	-1.23	0.04	-0.22
$\Delta E / \text{kJ}\cdot\text{mol}^{-1}$	0.0 <sup>a</sup>	20.4	34.9	36.3
$\Delta E_0 / \text{kJ}\cdot\text{mol}^{-1}$	0.0 <sup>b</sup>	21.4	33.5	36.3
$E_D^c / \text{kJ}\cdot\text{mol}^{-1}$	41.7	20.7	12.8	9.9

<sup>a</sup>Absolute Energy = -436.992464  $E_h$ ; <sup>b</sup>Absolute Energy zero point corrected = -436.869851  $E_h$ ;

<sup>c</sup>Dissociation energy.

**Table 1.** The four most stable isomer structures of HCOOH-PYR. (Reprinted with permission from Lorenzo Spada, Qian Gou, Barbara M. Giuliano, Walther Caminati. Interactions between Carboxylic Acids and Heteroaromatics: A Rotational Study of Formic Acid–Pyridine. *J. Chem. Phys. A*, Article ASAP, Publication Date (Web): February 17, 2016. DOI: 10.1021/acs.jpca.6b00387 Copyright (2016) American Chemical Society).

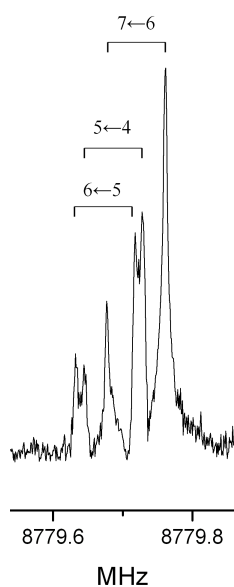
According to the *ab initio* data, isomer I, characterized by a O-H...N hydrogen bond and by a weak C-H...O hydrogen bond (WHB), is by far the most stable one. Its so much larger bonding energy than those of other isomers, is due mainly to a  $n_N \rightarrow \sigma^*_{\text{O-H}}$  electronic transfer<sup>6</sup> as for isomer II in which, however, the C-H...O interaction is replaced by a C-H... $\pi$  one, making the former one the only plausible candidate to be detected in the rotational spectrum upon supersonic expansion conditions.

## Experimental Section

The rotational spectra of the four isotopologues HCOOH-PYR, DCOOH-PYR, HCOOD-PYR, HCOOH-(<sup>15</sup>N)PYR have been recorded after the supersonic expansion, in the Bologna PJFTMW, of the molecule constituents, kept at 273 °K (commercially available, apart from HCOOD species

that was prepared by mixing HCOOH with D<sub>2</sub>O) and carried by Helium at stagnation pressure of 6 bars.

According to the theoretical calculations, the stronger  $\mu_a$  type lines have been first searched for the most abundant species. Around 8779.7 MHz (see Figure 1), a typical pattern due to the splitting caused by the presence of the <sup>14</sup>N quadrupole nucleus ( $I=1$ ) was detected and assigned to the  $6_{06} \leftarrow 5_{05}$  rotational transition.



**Figure 1.** The  $6_{06} \leftarrow 5_{05}$ ,  $\Delta F = +1$  rotational transition for the HCOOH-PYR species showing, also, the doubling due to the Doppler effect. (Reprinted with permission from Lorenzo Spada, Qian Gou, Barbara M. Giuliano, Walther Caminati. Interactions between Carboxylic Acids and Heteroaromatics: A Rotational Study of Formic Acid–Pyridine. *J. Chem. Phys. A*, Article ASAP, Publication Date (Web): February 17, 2016. DOI: 10.1021/acs.jpca.6b00387 Copyright (2016) American Chemical Society).

Later on, other  $\mu_a$ -type  $R$ -branch  $\Delta F = +1$  and some  $\Delta F = 0$  ones have been measured together with several weaker  $R$ -branch  $\Delta F = +1$   $\mu_b$ -type lines. All of them have been fitted by using the Pickett's SPFIT program, within the  $\bar{I}$ -representation of the Watson's  $S$  reduction. The comparison between the fitted rotational and quadrupole coupling constant values with those ones from the *ab initio* calculations suggests that the lines belonging to the isomer I. Then, following this first isotopologue assignment and after empirical corrections, the fitted rotational parameters (see Table 2) of the other three isotopologues have been determined from their respectively rotational spectra.



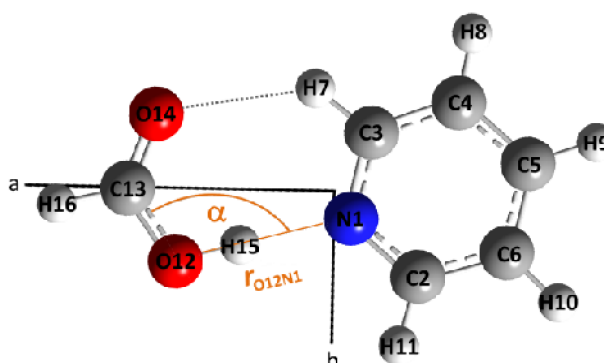
	HCOOH-PYR	DCOOH-PYR	HCOOD-PYR	HCOOH-( <sup>15</sup> N)PYR
<i>A</i> /MHz	4032.0599(7) <sup>a</sup>	4029.373(3)	4007.921(3)	4026.130(1)
<i>B</i> /MHz	811.1656(3)	789.0254(2)	806.9132(3)	811.1282(2)
<i>C</i> /MHz	675.8181(2)	660.3307(1)	672.1974(1)	675.6278(1)
$\chi_{aa}$ /MHz	-3.574(8)	-3.7(1)	-3.5(1)	-
$\chi_{bb}-\chi_{cc}$ /MHz	-2.11(1)	-2.13(4)	-2.09(4)	-
$\chi_{ab}$ /MHz	-2.6(8)	-1.74 <sup>b</sup>	-1.74 <sup>b</sup>	-
<i>D<sub>J</sub></i> /kHz	0.096(1)	[0.096] <sup>c</sup>	[0.096]	[0.096]
<i>D<sub>JK</sub></i> /kHz	0.30(2)	[0.30]	[0.30]	[0.30]
<i>d<sub>1</sub></i> /kHz	-0.018(1)	[-0.018]	[-0.018]	[-0.018]
<i>d<sub>2</sub></i> /kHz	-0.0023(8)	[-0.0023]	[-0.0023]	[-0.0023]
$\Delta_c^d$ /uÅ <sup>2</sup>	-0.565	-0.592	-0.575	-0.568
$\sigma^e$ /kHz	3.4	3.1	3.4	1.3
<i>N<sup>f</sup></i>	99	43	39	22

<sup>a</sup>Error in parentheses in units of the last digit. <sup>b</sup>Ab initio data. <sup>c</sup>Data in brackets fixed to the corresponding values of the parent species. <sup>d</sup>Inertial defect ( $\Delta_c = I_c - I_b - I_a$ ). <sup>e</sup>RMS error of the fit. <sup>f</sup>Number of fitted lines.

**Table 2.** Experimental rotational parameters of the isomer I of the HCOOH-PYR complex. (Reprinted with permission from Lorenzo Spada, Qian Gou, Barbara M. Giuliano, Walther Caminati. Interactions between Carboxylic Acids and Heteroaromatics: A Rotational Study of Formic Acid–Pyridine. *J. Chem. Phys. A*, Article ASAP, Publication Date (Web): February 17, 2016. DOI: 10.1021/acs.jpca.6b00387 Copyright (2016) American Chemical Society).

## Structural Information

A partial  $r_0$  structure has been obtained by fitting the N1-O12 distance ( $r_{O12N1}$ ) and the N1-O12-C13 valence angle ( $\alpha$ ) as highlighted in Figure 2.



**Figure 2.** Sketch of the observed conformer of HCOOH-PYR, atom numbering, main structural parameters and principal axes system.

Fitting these parameters (whose results are reported in Table 3), keeping fixed at their *ab initio* values the other ones, the experimental rotational constants relative to HCOOH-PYR, DCOOH-PYR and HCOOH-(<sup>15</sup>N)PYR species have been reproduced within 0.4 MHz while, on the other hand, those ones of HCOOD-PYR isotopologue are about 10 times larger.

	$r_0$	$r_e$
N1-O12/Å	2.662(1) <sup>a</sup>	2.733
$\alpha/^\circ$	111.4(1)	109.0
Hydrogen and weak hydrogen bond derived parameters		
N1-H15	1.661	1.730
N1-H15-O12	175.3	179.1
O14-H7	2.460	2.438
C3-H7-O14	132.0	131.8

<sup>a</sup>Error in parentheses in units of the last digit.

**Table 3.** Obtained and derived geometrical parameters relative to the hydrogen and weak hydrogen bonds, from the partial  $r_0$  adjustment geometry compared with the corresponding  $r_e$  values. (Reprinted with permission from Lorenzo Spada, Qian Gou, Barbara M. Giuliano, Walther Caminati. Interactions between Carboxylic Acids and Heteroaromatics: A Rotational Study of Formic Acid–Pyridine. *J. Chem. Phys. A*, Article ASAP, Publication Date (Web): February 17, 2016. DOI: 10.1021/acs.jpca.6b00387 Copyright (2016) American Chemical Society).

This behavior is generally attributable to the so-called reverse Ubbelohde effect which consists in a shortening of the two heavy atoms distance involved in the hydrogen bond upon deuteration as in the case of single O-H...O or O-H...N hydrogen bonds.

However, in this case, to reproduce the experimental HCOOD-PYR rotational constants, an increase of the N1-O12 distance of about 7 mÅ has to be taken into the account, following the behavior observed for a double minima potential proton transfer, typical of carboxylic acids, upon deuteration (Ubbelohde effect).

Focus the attention on the O-H...N interaction, a plausibly proton transfer occurs together with the Ubbelohde effect (upon deuteration), according to the strength of this hydrogen bond<sup>7</sup> ( $E_D = 41.7$  kJ·mol<sup>-1</sup> (*ab initio*) or 39.8 kJ·mol<sup>-1</sup> (from experiment, see below)). The shift of the proton from the oxygen to the nitrogen was already suggested by a NMR experiment<sup>8</sup> for the HCOOH-PYR. However, in the present study, the decreasing of the field gradient at the nitrogen nucleus, along the parallel oriented *c*-axes, in going from isolated pyridine ( $\chi_{cc} = 3.474(3)$  MHz) to the HCOOH-PYR ( $\chi_{cc} = 2.84(1)$  MHz), can be explain invoking the same shift behavior.

The substitution coordinates ( $r_s$ ) of the N1, H15 and H16 atom, numbering in Figure 2, are calculable as described in Chapter 1 for the determination of the molecular structure. Their values are compared in table 4 with those deriving from the  $r_0$  and  $r_e$  structures.

		$r_s$	$r_e$	$r_0$
N1	$ a /\text{Å}$	0.170(9) <sup>b</sup>	0.254	0.253
	$ b /\text{Å}$	0.432(3)	0.425	0.424
H15	$ a /\text{Å}$	1.812(1)	1.416	1.367
	$ b /\text{Å}$	0.872(2)	-0.856	-0.807
H16	$ a /\text{Å}$	4.184(1)	4.163	4.165
	$ b /\text{Å}$	0.294(5)	-0.357	-0.345

<sup>a</sup>Coordinate  $c$  set to zero by symmetry. <sup>b</sup>Error in parenthesis are in units of the last digits.

**Table 4.** The  $r_s$ ,  $r_0$  and  $r_e$  coordinates relative to substituted atoms in the principal axes system of the parent species. (Reprinted with permission from Lorenzo Spada, Qian Gou, Barbara M. Giuliano, Walther Caminati. Interactions between Carboxylic Acids and Heteroaromatics: A Rotational Study of Formic Acid–Pyridine. *J. Chem. Phys. A*, Article ASAP, Publication Date (Web): February 17, 2016. DOI: 10.1021/acs.jpca.6b00387 Copyright (2016) American Chemical Society).

In the case of H15 atom, a large discrepancy is determined for the  $a$ -coordinates from  $r_s$ ,  $r_0$  and  $r_e$  as usual for atoms involved in hydrogen bond upon deuteration.

## Dissociation Energy

According to the equation 1.61 and 1.62 in Chapter 1, the force constant  $k_s = 26.2 \text{ N m}^{-1}$  and the dissociation energy of  $39.8 \text{ kJ mol}^{-1}$  have been estimated for the HCOOH-PYR complex ( $R_{CM} = 4.26 \text{ Å}$ ). This is in good agreement with the *ab initio* value calculated be  $41.7 \text{ kJ mol}^{-1}$  as reported in Table 1.

### 3.1.2 2-Fluoropyridine – Water

#### Introduction

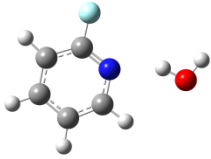
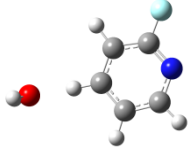
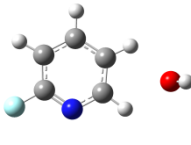
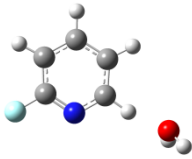
The features of the hydrogen and weak hydrogen bonds which can be established by water with molecules, since its dual role (proton donor and proton acceptor) and its widespread presence, is of great relevance to understand the chemical and biological processes occurring in nature. In this respect, rotational spectroscopic studies of organic molecule adducts with water<sup>9</sup> provide insights on the structural features, favourite interactions, dissociation energies, internal dynamics that water shows with different kind of chemical counterpart molecules. Hence, whilst perhalogenated alkenes

link water through a lone pair- $\pi^*$  interaction (see the paragraph below), halogen bonds take place with perhalogenated alkanes<sup>10</sup> while in the most of organic chemical groups, HBs and WHBs are the favourite interactions<sup>11,12,13</sup>. In aromatic molecules containing a nitrogen atom either a O-H $\cdots$ N HB is the main interaction occurring, for example, together with HBs as in the case of 2-hydroxypyridine-water complex<sup>14</sup> or the N-H $\cdots$ O HB takes place with water acting as proton acceptor<sup>15,16</sup>. In the present study the attention is focused on the role of substituents, such as fluorine, in position 2 of pyridine (2FPYR) with respect to the formation of the monowater adduct and on the observation of which is the favourite secondary weak hydrogen bond interaction stabilizing the complex.

## Theoretical Calculations

49 different structures have been determined by a conformational search performed by Molecular Mechanics (MacroModel 9.2 using the MMFFs force field)<sup>17</sup> within a relative energy window of 21 kJ mol<sup>-1</sup>. The resulting geometries converge to 4 stable isomers as determined by harmonic approximation frequency calculations of their optimized geometries at the MP2/6-311++G(d,p) level. The rotational constants, the dipole moment components, the quadrupole coupling constants (due to the presence of the <sup>14</sup>N nucleus,  $I = 1$ ) as well as the energies relative to the equilibrium and zero points are reported in Table 5, together with the dissociation energy BSSE corrected.

As in the case of PYR-HCOOH, the global minimum is calculated by the isomer showing an O-H $\cdots$ N HB together with a secondary C-H $\cdots$ O WHB. Due to the much lower acidity of H<sub>2</sub>O hydrogens than the responsible of the acidity in the HCOOH, the *ab initio* dissociation energy for isomer I is 25 kJ mol<sup>-1</sup> lower than the one found (with the same calculation method and basis set) for the most stable conformer of pyridine with HCOOH as proton donor.

	I	II	III	IV
				
$A, B, C/\text{MHz}$	2712,1472,954	3483,944,745	4684,950,793	3437,968,758
$\chi_{aa}, \chi_{bb}, \chi_{cc}/\text{MHz}$	-3.56,-1.59	-4.17,-1.37	1.53,-7.13	1.35,-6.99
$ \mu_a ,  \mu_b ,  \mu_c /\text{D}$	3.7,0.6,0.0	6.0,0.4,0.0	4.6,2.3,0.0	2.7,2.0,0.0
$\Delta E/\text{kJ}\cdot\text{mol}^{-1}$	0.0 <sup>[a]</sup>	13.9	14.1	15.4
$\Delta E_0/\text{kJ}\cdot\text{mol}^{-1}$	0.0 <sup>[b]</sup>	11.2	11.8	13.2
$E_D^c/\text{kJ}\cdot\text{mol}^{-1}$	15.7	4.7	4.2	2.6

<sup>a</sup>Absolute energies =  $-422.981029 E_h$ . <sup>b</sup>Absolute energies zero point corrected =  $-422.876685 E_h$ .

<sup>c</sup>Dissociation energy.

**Table 5.** Rotational parameters and energies of the four most stable isomer of 2FPYR-H<sub>2</sub>O calculated at the MP2/6-311++G(d,p) level. (Gou, Q.; Spada, L.; Vallejo-López, M.; Melandri, S.; Cocinero, E. J.; Lesarri, A.; Caminati, W. Intermolecular hydrogen bonding in 2-Fluoropyridine-Water. *Submitted*.)

## Experimental Section

The 2FPYR-H<sub>2</sub>O, 2FPYR-H<sub>2</sub><sup>18</sup>O, 2FPYR-DOH, 2FPYR-HOD and 2FPYR-D<sub>2</sub>O isotopologues have been generated by passing over a sample of 2FPYR (at 273 K using ice) and then H<sub>2</sub>O, H<sub>2</sub><sup>18</sup>O (98% enriched H<sub>2</sub><sup>18</sup>O), 1:1 mixture of H<sub>2</sub>O/D<sub>2</sub>O and D<sub>2</sub>O (99% enriched D<sub>2</sub>O) samples, respectively, helium at stagnation pressure of 3 bars. Then, the gas phase mixture has been supersonically expanded into the Bologna PJ-FTMW spectrometer. The rotational spectrum of the most abundant isopologue was collected starting from the *ab initio* predicted strongest  $\mu_a$ -type *R*-band lines  $4_{04} \leftarrow 3_{03}$  transition which is split because of the quadrupole coupling (<sup>14</sup>N has  $I = 1$ ).

After this first assignment, further  $\mu_a$ -type lines up to  $J = 8$  and  $K_a = 4$  have been fitted together with some much weaker  $\mu_b$ -type transition using the Pickett's SPFIT program, within *S*-reduction of Watson's semirigid rotational Hamiltonian in the  $\tilde{I}$  representation. No  $\mu_c$  type frequency transitions have been observed in agreement with the experimental inertial defect values reported in Table 6, suggesting the planar symmetry of the complex. Later on, the rotational spectra of the other

mentioned isotopologues have been measured. No splittings due to the deuterium ( $I = 1$ ) have been observed.

In the case of the deuterated isotopologues the centrifugal distortion constants have been fixed to the values of the parent species since it was possible to measure only the  $\mu_a$  type transitions due to the weakness of their rotational spectra. No lines belonging to the other isomers have been observed, suggesting the taking place of a possible relaxation process.

The rotational, the quadrupole coupling as well as the centrifugal distortion constants resulting from the fittings of the rotational transitions are reported in Table 6.

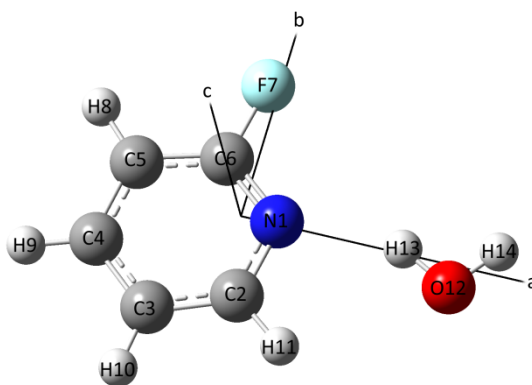
	2FPYR-H <sub>2</sub> O	2FPYR-H <sub>2</sub> <sup>18</sup> O	2FPYR-DOH	2FPYR-HOD	2FPYR-D <sub>2</sub> O
A/MHz	2738.178(1) <sup>a</sup>	2734.370(3)	2739.991(7)	2733.389(8)	2735.235(9)
B/MHz	1462.5220(4)	1369.5790(4)	1436.4306(5)	1397.4350(5)	1374.2071(5)
C/MHz	953.0579(2)	912.2303(2)	942.1317(2)	924.6688(2)	914.6656(3)
$\chi_{aa}$ /MHz	-3.568(6)	-3.51(6)	-3.65(6)	-3.55(7)	-3.77(6)
$\chi_{bb}-\chi_{cc}$ /MHz	-1.57(1)	-1.63(4)	-1.60(5)	-1.61(6)	-1.58(5)
$D_J$ /kHz	0.034(3)	0.039(2)	[0.034] <sup>b</sup>	[0.034]	[0.034]
$D_{JK}$ /kHz	11.24(2)	11.95(6)	[11.24]	[11.24]	[11.24]
$D_K$ /kHz	9.6(1)	[9.6]	[9.6]	[9.6]	[9.6]
$d_1$ /kHz	-0.178(2)	[0.178]	[-0.178]	[-0.178]	[-0.178]
$d_2$ /kHz	-0.223(2)	[-0.223]	[-0.223]	[-0.223]	[-0.223]
$\Delta_c/u\text{\AA}^2$	0.15 <sup>c</sup>	0.18	0.15	0.01	0.02
$N^d$	105	61	29	27	27
$\sigma^e$ /kHz	3.2	3.6	3.0	2.7	4.6

<sup>a</sup>Error in parentheses in units of the last digit. <sup>b</sup>Data in brackets are fixed at the corresponding values of the parent species. <sup>c</sup>Inertial defect <sup>d</sup>Number of lines in the fit. <sup>e</sup>Root-mean-square deviation of the fit.

**Table 6.** Rotational fitted parameters of the five isotopologues of the observed isomer of 2FPYR-H<sub>2</sub>O. (Gou, Q.; Spada, L.; Vallejo-López, M.; Melandri, S.; Cocinero, E. J.; Lesarri, A.; Caminati, W. Intermolecular hydrogen bonding in 2-Fluoropyridine-Water. *Submitted.*)

## Structural Information

Three structural parameters were fitted to obtain a partial  $r_0$  structure ( $R_{N1O12}$ ,  $\angle O12-N1-C2$  and  $\angle H13O8\cdots N1$  as in Figure 3) by reproducing the rotational constants from experiment, while the other geometrical parameters have been fixed to their *ab initio* values.



**Figure 3.** The observed isomer of 2FPYR-H<sub>2</sub>O in the principal axes of inertia with atom numbering. The H11-O12 and H13-N1 distances are determined to be 1.99 Å and 2.88 Å according to the  $r_0$  structure.

The results are reported in Table 7 where they are compared with their *ab initio* values.

	$R_{\text{N1O12}}/\text{Å}$	$\angle\text{O12-N1-C2}/^\circ$	$\angle\text{H14-O12-N1}/^\circ$
$r_0$	2.910(5) <sup>a</sup>	96.7(1)	116(4)
$r_e$	2.906	93.1	120.0

<sup>a</sup>Uncertainties in parentheses are expressed in units of the last digit.

**Table 7.** The geometrical parameters fitted and derived from the  $r_0$  and  $r_e$  structures of 2FPYR-water. (Gou, Q.; Spada, L.; Vallejo-López, M.; Melandri, S.; Cocinero, E. J.; Lesarri, A.; Caminati, W. Intermolecular hydrogen bonding in 2-Fluoropyridine-Water. *Submitted.*)

A further confirmation of the corrected rotational assignment of isomer I, apart from the comparison between the *ab initio* and the experimental rotational and quadrupole coupling constants, comes from the substitution coordinates ( $r_s$ ), in the principal axes of the parent species, of the atom constituting the water molecule since the availability of 2FPYR-H<sub>2</sub><sup>18</sup>O, 2FPYR-DOH and 2FPYR-HOD rotational constants. The obtained data are reported in table 8 comparing the  $r_0$  and  $r_e$  coordinates.

	<i>a</i>			<i>b</i>		
	$r_s$	$r_0$	$r_e$	$r_s$	$r_0$	$r_e$
O12	$\pm 3.449(1)^a$	3.442	3.443	$\pm 0.387(4)$	0.448	0.366
H13	$\pm 2.508(1)$	2.552	2.581	$[0]^b$	-0.067	-0.076
H14	$\pm 3.996(1)$	3.985	4.040	$\pm 0.597(2)$	-0.343	-0.385

<sup>a</sup>Error in parentheses in units of the last digit; <sup>b</sup>Fixed to zero since it results be an imaginary value.

**Table 8.** Comparison between  $r_s$ ,  $r_0$  and  $r_e$  coordinates of the constituting water atoms in 2FPYR-H<sub>2</sub>O according to the numbering of Figure 3. (Gou, Q.; Spada, L.; Vallejo-López, M.; Melandri, S.; Cocinero, E. J.; Lesarri, A.; Caminati, W. Intermolecular hydrogen bonding in 2-Fluoropyridine-Water. *Submitted.*)

### 3.1.3 3-Fluoropyridine – Water

#### Introduction

Fluorine, due to its electron withdrawing nature, gives rise to the inductive effect which can has a role in the changing of the geometry of fluoro substituted pyridine with respect to pyridine itself. However, as reported by two previous studies<sup>18,19</sup>, in the 2FPY, the N-C(F) bond length is appreciable shortened due to the interaction with the  $\pi$  bonding within the ring while, in this respect, in the case of 3-Fluoropyridine (3FPYR) nitrogen atom is too far away from fluorine to provide any contribution.

Following the results of the 2FPYR - water, the 3FPYR – water adduct provides the possibility to directly compare the effects of fluorine substitution in different positions in pyridine involved in microsolvation processes.

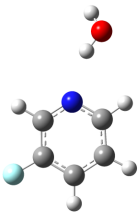
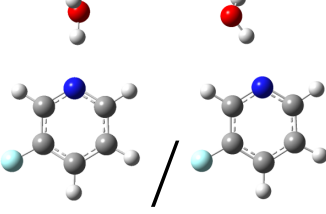
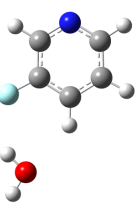
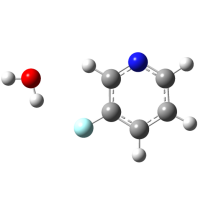
#### Theoretical Calculations

Four *ab initio* optimized geometries have been calculated by using the Gaussian 09 program package at the MP2/6-311++G(d,p) level. All the isomers are real minima as define by positive values of the calculated frequencies. The rotational constants as well as the quadrupole coupling constants, the planar moment of inertia and the energies, including also the zero point corrections, are reported in Table 9. Furthermore, parameters changing due to the basis set superposition error (BSSE) are listed together with, for 3FPYR\_W2 isomer, the different orientation of water.

As expected from the aforementioned studies, the O-H $\cdots$ N HB is the the most favourite interaction. Due to the asymmetry of the 3FPYR, two different C-H $\cdots$ O WHB between that monomer and water are possible: one with the C-H in position 2 and the other in position 5. This latter, as reported in table 9, in synergy with the strongest O-H $\cdots$ N contact, results be the most stable isomer. Two



higher energy stable isomers than the two described ones have been calculated, showing the O-H...F and a C-H...O WHBs linking the two subunits.

	3FPYR_W1	3FPYR_W2	3FPYR_W3	3FPYR_W4
				
$A/\text{MHz}$	4159/4096	3390/2900	3989/4017	3892/3936
$B/\text{MHz}$	1067/1046	1129/1254	1200/1168	1213/1174
$C/\text{MHz}$	852/835	852/877	923/905	925/904
$\mu_a/D$	-2.36/-2.24	3.25/-2.60	2.03/1.98	-0.34/-0.42
$\mu_b/D$	0.98/1.02	2.31/3.46	0.74/0.68	2.81/3.02
$\mu_c/D$	1.15/1.14	1.59/1.25	0.84/0.00	0.88/0.03
$\chi_{aa}/\text{MHz}$	-2.96/-3.74	-4.07/-5.49	-3.39/-4.03	1.54/1.62
$\chi_{bb}/\text{MHz}$	-0.11/-0.10	1.04/1.65	0.05/-0.09	-4.94/-5.81
$\chi_{cc}/\text{MHz}$	3.08/3.84	3.04/3.84	3.34/4.13	3.4/4.20
$P_{aa}/\text{u}\text{\AA}^2$	472.7/482.6	445.7/402.4	421.0/432.6	416.5/430.5
$P_{bb}/\text{u}\text{\AA}^2$	120.5/122.9	147.1/173.7	126.5/125.8	129.6/128.4
$P_{cc}/\text{u}\text{\AA}^2$	1.0/0.5	2.0/0.6	0.2/0.0	0.3/0.0
$\Delta E/\text{kJ}\cdot\text{mol}^{-1}$	0 <sup>b</sup> /0 <sup>c</sup>	0.4/0.3	10.9/10.4	14.5/13.8
$\Delta E_0/\text{kJ}\cdot\text{mol}^{-1}$	0 <sup>d</sup> /0 <sup>e</sup>	0.5/0.3	9.0/8.2	12.2/11.0

<sup>a</sup>Species 3FPY-W2 changes from the left to the right shape when including BSSE corrections.

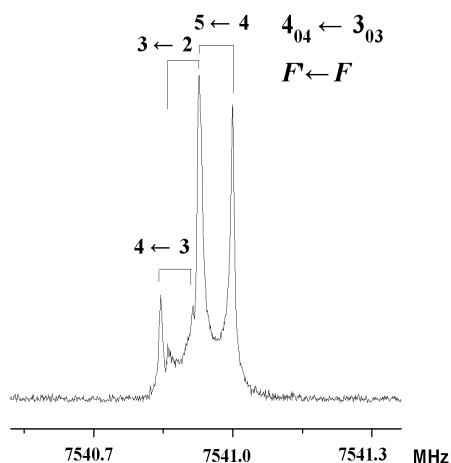
<sup>b,c,d,e</sup>Absolute energies are -422.970834, -422.96868, -422.866522, -422.86633 E<sub>h</sub>, respectively.

**Table 9.** Rotational parameters and energies calculated at the MP2/6-311++G(d,p) level without/with BSSE corrections of the energies. (Reprinted with permission from Camilla Calabrese, Qian Gou, Lorenzo Spada, Assimo Maris, Walther Caminati, Sonia Melandri, Effect of Fluorine Substitution on the Microsolvation of Aromatic Azines: The Microwave Spectrum of 3-Fluoropyridine-Water. *J. Phys. Chem. A*, Article ASAP, DOI: 10.1021/acs.jpca.6b00785, Publication Date (Web): March 09, 2016. Copyright © 2016 American Chemical Society.)

## Experimental Section

The 3FPYR-H<sub>2</sub>O, 3FPYR-H<sub>2</sub><sup>18</sup>O, 3FPYR-DOH, 3FPYR-HOD and 3FPYR-D<sub>2</sub>O isotopologues have been generated by passing over a sample of 3FPYR (at 273 K using ice) and then over H<sub>2</sub>O, H<sub>2</sub><sup>18</sup>O (98% enriched H<sub>2</sub><sup>18</sup>O), 1:1 mixture of H<sub>2</sub>O/D<sub>2</sub>O and D<sub>2</sub>O (99% enriched D<sub>2</sub>O) samples, respectively, helium at stagnation pressure of 5 bars. Then, the gas phase mixture has been supersonically expanded into the Bologna PJ-FTMW spectrometer. Following the results of table 9, the survey started with the search of the  $4_{04} \leftarrow 3_{03} \mu_a$ -type *R*-band of isomer 3FPY\_W1. This

rotational transition was found to be constituted by three components around 7541 MHz (see Figure 4) due to the presence of one  $^{14}\text{N}$  with nuclear spin moment  $I = 1$ . Later on, other several  $\mu_a$ -type and  $\mu_b$ -type transitions have been measured. No  $\mu_c$ -type lines have been observed in agreement with the  $C_s$  symmetry of the complex as deducible also from the close to zero values of the  $P_{cc}$  moments (see table 10) of inertia which define the mass distribution out of the  $ab$  plane.



**Figure 4.** The  $\mu_a$ -type  $4_{04} \leftarrow 3_{03}$  transition of the observed 3FPY-W1 isomer showing the Doppler effect and the quadrupolar splitting  $F' \leftarrow F$ . (Reprinted with permission from Camilla Calabrese, Qian Gou, Lorenzo Spada, Assimo Maris, Walther Caminati, Sonia Melandri, Effect of Fluorine Substitution on the Microsolvation of Aromatic Azines: The Microwave Spectrum of 3-Fluoropyridine-Water. *J. Phys. Chem. A*, Article ASAP, DOI: 10.1021/acs.jpca.6b00785, Publication Date (Web): March 09, 2016. Copyright © 2016 American Chemical Society.)

All the transitions have been fitted using Pickett's SPFIT program within  $S$ -reduction of Watson's semirigid rotational Hamiltonian in the  $I^f$  representation whose resulting rotational parameters are reported in table 10. No splittings due to the deuterium ( $I = 1$ ) have been observed.

	3FPYR–H <sub>2</sub> O	3FPYR–H <sub>2</sub> <sup>18</sup> O	3FPYR –DOH	3FPYR –HOD	3FPYR –DOD
A/MHz	4163.0585(9) <sup>a</sup>	4148.419(2)	4136.381(3)	4123.842(3)	4098.341(3)
B/MHz	1064.3651(1)	1003.1465(2)	1047.8077(4)	1024.6943(4)	1009.6845(4)
C/MHz	847.8457(1)	807.9682(2)	836.2324(5)	821.3607(4)	810.7445(4)
D <sub>J</sub> /kHz	0.1309(9)	0.126(2)	0.122(5)	0.122(4)	0.116(4)
D <sub>JK</sub> /kHz	4.90(1)	[4.90] <sup>b</sup>	[4.90]	[4.90]	[4.90]
D <sub>K</sub> /Hz	21.03(9)	[21.03]	[21.03]	[21.03]	[21.03]
d <sub>1</sub> /Hz	-41.3(8)	[-41.3]	[-41.3]	[-41.3]	[-41.3]
d <sub>2</sub> /Hz	-25.4(6)	[-25.4]	[-25.4]	[-25.4]	[-25.4]
χ <sub>aa</sub> /MHz	-3.085(8)	-3.12(3)	-3.04(7)	-3.15(7)	-3.08(7)
χ <sub>bb</sub> /MHz	-0.119(5)	-0.086(1)	-0.097(3)	-0.106(3)	-0.099(3)
χ <sub>cc</sub> /MHz	3.204(5)	3.204(1)	3.135(3)	3.255(3)	3.182(3)
P <sub>aa</sub> /uÅ <sup>2</sup>	474.75	503.73	482.25	492.97	500.29
P <sub>bb</sub> /uÅ <sup>2</sup>	121.33	121.76	122.11	122.32	123.07
P <sub>cc</sub> /uÅ <sup>2</sup>	0.07	0.06	0.07	0.23	0.25
N <sup>c</sup>	135	66	30	33	33
σ <sup>d</sup> /kHz	2.6	3.4	3.2	3.8	4.4

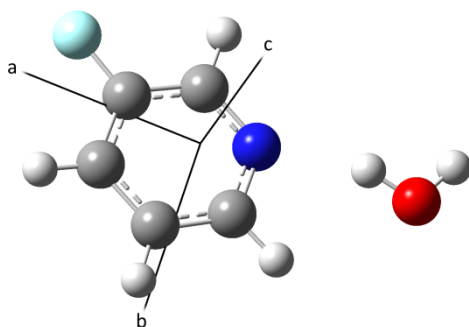
<sup>a</sup> Error in parentheses in units of the last digit. <sup>b</sup> Values in brackets fixed corresponding values of the parent species. <sup>c</sup> Number of lines in the fit. <sup>d</sup> Root-mean-square deviation of the fit.

**Table 10.** Experimental rotational, centrifugal distortion, quadrupole coupling constants and planar momenta of inertia for the of 3FPY\_W1 isomer. (Reprinted with permission from Camilla Calabrese, Qian Gou, Lorenzo Spada, Assimo Maris, Walther Caminati, Sonia Melandri, Effect of Fluorine Substitution on the Microsolvation of Aromatic Azines: The Microwave Spectrum of 3-Fluoropyridine-Water. *J. Phys. Chem. A*, Article ASAP, DOI: 10.1021/acs.jpca.6b00785, Publication Date (Web): March 09, 2016. Copyright © 2016 American Chemical Society).

Relaxation processes of the other isomers towards the 3FPYR\_W1 one can explain the lack of the experimental detection of the rotational transition frequencies for the other isomers.

## Structural Information

A partial  $r_0$  structure have been calculated by fitting the N...O distance and the O-H...N angle, which is involved in the HB (see Figure 5), keeping fixed at the *ab initio* values the other geometrical parameters.



**Figure 5.** Sketch of the observed 3FPY\_W1 with the atom numbering in the principal axes system.

The experimental constants of all the isotopologues have been reproduced, in this way, within a MHz apart from those relative to the 3FPYR-DOH species since their larger discrepancies suggests a plausible Ubbelohde effect<sup>4</sup> taking place upon deuteration. The obtain results are compared with those coming from the 2FPYR- H<sub>2</sub>O complex in table 11 showing that the fluorine substitution in different position of pyridine does not produce significantly differences in the geometry of the interactions with water. Furthermore, in both the complexes, the O-H...N interaction occurs together with a C-H...O one which is established with the hydrogen on the other side with respect to the fluorine substitution one.

		$R_{N...O}/\text{\AA}$	$\angle O-H...N/^\circ$
3FPYR-W	$r_0$	1.9839(6)	156.1(1)
	$r_e$	1.9785	157.5
2FPYR-W	$r_0$	1.988(5)	158(4)
	$r_e$	2.015	152

<sup>a</sup> Error expressed in unit of the last decimal digit.

**Table 11.** Comparison between  $R_{N...O}$  and  $\angle O-H...N$  parameters in the 2FPYR-water and 3FPYR-water complexes from  $r_e$  and  $r_0$  structures.

Furthermore, these values are similar to those ones of other water complexes of heterocyclic aromatic compounds pyrazine<sup>20</sup>, pyrimidine<sup>21</sup> and pyridazine<sup>22</sup> as reported in table 12, suggesting a not so different behavior as hydrogen bond acceptor and donor with respect to water links.

Water partner	$R_{N...O}/\text{\AA}$	$\angle\text{O-H}\cdots\text{N}/^\circ$
3FPYR	1.9839(6)	156.1(1)
2FPYR	1.988(5)	158(4)
Pyridazine	2.04	165.5
Pyrimidine	1.98	164.7
Pyrazine	1.94(2)	152(4)

**Table 12.** Comparison between complexes of water and some heterocyclic aromatic compounds.

Having to our disposal the rotational constants of the 3FPYR–H<sub>2</sub>O, 3FPYR–H<sub>2</sub><sup>18</sup>O, 3FPYR–DOH and 3FPYR–HOD, the substituted coordinates ( $r_s$ ), in the principal axes system of the most abundant isotopologue species, have been derived for the water atoms, using the Kraitchman's equations. The obtained coordinates are compared in Table 13 with those ones from the *ab initio* ( $r_e$ ) and effective structure ( $r_0$ ).

		$r_s$	$r_e$	$r_0$
O13	$a/\text{\AA}$	$\pm 3.8330(4)^a$	3.8116	-3.8264
	$b/\text{\AA}$	$\pm 0.485(3)$	-0.5223	-0.5060
H12	$a/\text{\AA}$	$\pm 2.7395(6)$	2.8664	-2.8761
	$b/\text{\AA}$	$\pm 0.895(2)$	-0.7145	-0.7025
H14	$a/\text{\AA}$	$\pm 4.2857(4)$	4.2379	-4.2386
	$b/\text{\AA}$	$\pm 1.103(1)$	-1.1320	-1.3718

<sup>a</sup>Error expressed in units of the last decimal digit. C-coordinates are zero for symmetry,

**Table 13.** Comparison between the substitution coordinates ( $r_s$ ) and those ones coming from the *ab initio* ( $r_e$ ) and from the effective structure ( $r_0$ ). (Reprinted with permission from Camilla Calabrese, Qian Gou, Lorenzo Spada, Assimo Maris, Walther Caminati, Sonia Melandri, Effect of Fluorine Substitution on the Microsolvation of Aromatic Azines: The Microwave Spectrum of 3-Fluoropyridine-Water. *J. Phys. Chem. A*, Article ASAP, DOI: 10.1021/acs.jpca.6b00785, Publication Date (Web): March 09, 2016. Copyright © 2016 American Chemical Society.)

## Dissociation Energy

An estimation of the dissociation energy of the 3FPYR-water complex have been performed using equation 1.61 and 1.62, resulting be  $30.2 \text{ kJ}\cdot\text{mol}^{-1}$  ( $k_s = 17.4 \text{ N}\cdot\text{m}^{-1}$  and  $R_{\text{CM}} = 4.55 \text{ \AA}$ ) quite similar with *ab initio* calculated one ( $16.44 \text{ kJ mol}^{-1}$ ).

### 3.1.4 Trifluoroanisole – Water

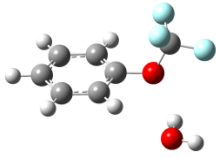
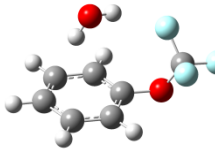
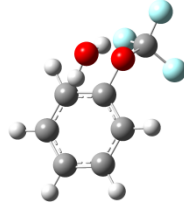
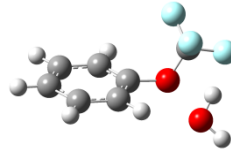
#### Introduction

In the previous reported studies, the microsolvated adducts of different fluorine substituted pyridine has been described, showing that the two complexes are linked with water by an O-H...N HB and a C-H...O WHB with similar geometrical features in both the complexes. In this respect, it is interesting to investigate if the fluorine substitution out of the ring produces any change on the features and on the type of HB and/or WHB involved. It has been shown the H → F substitution of the -OCH<sub>3</sub> group in going from the anisole<sup>23</sup> to the  $\alpha,\alpha,\alpha$ -trifluoroanisole<sup>24</sup> (TFA) gives rise to a change in the orientation of the aforementioned group from a planar to perpendicular shape with respect to the ring, respectively.

Water complex of anisole has been characterized by rotational spectroscopy showing a bifurcated O-H...O HB whose water bideuteration causing an isotopomeric conformational change<sup>25</sup>. Following this study, the investigation of the  $\alpha,\alpha,\alpha$ -trifluoroanisole – water (TFA-W) complex can provide insights to understand how the fluorination substitution affects the microsolvation processes.

#### Theoretical Calculation

Conformational space exploration has been performed by using MacroModel 9.2<sup>17</sup>. About 100 different conformers have been found belonging to an energy range below 13 kJ mol<sup>-1</sup> of which only four are real minima structures as proven by frequency calculations, at the MP2/6-311++G(d,p) level. Rotational constants, dipole moment components along the principal axes of inertia, energies at the equilibrium and at the zero point as well as the dissociation energies, with include the BSSE corrections, are reported in table 14.

	I	II	III	IV
				
A/MHz	1309	1502	1224	1239
B/MHz	662	620	627	673
C/MHz	505	571	531	482
$\mu_a/D$	1.1	-2.1	2.8	0.6
$\mu_b/D$	-0.6	-2.4	-2.9	0.3
$\mu_c/D$	-0.3	-0.6	0.0	0.3
$\Delta E/kJ\cdot mol^{-1}$	0.0 <sup>a</sup>	0.5	2.0	2.7
$\Delta E_0/kJ\cdot mol^{-1}$	0.5	0.0 <sup>b</sup>	0.1	2.3
$E_D^c/kJ\cdot mol^{-1}$	12.2	8.8	8.5	10.1

<sup>a</sup>Absolute energy: -719.396479 E<sub>h</sub>; <sup>b</sup>Absolute energy: -719.3754723 E<sub>h</sub>; <sup>c</sup>Dissociation energy.

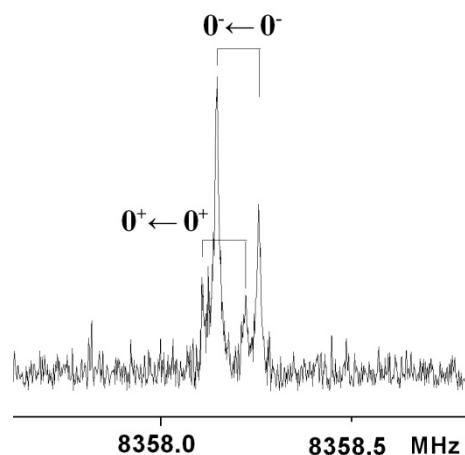
**Table 14.** The *ab initio* rotational parameters and the energies calculated at MP2/6-311++G(d,p) level for the four TFA-water complexes. (Reprinted with permission from Gou, Q.; Spada, L.; Vallejo-López, M.; Kang, L.; Novick, S. E.; Caminati, W., Fluorination Effects on the Shapes of Complexes of Water with Ethers: A Rotational Study of Trifluoroanisole–Water. *J. Phys. Chem. A*, 2014, 118 (6), pp. 1047–1051, Publication Date (Web): January 23, 2014. Copyright © 2016 American Chemical Society.).

Different HBs or WHBs are involved in the stabilization of the various isomers. In the global minimum one a hydrogen O-H···O and a weak hydrogen C-H···O bonds links the TFA with water while both II and III forms show one O-H··· $\pi$  interaction together with either a O-H···F or a O-H···O contact, respectively. In isomer IV, a C-H···O and a O-H···F weak hydrogen bonds are observed.

## Experimental Section

A 1:1 mixture of TFA and water at stagnation pressure of 3 bars was expanded into the cavity of the Bologna PJ-FTMW. According to table 14, the rotational spectrum was collected starting from the  $\mu_a$ -type *R*-branch transitions for the most stable isomer. Two component lines with an intensity ratio 1:3 have been observed around 8374.88 MHz corresponding to the  $8_{08} \leftarrow 7_{07}$  rotational transition within the  $0^+$  and  $0^-$  states, respectively. They originate from the tunnel quantum effect which is caused by the internal rotation of water around its  $C_{2v}$  axis, exchanging a pair of fermions, which is described by a two equivalent minima potential. This splitting, compared with that coming from the anisole-water complex<sup>25</sup>, is smaller. Then, several other  $\mu_a$ -type *R*-branch (see in Figure 6

the  $8_{18} \leftarrow 7_{17}$  transition) the transitions as well as much weaker  $\mu_b$  and  $\mu_c$  have been measured. No lines belonging to other isomers could be observed suggesting the occurring of the relaxation processes upon supersonic conditions towards the most stable isomer.



**Figure 6.** The  $8_{18} \leftarrow 7_{17}$  transition within the  $0^+$  and  $0^-$  states for the isomer I of the TFA-water complex. (Reprinted with permission from Gou, Q.; Spada, L.; Vallejo-López, M.; Kang, L.; Novick, S. E.; Caminati, W., Fluorination Effects on the Shapes of Complexes of Water with Ethers: A Rotational Study of Trifluoroanisole–Water. *J. Phys. Chem. A*, 2014, 118 (6), pp. 1047–1051, Publication Date (Web): January 23, 2014. Copyright © 2016 American Chemical Society.)

All the transition have been fitted by using the Pickett's SPFIT program in the Watson  $S$ -reduction and  $I'$ -representation. However, it was not possible to determine any Coriolis coupling constants and the energy between the two states because of the not significantly interaction between these latter ones. Later on, the same procedure has been performed for the TFA- $\text{H}_2^{18}\text{O}$ , TFA-HOD, TFA-DOH, TFA-DOD by expanding, respectively, the TFA mixtures with  $\text{H}_2^{18}\text{O}$  (98% enriched  $\text{H}_2^{18}\text{O}$ ), 1:1 mixture of  $\text{H}_2\text{O}/\text{D}_2\text{O}$  and  $\text{D}_2\text{O}$  (99% enriched  $\text{D}_2\text{O}$ ) samples in the same conditions of the TFA- $\text{H}_2\text{O}$  complex. All the results are reported in Table 15 and 16.



	TFA-H <sub>2</sub> O		TFA-H <sub>2</sub> <sup>18</sup> O	
	0 <sup>+</sup>	0 <sup>-</sup>	0 <sup>+</sup>	0 <sup>-</sup>
A/MHz	1291.6717(6) <sup>a</sup>	1292.6534(6)	1233.72(1)	1233.70(1)
B/MHz	656.3183(2)	656.3193(2)	652.709(4)	652.713(4)
C/MHz	500.8509(2)	500.8532(2)	490.0453(2)	490.0479(2)
D <sub>J</sub> /kHz	0.0385(7)		[0.0385] <sup>b</sup>	
D <sub>JK</sub> /kHz	0.901(8)		[0.901]	
D <sub>K</sub> /kHz	0.64(2)		[0.64]	
d <sub>1</sub> /Hz	-5.0(3)		[-5.0]	
d <sub>2</sub> /Hz	-8.2(2)		[-8.2]	
σ <sup>c</sup> /kHz	2.5		2.7	
N <sup>d</sup>	96		18	

<sup>a</sup>Error in parentheses in units of the last digit. <sup>b</sup>Fixed at the values of the parent species. <sup>c</sup>RMS error of the fit. <sup>d</sup>Number of lines in the fit.

**Table 15.** Rotational, centrifugal distortion constants relative to the 0<sup>+</sup> and 0<sup>-</sup> sublevels for the most abundant TFA- H<sub>2</sub>O and TFA-H<sub>2</sub><sup>18</sup>O isotopologues for the observed isomer. (Reprinted with permission from Gou, Q.; Spada, L.; Vallejo-López, M.; Kang, L.; Novick, S. E.; Caminati, W., Fluorination Effects on the Shapes of Complexes of Water with Ethers: A Rotational Study of Trifluoroanisole–Water. *J. Phys. Chem. A*, 2014, 118 (6), pp. 1047–1051, Publication Date (Web): January 23, 2014. Copyright © 2016 American Chemical Society.).

The splitting due to the internal rotation was observed for the TFA- H<sub>2</sub>O and TFA-H<sub>2</sub><sup>18</sup>O isotopologues (the 0<sup>+</sup> and 0<sup>-</sup> states rotational constants are reported in table 15) but not in the case of TFA-HOD, TFA-DOH, TFA-DOD because of the heavier reduced mass of the motion. The centrifugal distortion constants for the deuterated isotopologues have been fixed at the values of the TFA- H<sub>2</sub>O isotopologue.

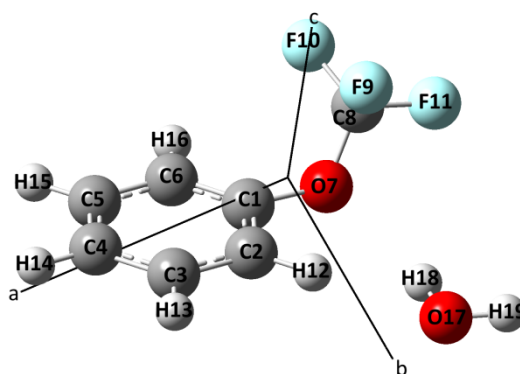
	TFA-HOD	TFA-DOH	TFA-DOD
A/MHz	1252.33(1) <sup>b</sup>	1274.47(1)	1236.158(1)
B/MHz	652.523(3)	653.994(3)	650.161(4)
C/MHz	493.0183(2)	498.1981(2)	490.4597(2)
σ <sup>c</sup> /kHz	3.7	2.6	4.0
N <sup>d</sup>	9	9	9

<sup>a</sup>The quartic centrifugal distortion parameters have been fixed at the values of the parent species. <sup>b</sup>Error in parentheses in units of the last digit. <sup>c</sup>RMS error of the fit. <sup>d</sup>Number of lines in the fit.

**Table 16.** Rotational parameters of for the TFA-HOD, TFA-DOH and TFA-DOD isotopologues. (Reprinted with permission from Gou, Q.; Spada, L.; Vallejo-López, M.; Kang, L.; Novick, S. E.; Caminati, W., Fluorination Effects on the Shapes of Complexes of Water with Ethers: A Rotational Study of Trifluoroanisole–Water. *J. Phys. Chem. A*, 2014, 118 (6), pp. 1047–1051, Publication Date (Web): January 23, 2014. Copyright © 2016 American Chemical Society.).

## Structural Information

A partial  $r_0$  structure have been derived by adjusting three structural parameters ( $R_{\text{H12O17}}$ ,  $\angle\text{C2H12}\cdots\text{O17}$  and  $\angle\text{O17}\cdots\text{C2-H12C1}$ , see Figure 7) which reproduce the rotational constants experimentally determined within few MHz, while keeping the other geometrical parameters fixed to their *ab initio* values.



**Figure 7.** Atom numbering of the TFA-W complex in the principal axes of inertia.

A comparison between the values of the three aforementioned parameters from  $r_0$  and  $r_e$  structures is reported in Table 17.

Fitted parameters			
	$R_{\text{H12O17}}/\text{\AA}$	$\angle\text{C2H12}\cdots\text{O17}/^\circ$	$\angle\text{O17}\cdots\text{C2-H12C1}/^\circ$
$r_0$	2.574(5) <sup>a</sup>	130.8(5)	-36.6(3)
$r_e$	2.447	132.0	-36.4
Derived parameters			
	$R_{\text{O7H18}}/\text{\AA}$	$\angle\text{O7}\cdots\text{H18O17}/^\circ$	
$r_0$	2.294(5)	140.5(5)	
$r_e$	2.170	143.1	

<sup>a</sup>Uncertainties (in parentheses) are expressed in units of the last digit.

**Table 17.**  $r_0$  and  $r_e$  hydrogen bond parameters of TFA-water. (Reprinted with permission from Gou, Q.; Spada, L.; Vallejo-López, M.; Kang, L.; Novick, S. E.; Caminati, W., Fluorination Effects on the Shapes of Complexes of Water with Ethers: A Rotational Study of Trifluoroanisole–Water. *J. Phys. Chem. A*, 2014, 118 (6), pp. 1047–1051, Publication Date (Web): January 23, 2014. Copyright © 2016 American Chemical Society).

A further confirmation of the correct isomer assignment comes from the calculation of the substituted coordinates ( $r_s$ ). In the present study, only those ones defining the position of the oxygen of the water along the principal axes of inertia has been reported since the plausible Ubbelohde

effect<sup>4</sup> gives meaningless values of the coordinates for the water hydrogens upon deuteration. The oxygen  $r_s$  coordinates are compared with those from the  $r_0$  structure in Table 18.

	$a/\text{Å}$	$b/\text{Å}$	$c/\text{Å}$
$r_s$	$\pm 1.397(1)^a$	$\pm 3.0439(5)$	$\pm 0.325(5)$
$r_0$	1.371	3.058	-0.500

<sup>a</sup>Error in parentheses in units of the last digit.

**Table 18.** Oxygen (water) position as derived from the  $r_s$  and  $r_0$  coordinates. (Reprinted with permission from Gou, Q.; Spada, L.; Vallejo-López, M.; Kang, L.; Novick, S. E.; Caminati, W., Fluorination Effects on the Shapes of Complexes of Water with Ethers: A Rotational Study of Trifluoroanisole–Water. *J. Phys. Chem. A*, 2014, 118 (6), pp. 1047–1051, Publication Date (Web): January 23, 2014. Copyright © 2016 American Chemical Society.)

### 3.1.5 Conclusions

The rotational spectra of four hydrogen bonded molecular complexes in synergy with secondary weak hydrogen bonds have been recorded. The analysis of several isotopologues structures make it possible the structural refinements, deriving the  $r_0$  structures as well as the position of the oxygen in water complexes by substitution coordinates ( $r_s$ ). In the PYR-HCOOH adduct a plausible proton transfer together with a possible Ubbelohde effect an increase of the N – O (pyridine nitrogen – O of the HO-CHO) distance of about 7 mÅ is required upon H→D. A secondary C-H···O WHB interaction, in synergy with a stronger O-H···N HB stabilizing the complex whose dissociation energy is about 40 kJ·mol<sup>-1</sup>, higher than that from the 3FPYR-water in agreement with the different features of the O-H from HCOOH and from H<sub>2</sub>O, respectively. The C-H···O contact taking place in all the water complexes with 2FPYR, 3FPYR and TFA where a stronger O-H···N and O-H···O HBs, respectively, are the main interaction.

No appreciable different in the geometries of 2FPYR and 3FPYR are observable upon solvation.

In the case of TFA-water, a splitting of the rotational transitions due to the tunnelling relative to the internal motion of the water around its  $C_{2v}$  axis has been observed, resulting smaller than that found in the anisole-water complex.

## 3.2 WEAK HYDROGEN BONDING

### 3.2.1 Difluoromethane – Dichloromethane

#### Introduction

Freons (halocarbon compounds), the well known molecules causing the ozone depletion, are the most suitable candidates to study the WHBs such as the C-H...F-C and C-H...Cl-C types. In particular, rotational spectroscopy in supersonic expansion conditions provides useful information on isolated molecules or molecular complexes in absence of matrix or solvent effects, unveiling the genuine nature of the involved interactions.

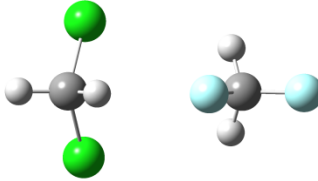
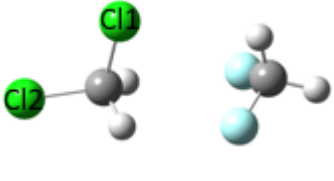
In this respect, several adducts, showing the C-H...F-C<sup>26,27,28,29</sup> contacts have been observed for which the relatively dissociation energies and the bond lengths have been determined.

In the case of the C-H...Cl-C WHB interaction, few microwave studies have been performed<sup>30,31</sup>, suggesting that when a competition between C-H...F-C and C-H...Cl-C interactions is possible, the C-H...Cl-C contacts is preferred.

The Difluoromethane (CH<sub>2</sub>F<sub>2</sub>) – Dichloromethane (CH<sub>2</sub>Cl<sub>2</sub>)<sup>32</sup> adduct marks the divide between the two aforementioned WHBs in order to described a behaviour trend in forming those type of interactions, when more than one C-H...Cl-C and/or C-H...F-C contacts are possible in the molecular system.

#### Theoretical Calculations

*Ab initio* calculations at the MP2/6-311++G(d,p) level have been performed for two isomers of CH<sub>2</sub>F<sub>2</sub> - CH<sub>2</sub>Cl<sub>2</sub>, by using the Gaussian03 Program, showing two C-H...Cl-C and one C-H...F-C or two C-H...F-C and one C-H...Cl-C contacts, respectively. The rotational constants and dipole moment components along *a, b, c* as well as the BSSE corrected energies are reported in Table 19. Furthermore, the quadrupole coupling constants for the two chlorine atoms (both <sup>35</sup>Cl and <sup>37</sup>Cl have *I* = 3/2) are listed for both the C<sub>s</sub> symmetry molecular complexes.

	I	II
		
<i>Symmetry</i>	$C_s$	$C_s$
$A, B, C/\text{MHz}$	2707,976,792	3410,861,790
$\chi_{aa}, \chi_{bb}, \chi_{cc}(\text{Cl1})/\text{MHz}$	36.26, -44.92	29.31, -104.60
$\chi_{ab}, \chi_{ac}, \chi_{bc}(\text{Cl1})/\text{MHz}$	-10.38, 7.87, 47.25	-21.24, 0.00, 0.00
$\chi_{aa}, \chi_{bb}, \chi_{cc}(\text{Cl2})/\text{MHz}$		-67.27, -9.20
$\chi_{ab}, \chi_{ac}, \chi_{bc}(\text{Cl2})/\text{MHz}$		-22.75, 0.00, 0.00
$\mu_a, \mu_b, \mu_c/\text{D}$	-1.47, -0.00, 0.05	2.96, 0.17, 0.0
$\Delta E/\text{cm}^{-1}$	0 <sup>a</sup>	44
$\Delta E_{\text{BSSE}}/\text{cm}^{-1}$	0 <sup>b</sup>	26

<sup>a</sup>Absolute energy = -1197.019948  $E_h$ . <sup>b</sup>Absolute energy BSSE corrected = -1197.016447  $E_h$ .

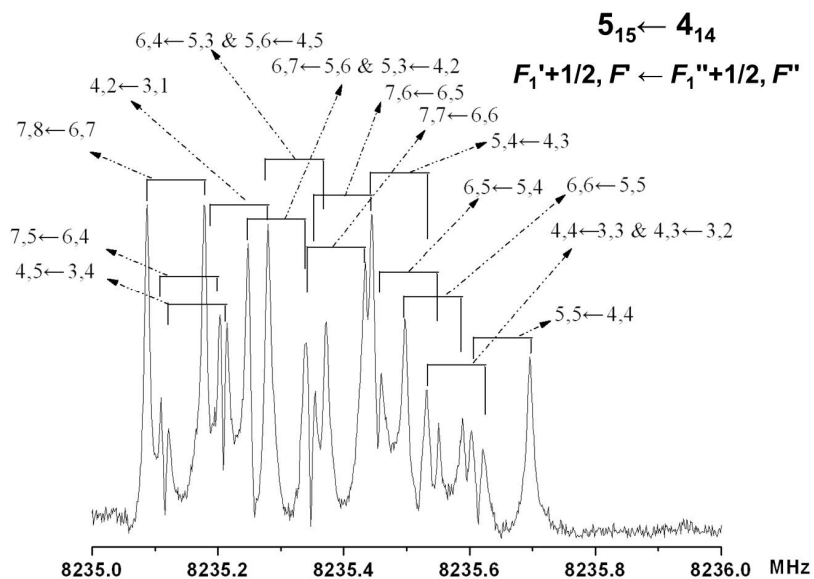
**Table 19.** *Ab initio* rotational parameters for two isomers of  $\text{CH}_2\text{F}_2\text{-CH}_2\text{Cl}_2$  calculated at the MP2/6-311++G(d,p) level. (Reused with permission from Qian Gou, Lorenzo Spada, Montserrat Vallejo-López, Zbigniew Kisiel, Walther Caminati. Interactions between Freons: A Rotational Study of  $\text{CH}_2\text{F}_2\text{-CH}_2\text{Cl}_2$ . *Chem. Asian J.* 2014, 9, 1032 – 1038 © 2014 Wiley-VCH Verlag GmbH&Co. KGaA, Weinheim).

## Experimental Section

A gas mixture of a 1% of  $\text{CH}_2\text{F}_2$  and of  $\text{CH}_2\text{Cl}_2$  at stagnation pressure 5 bars with Helium, has been expanded into the cavity of the Bologna PJ-FTMW spectrometer.

The rotational spectrum acquisition started with the search of the  $\mu_a$ -type *R*-branch transitions for isomer I according to the *ab initio* values of dipole moment components and to the relative energies. A ~4 MHz wide band, with the center around 8485.4 MHz, has been first assigned to the  $5_{05}\leftarrow 4_{04}$  transition of the double  $^{35}\text{Cl}$  isotopologue of the  $\text{CH}_2\text{F}_2\text{-CH}_2\text{Cl}_2$  adduct of isomer I. Later on several other  $\mu_a$ -type *R*-branch have been measured (see the  $5_{15}\leftarrow 4_{14}$  transition in Figure 8) while no  $\mu_b$  and  $\mu_c$  have been observed in agreement with the zero (by symmetry) and almost zero dipole moment components, respectively.

All the lines have been fitted by using the Pickett's SPFIT program Watson's  $S''$  reduction in the  $I'$  representation.



**Figure 8.** The  $5_{15} \leftarrow 4_{14}$  transition for the isomer I of the  $\text{CH}_2\text{F}_2\text{-CH}_2\text{Cl}_2$  showing the complex pattern due to the quadrupole coupling of two  $^{35}\text{Cl}$  atoms. (Reused with permission from Qian Gou, Lorenzo Spada, Montserrat Vallejo-López, Zbigniew Kisiel, Walther Caminati. Interactions between Freons: A Rotational Study of  $\text{CH}_2\text{F}_2\text{-CH}_2\text{Cl}_2$ . *Chem. Asian J.* 2014, 9, 1032 – 1038 © 2014 Wiley-VCH Verlag GmbH&Co. KGaA, Weinheim).

Then, only one set of lines with a relative intensity  $2/3$ , compared with the same transitions of the  $\text{CH}_2\text{F}_2\text{-CH}_2^{35}\text{Cl}^{35}\text{Cl}$  isotopologue were assigned, belonging to the  $\text{CH}_2\text{F}_2\text{-CH}_2^{35}\text{Cl}^{37}\text{Cl}$  isotopologue, in agreement with the supposed  $C_s$  symmetry of the isomer I. Because of their much smaller intensity than the other possible isotopologues, no lines belonging to the  $\text{CH}_2\text{F}_2\text{-CH}_2^{37}\text{Cl}^{37}\text{Cl}$  have been observed. The results are reported in Table 20.

	CH <sub>2</sub> F <sub>2</sub> -CH <sub>2</sub> <sup>35</sup> Cl <sup>35</sup> Cl	CH <sub>2</sub> F <sub>2</sub> -CH <sub>2</sub> <sup>35</sup> Cl <sup>37</sup> Cl
A/MHz	2663.073(3) <sup>a</sup>	2604.320(3)
B/MHz	958.4016(2)	951.1963(1)
C/MHz	785.1948(1)	775.4507(1)
D <sub>J</sub> /kHz	0.7171(7)	0.710(1)
D <sub>JK</sub> /kHz	10.813(6)	9.88(7)
d <sub>1</sub> /kHz	-0.1604(7)	[-0.1604] <sup>b</sup>
d <sub>2</sub> /kHz	-0.0613(4)	[-0.0613] <sup>b</sup>
χ <sub>aa</sub> ( <sup>35</sup> Cl)/MHz	37.399(5)	37.17(3)
χ <sub>bb</sub> -χ <sub>cc</sub> ( <sup>35</sup> Cl)/MHz	-43.68(2)	-42.34(3)
χ <sub>ab</sub> ( <sup>35</sup> Cl)/MHz	±9.00(7)	[11.16] <sup>c</sup>
χ <sub>ac</sub> ( <sup>35</sup> Cl)/MHz	7.0(1)	[8.43] <sup>c</sup>
χ <sub>bc</sub> ( <sup>35</sup> Cl)/MHz	∓49.71(6)	-50.03(2)
χ <sub>aa</sub> ( <sup>37</sup> Cl)/MHz		29.62(2)
χ <sub>bb</sub> -χ <sub>cc</sub> ( <sup>37</sup> Cl)/MHz		-35.44(2)
χ <sub>ab</sub> ( <sup>37</sup> Cl)/MHz		[-7.52] <sup>c</sup>
χ <sub>ac</sub> ( <sup>37</sup> Cl)/MHz		[6.19] <sup>c</sup>
χ <sub>bc</sub> ( <sup>37</sup> Cl)/MHz		39.23(1)
N <sup>d</sup>	349	160
σ <sup>e</sup> /kHz	2.9	3.1

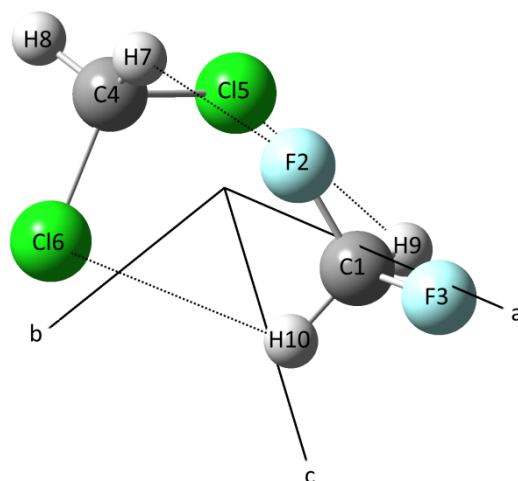
<sup>a</sup>Uncertainties in units of the last digit. <sup>b</sup>Fixed to the most abundant species values. <sup>c</sup>Fixed to the *ab initio* values. <sup>d</sup>Number of lines in the fit. <sup>e</sup>Standard deviation of the fit.

**Table 20.** Rotational parameters from the fitted transitions for two isotopologues of isomer I. (Reused with permission from Qian Gou, Lorenzo Spada, Montserrat Vallejo-López, Zbigniew Kisiel, Walther Caminati. Interactions between Freons: A Rotational Study of CH<sub>2</sub>F<sub>2</sub>-CH<sub>2</sub>Cl<sub>2</sub>. *Chem. Asian J.* 2014, 9, 1032 – 1038 © 2014 Wiley-VCH Verlag GmbH&Co. KGaA, Weinheim).

No lines belonging to isomer II have been measured. This can be due to the kinetic relaxation processes occurring in the jet.

### Structural Information

The substituted coordinates (*r<sub>s</sub>*) along the principal axes of inertia of the chlorine atoms (see Figure 9) have been determined.



**Figure 9.** The isomer I of the  $\text{CH}_2\text{F}_2\text{-CH}_2\text{Cl}_2$  adduct, with atom numbering, along the principal axes of inertia.

Their values, which are compared with those from the *ab initio* structures in Table 21, are a further confirmation of the corrected isomeric assignment and of the  $C_s$  symmetry of the complex.

	$a/\text{\AA}$	$b/\text{\AA}$	$c/\text{\AA}$
$r_s$	$\pm 1.399(1)^a$	$\pm 1.466(1)$	$\pm 0.223(7)$
$r_e$	1.389	$\pm 1.473^b$	0.236

<sup>a</sup>Error in units of the last digit. <sup>b</sup>The sign depends on which chlorine atom is considered since the  $C_s$  symmetry along *ab* plane.

**Table 21.** The substitution coordinates for the chlorine atoms in the principal axes system. (Reused with permission from Qian Gou, Lorenzo Spada, Montserrat Vallejo-López, Zbigniew Kisiel, Walther Caminati. Interactions between Freons: A Rotational Study of  $\text{CH}_2\text{F}_2\text{-CH}_2\text{Cl}_2$ . *Chem. Asian J.* 2014, 9, 1032 – 1038 © 2014 Wiley-VCH Verlag GmbH&Co. KGaA, Weinheim).

A partial effective structure ( $r_0$ ) has been calculated by fitting three geometrical parameters ( $R_{\text{C1C4}}$ ,  $\angle\text{H7C4}\cdots\text{C1}$  and  $\angle\text{F2C1}\cdots\text{C4}$ ) in order to reproduce the experimental rotational constants of the available isotopologues, keeping constants at their *ab initio* values the remaining parameters. The results from the fitting are reported in Table 22.



	$R_{\text{ClC}_4}/\text{\AA}$	$\angle\text{H7C}_4\cdots\text{C1}/^\circ$	$\angle\text{F2C1}\cdots\text{C4}/^\circ$
$r_0$	3.755(1) <sup>a</sup>	62.5(1)	55.7(1)
$r_e$	3.751	63.5	50.4

<sup>a</sup>Uncertainties in units of the last digit.

**Table 22.** The fitted  $r_0$  parameters compared with the corresponding values from the *ab initio* calculations ( $r_e$ ) for isomer I of  $\text{CH}_2\text{F}_2\text{-CH}_2\text{Cl}_2$ . The values of 2.489(2) Å and of 3.147(2) Å are derived (from  $r_0$ ) for the C-H $\cdots$ F and C-H $\cdots$ Cl contacts, respectively<sup>32</sup>. (Reused with permission from Qian Gou, Lorenzo Spada, Montserrat Vallejo-López, Zbigniew Kisiel, Walther Caminati. Interactions between Freons: A Rotational Study of  $\text{CH}_2\text{F}_2\text{-CH}_2\text{Cl}_2$ . *Chem. Asian J.* 2014, 9, 1032 – 1038 © 2014 Wiley-VCH Verlag GmbH&Co. KGaA, Weinheim).

Structural information relative to the complex can be derived from the analysis of the quadrupole coupling constant results from Table 20. In fact, since it was possible to determine the values of the complete set of the quadrupolar constants along the principal axes system ( $\chi_{aa}$ ,  $\chi_{bb}$ ,  $\chi_{cc}$ ,  $\chi_{ab}$ ,  $\chi_{bc}$  and  $\chi_{ac}$ ), the quadrupole tensor components along the  $x,y,z$  principal axes (orienting in a way that  $z$  is close to the the molecular field gradient  $\equiv$  C-Cl axis) can be obtained by diagonalisation of the first matrix.

The obtained results as well as the quadrupole asymmetry parameter ( $\eta$ ), the estimation of  $\alpha$  angle and the  $\theta_{zb}$  angle between the  $z$  and  $b$  axes of the two different axes systems, giving the estimation of the  $\angle\text{Cl-C-Cl}$  angle ( $\angle\text{ClC-Cl} = (180 - 2\theta_{zb})$ ), are similar<sup>32</sup> to those ones of the  $\text{CH}_2\text{Cl}_2$  molecule<sup>33</sup>.

## Dissociation Energy

According to the 1.61 and 1.62 equations the dissociation energy of the isomer I of the  $\text{CH}_2\text{F}_2\text{-CH}_2\text{Cl}_2$  complex have been estimated from the fitted rotational parameters of Table 20 to be 7.6 kJ mol<sup>-1</sup> ( $k_s = 6.4 \text{ N}\cdot\text{m}^{-1}$  and  $R_{\text{CM}} = 3.77 \text{ \AA}$ ).

## 3.2.2 Difluoromethane – Chlorofluoromethane

### Introduction

In the previous study, the characterization of the  $\text{CH}_2\text{F}_2\text{-CH}_2\text{Cl}_2$  molecular complex suggests that when the C-H $\cdots$ F-C and C-H $\cdots$ Cl-C interactions are possible, the largest number of the C-H $\cdots$ Cl-C contacts is observed.

The interaction distances at which the C-H $\cdots$ F-C and the C-H $\cdots$ Cl-C WHBs take place following the different radius values of the halogens acting as weak hydrogen bond acceptors. Whilst the

typical range of C-H...F-C is, as already mentioned, within the 2.5-2.9 Å range, the C-H...Cl-C occurs at larger distances (3.0 – 3.1 Å).

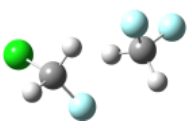
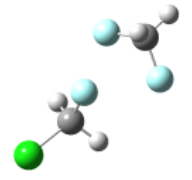
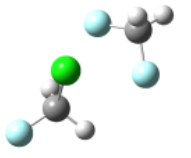
It is interesting, thus, to investigate, also due to the availability of the rotational investigation of CH<sub>2</sub>F<sub>2</sub> dimer, how the single chlorine substitution in going from CH<sub>2</sub>F<sub>2</sub><sup>26</sup> to CH<sub>2</sub>FCl to CH<sub>2</sub>Cl<sub>2</sub>, as partner molecules of CH<sub>2</sub>F<sub>2</sub>, modifies the shape and the bonding energies of the respective molecular adducts.

### Theoretical Calculations

The structures of three different isomers have been optimized at the MP2/6-311++G(d,p) level using the Gaussian03 Quantum Chemistry Package for the CH<sub>2</sub>F<sub>2</sub>-CH<sub>2</sub>ClF adduct. The calculated geometries, reported in Table 23, together with their respectively rotational parameters useful for the spectrum assignment, are linked by WHBs of the C-H...Cl-C and/or C-H...F-C type contacts.

The relative energies at the equilibrium ( $\Delta E$ ), including the zero point ( $\Delta E_0$ ) and the BSSE corrections ( $\Delta E_{BSSE}$ ) are also listed in table 23, showing different indications of the global minimum according to the corrections which are considered: isomer I according to  $\Delta E_0$  or isomer II from  $\Delta E_{BSSE}$ .

Furthermore, the dissociation energies ( $E_D$ ) of the isomers have been calculated, resulting be similar in magnitude.

	I	II	III
			
<i>Symmetry</i>	$C_1$	$C_s$	$C_s$
<i>A</i> /MHz	4443	6377	3944
<i>B</i> /MHz	1080	912	1155
<i>C</i> /MHz	975	886	1075
$1.5\chi_{aa}$ /MHz	49.2	-101.9	45.4
$0.25(\chi_{bb}-\chi_{cc})$ /MHz	-19.7	1.7	-25.9
$\chi_{bc}$ /MHz	29.2	0.0	0.0
$\chi_{ab}$ /MHz	16.1	0.0	3.9
$\chi_{ac}$ /MHz	1.9	2.5	0.0
$\mu_a$ /D	-1.91	-2.24	3.12
$\mu_b$ /D	-1.19	0.00	0.59
$\mu_c$ /D	0.02	-0.06	0.00
$\Delta E^a$ /cm <sup>-1</sup>	0 <sup>a</sup>	62	102
$\Delta E_{BSSE}^b$ /cm <sup>-1</sup>	2	0 <sup>b</sup>	67
$\Delta E_0^c$ /cm <sup>-1</sup>	0 <sup>c</sup>	36	54
$E_D^d$ /kJ mol <sup>-1</sup>	5.3	5.6	5.1

<sup>a</sup>Absolute energy =  $-837.044733 E_h$ . <sup>b</sup>Absolute energy BSSE corrected =  $-837.041714 E_h$ .

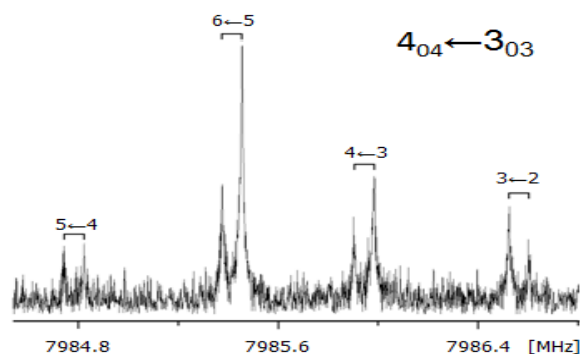
<sup>c</sup>Absolute energy zero point corrected =  $-836.978378 E_h$ . <sup>d</sup>Dissociation energy

**Table 23.** The rotational parameters and the energies calculated at the MP2/6-311++G(d,p) level for three isomers of the CH<sub>2</sub>F<sub>2</sub>-CH<sub>2</sub>ClF complex. (Spada, L.; Gou, Q.; Tang, S.; Caminati, W. Weak hydrogen bonds in adducts between freons: the rotational study of CH<sub>2</sub>F<sub>2</sub>-CH<sub>2</sub>ClF. *New J. Chem.*, 2015,39, 2296-2299). - Reproduced by permission of The Royal Society of Chemistry (RSC) on behalf of the Centre National de la Recherche Scientifique (CNRS) and the RSC.

## Experimental Section

The 1:1 gas mixture, at 1% in Helium (stagnation pressure of 5 bars), of CH<sub>2</sub>F<sub>2</sub> and CH<sub>2</sub>ClF was expanded into the cavity of the Bologna PJ-FTMW spectrometer.

According to the *ab initio* results, the  $\mu_a$ -type transitions are expected to be the strongest component for all the isomers. The rotational spectrum was, thus, collected starting from the search of the  $4_{04} \leftarrow 3_{03}$  transition. A typical four components pattern due to the quadrupole coupling of one <sup>35</sup>Cl atom ( $I = 3/2$ ) was found centered at 7985.6 MHz as shown in Figure 10.



**Figure 10.** Quadrupole splitting ( $F'+1/2 \leftarrow F''+1/2$ ) displayed for the  $4_{04} \leftarrow 3_{03}$  rotational transition of the most abundance species of isomer I. (Spada, L.; Gou, Q.; Tang, S.; Caminati, W. Weak hydrogen bonds in adducts between freons: the rotational study of  $\text{CH}_2\text{F}_2\text{-CH}_2\text{ClF}$ . *New J. Chem.*, 2015,39, 2296-2299). - Reproduced by permission of The Royal Society of Chemistry (RSC) on behalf of the Centre National de la Recherche Scientifique (CNRS) and the RSC.

After this first assignment, other  $\mu_a$ -type lines up to  $J = 9$  and  $K_a=3$  have been measured together with weaker  $\mu_b$ -type transitions. The predicted almost zero  $\mu_c$  type lines have not been observed.

At about 120 MHz below the frequencies of the  $4_{04} \leftarrow 3_{03}$  transition for the most abundant isotopologue, the three times weaker 4 components lines for the  $\text{CH}_2\text{F}_2\text{-CH}_2^{37}\text{ClF}$  species have been observed. Several other  $\mu_a$  and  $\mu_b$  types transitions were measured and fitted using, for both the isotopologues, the Pickett's SPFIT program within the semirigid Watson's Hamiltonian ( $I^r$  representation,  $S$ -reduction).

The obtained results are reported in Table 24.

	CH <sub>2</sub> F <sub>2</sub> -CH <sub>2</sub> <sup>35</sup> ClF	CH <sub>2</sub> F <sub>2</sub> -CH <sub>2</sub> <sup>37</sup> ClF
A/MHz	4361.912(3) <sup>a</sup>	4295.106(4)
B/MHz	1053.0440(5)	1038.0981(5)
C/MHz	949.3755(3)	934.1084(3)
D <sub>J</sub> /kHz	1.381(2)	1.378(4)
D <sub>JK</sub> /kHz	9.30(1)	8.51(6)
D <sub>K</sub> /kHz	16.8(6)	17.3(7)
d <sub>1</sub> /kHz	-0.220(3)	-0.223(4)
d <sub>2</sub> /kHz	-0.020(2)	-0.018(7)
1.5χ <sub>aa</sub> /MHz	52.78(1)	41.36(3)
0.25(χ <sub>bb</sub> -χ <sub>cc</sub> )/MHz	-20.329(4)	-16.058(5)
χ <sub>bc</sub> /MHz	31.6(1)	24.7(2)
χ <sub>ab</sub> /MHz	11.4(9)	10(1)
χ <sub>ac</sub> /MHz	-1.9 <sup>b</sup>	-1.5 <sup>b</sup>
N <sup>c</sup>	128	72
σ <sup>c</sup> /kHz	1.9	1.7

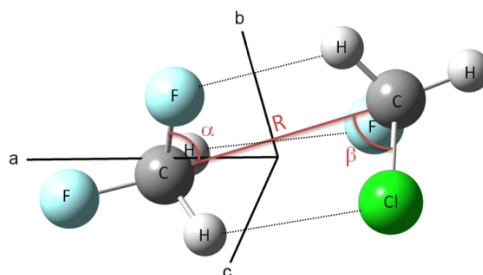
<sup>a</sup>Error in parentheses in units of the last digit. <sup>b</sup>Fixed to the *ab initio* value. <sup>c</sup>Number of lines in the fit. <sup>c</sup>Standard deviation of the fit.

**Table 24.** The experimental rotational parameters of two isotopologues of the Isomer I of the CH<sub>2</sub>F<sub>2</sub>-CH<sub>2</sub>ClF molecular adduct. (Spada, L.; Gou, Q.; Tang, S.; Caminati, W. Weak hydrogen bonds in adducts between freons: the rotational study of CH<sub>2</sub>F<sub>2</sub>-CH<sub>2</sub>ClF. *New J. Chem.*, 2015,39, 2296-2299). - Reproduced by permission of The Royal Society of Chemistry (RSC) on behalf of the Centre National de la Recherche Scientifique (CNRS) and the RSC.

No other isomers have been observed in the spectrum, indicating a possible kinetic relaxation towards isomer I upon supersonic expansion conditions.

### Structural information

A partial *r*<sub>0</sub> structure have been calculated by fitting three geometrical parameters (*R*, *α*, *β* in Figure 11) in a way to reproduce, within 1 MHz, the experimental rotational constants while keeping fixed the other ones to their *ab initio* values.



**Figure 11.** The isomer I of the  $\text{CH}_2\text{F}_2\text{-CH}_2\text{ClF}$  adduct in the principal axes of inertia showing the fitted parameters ( $R$ ,  $\alpha$ ,  $\beta$ ) to calculate the partial  $r_0$  structure. (Spada, L.; Gou, Q.; Tang, S.; Caminati, W. Weak hydrogen bonds in adducts between freons: the rotational study of  $\text{CH}_2\text{F}_2\text{-CH}_2\text{ClF}$ . *New J. Chem.*, 2015,39, 2296-2299). - Reproduced by permission of The Royal Society of Chemistry (RSC) on behalf of the Centre National de la Recherche Scientifique (CNRS) and the RSC.

The obtained results are compared with the ones from the *ab initio* structure in Table 25.

	$r_0$	$r_e$
$R/\text{\AA}$	3.661(2) <sup>a</sup>	3.564
$\alpha/^\circ$	59.2(1)	58.8
$\beta/^\circ$	82.8(1)	85.2

<sup>a</sup>Error in parentheses in units of the last digit

**Table 25.** Comparison of  $R$ ,  $\alpha$ ,  $\beta$  parameters from the relative  $r_0$  and  $r_e$  structures for isomer I. (Spada, L.; Gou, Q.; Tang, S.; Caminati, W. Weak hydrogen bonds in adducts between freons: the rotational study of  $\text{CH}_2\text{F}_2\text{-CH}_2\text{ClF}$ . *New J. Chem.*, 2015,39, 2296-2299). - Reproduced by permission of The Royal Society of Chemistry (RSC) on behalf of the Centre National de la Recherche Scientifique (CNRS) and the RSC.

The features of the  $\text{C-H}\cdots\text{Cl-C}$  and/or  $\text{C-H}\cdots\text{F-C}$  interactions as well as the  $\text{C}\cdots\text{C}$  distances of the  $(\text{CH}_2\text{F}_2)_2$ ,  $\text{CH}_2\text{F}_2\text{-CH}_2\text{ClF}$  and  $\text{CH}_2\text{F}_2\text{-CH}_2\text{Cl}_2$  are compared in Table 26. Following the previous complexes sequence, one can see that the  $\text{C}\cdots\text{C}$  distance increase of about 0.1 Å for each addition of one Cl atom. The  $\text{C-H}\cdots\text{Cl-C}$  contacts take place at similar distances around the value of 3.15 Å while in the case of  $\text{C-H}\cdots\text{F-C}$  interaction are within the usual 2.5 – 2.9 Å distance range.

	$r(\text{F}\cdots\text{H})/\text{\AA}$	$r(\text{H}\cdots\text{Cl})/\text{\AA}$	$r(\text{C}\cdots\text{C})/\text{\AA}$
$(\text{CH}_2\text{F}_2)_2$	2.628, 2.759	--	3.55(1)
$\text{CH}_2\text{F}_2\text{-CH}_2\text{ClF}$	2.633, 2.861	3.169	3.661
$\text{CH}_2\text{F}_2\text{-CH}_2\text{Cl}_2$	2.489(2)	3.147(2)	3.755(1)

**Table 26.** The comparison of the C-H $\cdots$ Cl-C, C-H $\cdots$ F-C WHBs and C $\cdots$ C distances by addition of one Cl atom from  $(\text{CH}_2\text{F}_2)_2$ , through  $\text{CH}_2\text{F}_2\text{-CH}_2\text{ClF}$  to  $\text{CH}_2\text{F}_2\text{-CH}_2\text{Cl}_2$ . (Spada, L.; Gou, Q.; Tang, S.; Caminati, W. Weak hydrogen bonds in adducts between freons: the rotational study of  $\text{CH}_2\text{F}_2\text{-CH}_2\text{ClF}$ . *New J. Chem.*, 2015,39, 2296-2299). - Reproduced by permission of The Royal Society of Chemistry (RSC) on behalf of the Centre National de la Recherche Scientifique (CNRS) and the RSC.

The substituted coordinates ( $r_s$ ) of the chlorine atom have been calculated from the experimental rotational constants of the two observed isotopologues of isomer I, whose results are reported in Table 27 where are compared with the respective coordinates from the  $r_e$  and  $r_0$  structures.

	$r_s$	$r_e$	$r_0$
$a/\text{\AA}$	$\pm 1.870(1)^a$	-1.922	-1.898
$b/\text{\AA}$	$\pm 0.965(2)$	-0.929	-0.960
$c/\text{\AA}$	$\pm 0.05(3)$	-0.097	-0.095

<sup>a</sup>Error in parentheses in units of the last digit.

**Table 27.** The comparison of the chlorine coordinates, along the principal axes of inertia, from the  $r_s$ ,  $r_e$  and  $r_0$  structures. (Spada, L.; Gou, Q.; Tang, S.; Caminati, W. Weak hydrogen bonds in adducts between freons: the rotational study of  $\text{CH}_2\text{F}_2\text{-CH}_2\text{ClF}$ . *New J. Chem.*, 2015,39, 2296-2299). - Reproduced by permission of The Royal Society of Chemistry (RSC) on behalf of the Centre National de la Recherche Scientifique (CNRS) and the RSC.

### Dissociation Energy

The dissociation energy value ( $E_D = 5.3 \text{ kJ}\cdot\text{mol}^{-1}$ , with  $k_s = 4.6 \text{ N}\cdot\text{m}^{-1}$  and  $R_{\text{CM}} = 3.72 \text{ \AA}$ ). for the observed isomer has been estimated from the experimental data using the equations 1.61 and 1.62. This result is in good agreement with the ab initio one, similar to those for  $(\text{CH}_2\text{F}_2)_2$  ( $E_D = 6.6 \text{ kJ}\cdot\text{mol}^{-1}$ ) and  $\text{CH}_2\text{F}_2\text{-CH}_2\text{Cl}_2$  ( $E_D = 7.6 \text{ kJ}\cdot\text{mol}^{-1}$ ) ones.

### 3.2.3 Pyridine – Methane

Until now, the description of WHBs has been performed analysing the established interactions of the C-H $\cdots$ Cl-C and C-H $\cdots$ F-C types which take place at distances around  $3 \text{ \AA}$  and in the  $2.5 - 2.9 \text{ \AA}$  range, respectively with estimated energies of about  $2 \text{ kJ}\cdot\text{mol}^{-1}$ . When the competition between the two is possible, it has been observed that the former is the favourite one.

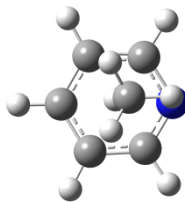
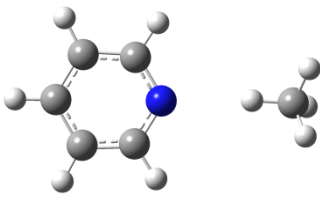
Pyridine (PYR) and Methane (MET) can be linked together through different WHBs: the C-H...N interaction, forming a  $\sigma$  type complex, or the C-H... $\pi$  interaction giving rise to a  $\pi$  types adduct, because of, respectively, the involving either of the nitrogen lone pair or the  $\pi$  system of pyridine.

Depending on which of these interaction is the favourite one, two different complex shapes are possible where, according to the previous interactions, MET is located either perpendicular or in the plane with respect to pyridine.

This study represents, also, the first investigation of a molecular adduct between an aromatic compound with an alkane by means of rotational spectroscopy.

### Theoretical calculation

According to the previous considerations, two adducts have been calculated at the MP2/6-311++G(d,p) level by using Gaussian03 program package: isomer I, showing as favourite interaction the C-H... $\pi$  contact, and isomer II where PYR and MET are linked by a C-H...N WHB. The rotational parameters useful for the spectrum assignment are reported in Table 28 together with the relative energy calculated at the equilibrium and including the zero point corrections as well as the BSSE corrected ones.

		
$A/\text{MHz}$	2901	5793
$B/\text{MHz}$	1895	1128
$C/\text{MHz}$	1873	950
$\chi_{aa}/\text{MHz}$	3.29	-4.86
$\chi_{bb}-\chi_{cc}/\text{MHz}$	-6.28	-1.95
$ \mu_a /\text{D}$	0.4	2.7
$ \mu_b /\text{D}$	2.3	0.2
$ \mu_c /\text{D}$	0.0	0.0
$\Delta E/\text{cm}^{-1}$	0 <sup>a</sup>	346
$\Delta E_{\text{BSSE}}/\text{cm}^{-1}$	0 <sup>b</sup>	19
$\Delta E_0/\text{cm}^{-1}$	0 <sup>c</sup>	65

<sup>a</sup>Absolute energy = -287.992494  $E_h$ . <sup>b</sup>Absolute energy BSSE corrected = -287.858116  $E_h$ . <sup>c</sup>Absolute energy zero point corrected = -287.990053  $E_h$ .

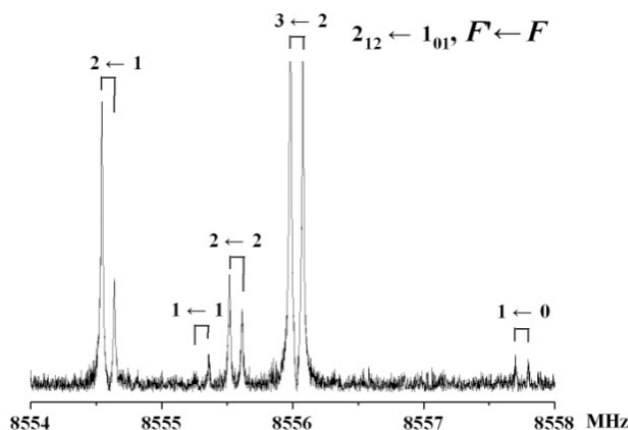


**Table 28.** The two calculated isomers for the PYR-MET complex at the MP2/6-311++G(d,p) level. (Adapted from Q. Gou, L. Spada, M. Vallejo-López, A. Lesarri, E. J. Cocinero and W. Caminati, Phys. Chem. Chem. Phys., 2014, 16, 13041 - Reproduced by permission of the PCCP Owner Societies).

## Experimental Section

PYR-MET and (<sup>15</sup>N)PYR-MET 1:1 molecular complexes have been generated by passing over PYR and (<sup>15</sup>N)PYR, respectively, maintained at 273 K in a sample container, a 5% mixture of MET in Helium at the stagnation pressure of 6 bars. The rotational spectrum has been collected by using the Bologna PJ-FTMW spectrometer.

According to the data reported in Table 28, the search of the rotational transitions was started from the  $\mu_b$ -types lines of isomer I. Several components transition belonging to the  $2_{12} \leftarrow 1_{01}$  (see Figure 12) of isomer I, due to the presence of the <sup>14</sup>N atom ( $I = 1$ ), was first observed around 8556 MHz.



**Figure 12.** The  $2_{12} \leftarrow 1_{01}$  rotational transition showing five quadrupolar components according to  $\Delta F = 0, 1$ . (Q. Gou, L. Spada, M. Vallejo-López, A. Lesarri, E. J. Cocinero and W. Caminati, Phys. Chem. Chem. Phys., 2014, 16, 13041 - Reproduced by permission of the PCCP Owner Societies).

After this first assignment, other  $\mu_b$ -types and much weaker  $\mu_a$ -types lines have been measured and fitted using the Pickett's SPFIT program ( $S$  reduction and  $I'$  representation). Later on, the rotational spectrum of (<sup>15</sup>N)PYR-MET isotopologue, whose lines are not split since  $I = 1/2$ , has been observed and assigned following the same procedure. The results, for both isotopologues, are shown in Table 29.

	PYR-MET	( <sup>15</sup> N)PYR-MET
<i>A</i> /MHz	2995.7148(9) <sup>a</sup>	2961.1510(6)
<i>B</i> /MHz	1873.3363(6)	1872.2691(6)
<i>C</i> /MHz	1853.4941(6)	1838.9538(5)
<i>D<sub>J</sub></i> /kHz	5.46(1)	5.33(2)
<i>D<sub>JK</sub></i> /kHz	53.70(6)	[53.70] <sup>b</sup>
<i>D<sub>K</sub></i> /kHz	-56.59(8)	[-56.59]
<i>d<sub>1</sub></i> /kHz	-0.23(2)	[-0.23]
$\chi_{aa}$ /MHz	3.251(5)	-
$\chi_{bb}-\chi_{cc}$ /MHz	-6.137(7)	-
<i>N</i> <sup>c</sup>	55	18
$\sigma$ /kHz <sup>d</sup>	2.6	2.2

<sup>a</sup>Uncertainties are in units of the last digit. <sup>b</sup>Fixed to the values of the PYR-MET isotopologue.

<sup>c</sup>Number of transitions in the fit. <sup>d</sup>Standard deviation of the fit.

**Table 29.** The fitted rotational parameters for the two isotopologues of isomer I. (Q. Gou, L. Spada, M. Vallejo-López, A. Lesarri, E. J. Cocinero and W. Caminati, Phys. Chem. Chem. Phys., 2014, 16, 13041 - Reproduced by permission of the PCCP Owner Societies).

No lines belonging to the isomer II have been observed suggesting a plausible isomeric relaxation toward isomer I.

No splitting due to the transitions according to the three nuclear-spin states *A*, *F* and *E* of methane were observed, suggesting their overlap since, the much heavier mass of the present adduct than those ones of complexes with methane where three and two components are observable (CH<sub>4</sub>-H<sub>2</sub>O<sup>34</sup> and CH<sub>4</sub>-OCS<sup>35</sup>, respectively).

## Structural Information and Dynamics

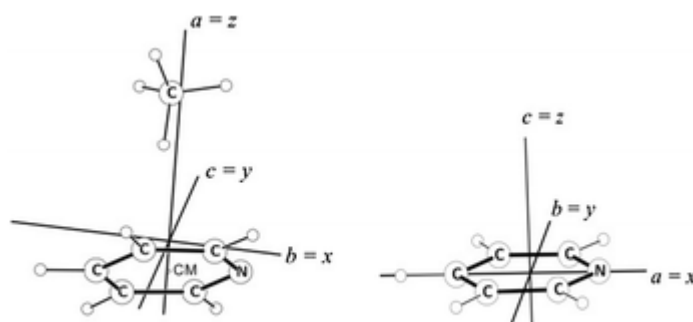
The substitution coordinates of the nitrogen atom along the principal axes system of the PYR-MET isotopologue have been calculated according to the Kraitchman's equations as reported in Table 30 suggesting a *C<sub>s</sub>* symmetry of the isomer I since the imaginary value of the obtained *c*-coordinate.

	<i>a</i> /Å	<i>b</i> /Å
<i>r</i> <sub>0</sub>	±0.411(4) <sup>a</sup>	±1.424(1)
<i>r</i> <sub>e</sub>	-0.441	1.427

<sup>a</sup>Uncertainties are expressed in units of the last digit. The *c*-coordinates are fixed to zero by symmetry.

**Table 30.** The nitrogen *r<sub>s</sub>* coordinates (Å) in the principal axes system of the PYR-MET which are compared with the *ab initio* ones. (Q. Gou, L. Spada, M. Vallejo-López, A. Lesarri, E. J. Cocinero and W. Caminati, Phys. Chem. Chem. Phys., 2014, 16, 13041 - Reproduced by permission of the PCCP Owner Societies).

The large values of  $D_J$  and  $D_{JK}$  suggests that the vibrations parallel to the ring plane (bendings) have a really small barrier. Hence, together with the low energy stretching vibration between the centers of mass of the PYR and MET, these three large amplitude motions give rise to the Coriolis interactions<sup>36</sup>. This can be seen (together with, also, a displacement of MET along the  $z$  axes), taking into the account the differences of planar moment of inertia along  $x$  ( $\Delta M_{xx}$ ) and  $y$  ( $\Delta M_{yy}$ ) in going from PYR to PYR-MET (the respectively  $x,y,z$  axes system for the PYR and for PYR-MET are almost parallel, see Figure 13) whose values are negatives.



**Figure 13.** The principal axes of inertia and their relations with  $x,y,z$  axes system for PYR-MET and PYR. (Q. Gou, L. Spada, M. Vallejo-López, A. Lesarri, E. J. Cocinero and W. Caminati, Phys. Chem. Chem. Phys., 2014, 16, 13041 - Reproduced by permission of the PCCP Owner Societies).

Furthermore, assuming a free internal rotation for the MET since  $A_{(\text{PYR-MET})} > C_{\text{PYR}}$  (it does not produce any change on  $I_a$ ) and the two bendings motion displacement along  $x$  ( $X$ ) within the  $xz$  plane and  $y$  ( $Y$ ), the potential energy is given by:

$$V(X, Y) = (1/2)[k_x Y^2 + k_y (X - X_e)^2] \quad (1)$$

Where  $X_e$  is the displacement, at the equilibrium position, of the center of mass of MET from the PYR  $z$ -axis within the symmetry plane.

Taking into the account equation (1) in a bidimensional flexible model<sup>37</sup> reproducing the experimental  $\Delta M_{xx}$  and  $\Delta M_{yy}$ , two of the three parameters in that equation are determined as reported in Table 31 as well as the MET center of mass coordinate along  $z$  ( $Z_0$ ).

(a) Experimental and calculated data				
	$M_{gg}(\text{u}\text{\AA})$		$\Delta M_{gg}(\text{u}\text{\AA})$	
	PYR	PYR-CH <sub>4</sub>	Exptl.	Calc.
X	87.738( $M_{aa}$ )	85.794( $M_{bb}$ )	-1.944	-1.944
Y	83.974( $M_{bb}$ )	82.906( $M_{cc}$ )	-1.068	-1.069
Z	0( $M_{cc}$ )	186.888( $M_{aa}$ )	186.888	186.842
(b) Determined parameters				
$k_x = k_y = 0.36(1) \text{ N m}^{-1}$		$X_e = 0.375(1) \text{ \AA}$	$Z_0 = 3.544(1) \text{ \AA}$	

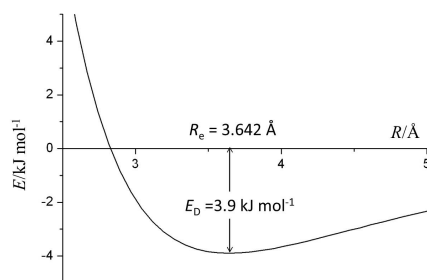
**Table 31.** The results of the bidimensional flexible model together with the values of the  $M_{gg}$  (with  $g = a, b, c$ ) for PYR and for PYR-MET and their differences. (Q. Gou, L. Spada, M. Vallejo-López, A. Lesarri, E. J. Cocinero and W. Caminati, *Phys. Chem. Chem. Phys.*, 2014, 16, 13041 - Reproduced by permission of the PCCP Owner Societies).

## Dissociation Energy

The usual procedure for estimating the dissociation energy results be too approximated for this floppy system according to the high  $D_J$  and  $D_{JK}$  values which consider the stretching motion between two centers of mass of the two molecular partner as not affected by the other vibrations.

Assuming its independency from the other two low energy large amplitude motion bendings, the force constant can be evaluated be  $2.73 \text{ N}\cdot\text{m}^{-1}$  ( $R_{CM} = 3.66 \text{ \AA}$ , from MP2/6-311++G(d,p) calculation) according to equation 1.61 whose relative “frequency” is  $\nu_s = 59.0 \text{ cm}^{-1}$ .<sup>38</sup>

The equilibrium center of mass distance ( $R_e$ ) between the PYR and MET and the values of the dissociation energy ( $E_D$ ) have been adjusted, within the Lennard-Jones potential (see Figure 14), reproducing the stretching frequency ( $\nu_s = 59.0 \text{ cm}^{-1}$ ) and the sum of the experimental rotational constants  $B$  and  $C$  by means of a monodimensional flexible model<sup>37</sup>.



**Figure 14.** Dissociation energy values vs center of mass distances within the Lennard-Jones potential reproducing the  $\nu_s$  and the experimental  $B+C$  values by means of monodimensional flexible model obtaining:  $R_e = 3.642(1)$  and  $E_D = 3.9(1) \text{ kJ}\cdot\text{mol}^{-1}$ . (Q. Gou, L. Spada, M. Vallejo-López, A. Lesarri, E. J. Cocinero and W. Caminati, *Phys. Chem. Chem. Phys.*, 2014, 16, 13041 - Reproduced by permission of the PCCP Owner Societies).

### 3.2.4 Pyridine –Fluoromethane

#### Introduction

Following the previous study, the effect of the fluorine substitution in methane is explored in the complex of fluoromethane (CH<sub>3</sub>F) with pyridine (PYR).

In the case of PYR-MET adduct, it has been shown that a  $\pi$  type isomer is formed due to the preference towards the C-H $\cdots\pi$  interaction instead of a C-H $\cdots$ N one.

On the other hand, a rotational investigation of PYR-CHF<sub>3</sub> shows that the triple fluorine substitution of methane favours the  $\sigma$  type complex through a C-H $\cdots$ N contact in cooperativity with a secondary C-H $\cdots$ F WHB which is broken and reformed because of the occurring of the internal rotation of the -CF<sub>3</sub> group ( $V_3 = 0.572(3)$  kJ $\cdot$ mol<sup>-1</sup>)<sup>39</sup> around its C<sub>3v</sub> axis.

It has been shown, also, that for the PYR-CF<sub>4</sub><sup>40</sup>, the  $\sigma$  type complex is favourite through the N lone pair interaction with the  $\sigma$  hole<sup>41</sup> on the carbon of the CF<sub>4</sub> group.

The main goal of the present study is to verify if a single fluorine substitution changes the shape of the complex with respect to the  $\pi$  type one found for PYR-MET or if due to its larger acidity than this latter complex it behaves in the same way of PYR- CHF<sub>3</sub>.

In this latter case, it is interesting, also, to understand the link between the reduced barrier of the internal rotation motion with the type of established WHBs and their features.

#### Theoretical Calculations

Thanks to the using of MacroModel 9.2<sup>17</sup>, the isomeric space of PYR- CH<sub>3</sub>F was explored finding 28 isomer structures with relative energy within 50 kJ $\cdot$ mol<sup>-1</sup>.

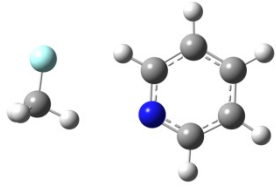
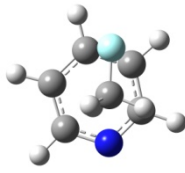
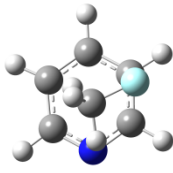
Three real minima isomer geometries, according to frequency calculations at the MP2/6-311++G(d,p) level, have been determined, whose relative energies, at the equilibrium point, are within 5 kJ $\cdot$ mol<sup>-1</sup>.

The rotational constants of those structures as well as the quadrupole coupling constants and the dipole moment components are reported in Table 32.

The most stable isomer, according the zero point corrected energy, is a C<sub>s</sub>,  $\sigma$ -type one ( $\sigma$ -I) where the two subunits are linked by a C-H $\cdots$ N and a C-H $\cdots$ F-C WHBs, while the about 200 cm<sup>-1</sup> higher energy isomers ( $\pi$ -I and  $\pi$ -II) than the most stable one, are  $\pi$ -type showing the C-H $\cdots$   $\pi$  interaction.

Furthermore, the evaluation of the dissociation energies has been performed by taking into the

account the BSSE using the counterpoise procedure.

	$\sigma$ -I	$\pi$ -I	$\pi$ -II
			
$A/\text{MHz}$	4813	2879	2927
$B/\text{MHz}$	835	1272	1280
$C/\text{MHz}$	715	1233	1223
$\chi_{aa}/\text{MHz}$	-2.91	1.94	2.86
$\chi_{bb}-\chi_{cc}/\text{MHz}$	-3.76	-5.04	-4.20
$\mu_a/\text{D}$	-2.05	-0.29	0.91
$\mu_b/\text{D}$	0.64	0.69	0.81
$\mu_c/\text{D}$	0.00	0.39	-2.01
$\Delta E/\text{cm}^{-1}$	6	13	0 <sup>a</sup>
$\Delta E_0/\text{cm}^{-1}$	0 <sup>b</sup>	211	217
$E_D/\text{kJ}\cdot\text{mol}^{-1}$	7.47	1.45	1.36

<sup>a</sup>Absolute energy= -387.062408  $E_h$ . <sup>b</sup>Absolute energy zero point corrected= -386.934122  $E_h$ .

**Table 32.** Ab initio shapes and spectroscopic parameters of the three most stable conformers of Py-FMET. (L. Spada, Q. Gou, M. Vallejo-López, A. Lesarri, E. J. Cocinero, W. Caminati. *Phys. Chem. Chem. Phys.*, 2014, 16, 2149-2153 - Reproduced by permission of the PCCP Owner Societies).

## Experimental Section

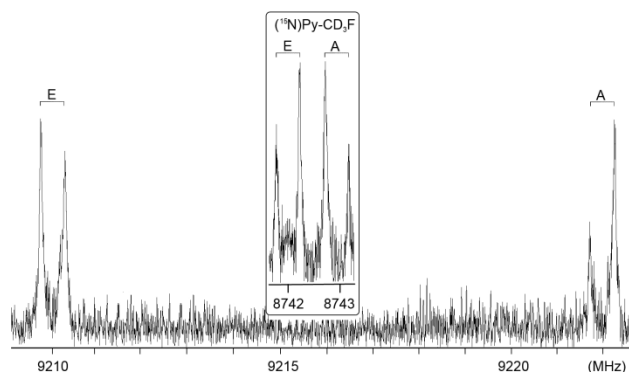
The 1% gas mixture of  $\text{CH}_3\text{F}$  in Helium at stagnation pressure of 3 bars was flowing over the PYR sample kept at 273 K and expanded into the cavity of the Bologna PJ-FTMW and, later on, also the PYR- $\text{CD}_3\text{F}$  and ( $^{15}\text{N}$ )PYR- $\text{CH}_3\text{F}$  have been formed in the same way using, respectively, a 99% enriched  $\text{CD}_3\text{F}$  and a 98% enriched ( $^{15}\text{N}$ )PYR samples.

Following the predictions of Table 32, the  $\mu_a$ -type transitions of isomer  $\sigma$ -I were first searched, observing around 7713.6 MHz and 13 MHz below, the typical pattern due to the presence of  $^{14}\text{N}$  ( $I = 1$ ) quadrupole coupling within the  $A$  and  $E$  states, respectively (methyl  $V_3$  barrier internal rotation), for the  $5_{05} \leftarrow 4_{04}$  transition.

Later on, several others  $\mu_a$ -type and  $\mu_b$ -type  $R$ -branch lines have been fitted using the XIAM program with the Watson's  $S$  reduced semirigid-rotor Hamiltonian ( $I^r$  representation) for the PYR-

CH<sub>3</sub>F and then the same procedure has been performed for PYR-CD<sub>3</sub>F, (<sup>15</sup>N)PYR-CH<sub>3</sub>F and (<sup>15</sup>N)PYR-CD<sub>3</sub>F isotopologues.

In Figure 15 is shown the 6<sub>06</sub>←5<sub>05</sub> transitions for the latter two species, comparing the different splittings due to -CH<sub>3</sub> group internal rotation in absence of the quadrupolar coupling because <sup>15</sup>N has nuclear spin  $I=1/2$ .



**Figure 15.** Comparison of the different splittings due to internal rotation for the 6<sub>06</sub>←5<sub>05</sub> transitions of the PYR(<sup>15</sup>N)-CH<sub>3</sub>F and PYR(<sup>15</sup>N)-CD<sub>3</sub>F isotopologues because of the different reduced mass of the motion. (L. Spada, Q. Gou, M. Vallejo-López, A. Lesarri, E. J. Cocinero, W. Caminati. Phys. Chem. Chem. Phys., 2014, 16, 2149-2153 - Reproduced by permission of the PCCP Owner Societies).

The results are reported in Table 33 containing also the fitted values for the  $V_3$  barrier, the angles between the internal rotation axes with the principal axes system ( $\angle(i,g)$ ,  $g = a, b, c$ ) and the moment of inertia for the -CH<sub>3</sub> group ( $I_\alpha$ ).

	Py-CH <sub>3</sub> F	Py( <sup>15</sup> N)-CH <sub>3</sub> F	Py-CD <sub>3</sub> F	Py( <sup>15</sup> N)-CD <sub>3</sub> F
A/MHz	4833.0493(5) <sup>a</sup>	4807.142(2)	4620.377(2)	4598.017(1)
B/MHz	835.9621(2)	835.9118(2)	789.9878(7)	789.875(1)
C/MHz	716.6834(2)	716.0581(1)	681.1657(2)	680.5990(1)
D <sub>J</sub> /kHz	0.369(1)	[0.369] <sup>b</sup>	0.309(1)	[0.309]
D <sub>JK</sub> /kHz	3.99(1)	[3.99]	3.41(3)	[3.41]
d <sub>1</sub> /kHz	-0.0587(8)	[-0.0587]	-0.045 (1)	[-0.045]
d <sub>2</sub> /kHz	-0.0133(5)	[-0.0133]	-0.008(3)	[-0.008]
χ <sub>aa</sub> /MHz	-2.945(9)	-	-3.11(2)	-
χ <sub>bb</sub> -χ <sub>cc</sub> /MHz	-3.740(8)	-	-3.67(1)	-
V <sub>3</sub> /cm <sup>-1</sup>	123.819(3)	129.834(5)	133.4(2)	134.0(4)
I <sub>α</sub> /uÅ <sup>2c</sup>	3.402	3.248	6.496	6.496
∠(i,a)/°	88.03(1)	88.08(1)	87.22(1)	86.7(2)
N <sup>d</sup>	168	28	114	28
σ/kHz <sup>e</sup>	3.7	2.4	3.3	2.5

<sup>a</sup>Error in parentheses in units of the last digit. <sup>b</sup>Values in brackets fixed to the corresponding value of the parent species. <sup>c</sup>Fixed to the values for the CH<sub>3</sub>F or CD<sub>3</sub>F molecules. <sup>d</sup>Number of lines in the fit. <sup>e</sup>Root-mean-square deviation of the fit.

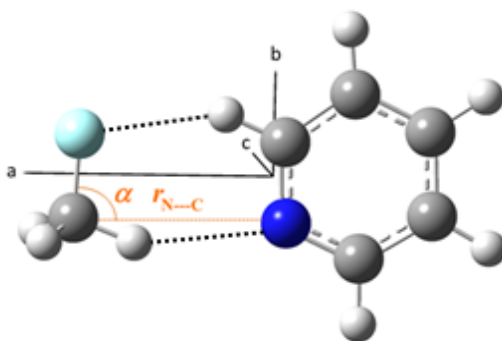
**Table 33.** Rotational and internal rotation parameters for the observed  $\sigma$ -I isomer of four isotopologues. (L. Spada, Q. Gou, M. Vallejo-López, A. Lesarri, E. J. Cocinero, W. Caminati. *Phys. Chem. Chem. Phys.*, 2014, 16, 2149-2153 - Reproduced by permission of the PCCP Owner Societies).

No signals due to the other isomers have been detected suggesting a kinetic relaxation upon supersonic expansion toward isomer ( $\sigma$ -I).

### Structural Information

A partial  $r_0$  structure has been calculated by fitting two parameters (the others are fixed to their *ab initio* values) involving in the WHBs linking isomer I of PYR-CH<sub>3</sub>F C<sub>s</sub> isomer  $\sigma$ -I: the C...N distance ( $r_{N...C}$ ) between the carbon of CH<sub>3</sub>F and nitrogen of pyridine and the angle ∠F-C...N ( $\alpha$ ) as reported in Figure 16. The results of the  $r_0$  fitting are reported in Table 34 together with the *ab initio* ones. The experimental rotational constants of the four isopologues have been reproduced within few MHz.





**Figure 16.** Molecular structure, WHB parameters along the principal axes of inertia for PYR-CH<sub>3</sub>F.

	$r_{N...C}/\text{\AA}$	$\alpha/^\circ$
$r_0$	3.592(6) <sup>a</sup>	81.6(5) <sup>a</sup>
$r_e$	3.521	87.7

<sup>a</sup>Error in parentheses in units of the last digit.

**Table 34.** The  $r_0$  and  $r_e$  calculated  $r_{N...C}$  distance and  $\alpha$  angle of isomer  $\sigma$ -I of PYR-CH<sub>3</sub>F. (L. Spada, Q. Gou, M. Vallejo-López, A. Lesarri, E. J. Cocinero, W. Caminati. *Phys. Chem. Chem. Phys.*, 2014, 16, 2149-2153 - Reproduced by permission of the PCCP Owner Societies).

In going from the PYR-CH<sub>3</sub>F to the PYR-CF<sub>3</sub>H, the C-H...F and C-H...N distances deriving from the  $r_0$  structures follow the opposite trend (2.37 Å and 2.67 Å, respectively for PYR-CH<sub>3</sub>F vs 2.70 Å and 2.32 Å for PYR-CF<sub>3</sub>H). This observation, together with the internal rotation motion around the C-F bond in PYR-CH<sub>3</sub>F ( $V_3 = 1.55 \text{ kJ}\cdot\text{mol}^{-1}$ ) and around C-H in PYR-CF<sub>3</sub>H ( $V_3 = 0.572 \text{ kJ}\cdot\text{mol}^{-1}$ )<sup>39</sup> suggests that the C-H...F and C-H...N interactions have different strengths in the two complexes, in agreement with the lower acidity value of the hydrogens in the CH<sub>3</sub>F group and vice versa. This implicates the destroying and the re-forming of the C-H...F and C-H...N contacts, respectively, undergoing a internal rotation motions.

The position of the N atom ( $r_s$ ) within the principal axes system of the (<sup>14</sup>N)PYR-CH<sub>3</sub>F has been calculated using the Kraitchman's equations, whose results are compared in Table 35 with the *ab initio* ones ( $r_e$ ), confirming the correct isomer assignment.

	$r_s$	$r_e$
$a/\text{Å}$	$\pm 0.236(6)^a$	-0.227
$b/\text{Å}^b$	$\pm 0.753(2)$	0.767

<sup>a</sup>Error in parentheses in units of the last digit. <sup>b</sup>The  $c$ -coordinates are zero by symmetry.

**Table 35.** The N atom substitution and *ab initio* coordinates along the principal axes of inertia of the (<sup>14</sup>N)PYR- CH<sub>3</sub>F isotopologue. (L. Spada, Q. Gou, M. Vallejo-López, A. Lesarri, E. J. Cocinero, W. Caminati. Phys. Chem. Chem. Phys., 2014, 16, 2149-2153 - Reproduced by permission of the PCCP Owner Societies).

## Dissociation Energy

Assuming to be valid the equation 1.61 and 1.62, the estimation of the dissociation energy for PYR-CH<sub>3</sub>F complex is performed, resulting be equal to 11.4 kJ·mol<sup>-1</sup> ( $k_s = 6.4 \text{ N}\cdot\text{m}^{-1}$  and  $R_{\text{CM}} = 4.64 \text{ Å}$ ) quite similar to the *ab initio* predicted one (7.9 kJ·mol<sup>-1</sup>) and to the value for the PYR-CF<sub>3</sub>H (14.9 kJ·mol<sup>-1</sup>) and PYR-CF<sub>4</sub> (10.6 kJ·mol<sup>-1</sup>)<sup>40</sup> molecular systems.

## 3.2.5 Pyridine – Difluoromethane

### Introduction

The pyridine – difluoromethane (PYR-CH<sub>2</sub>F<sub>2</sub>) complex is the intermediate adduct in going from the pyridine-CH<sub>4</sub> to pyridine-CF<sub>4</sub><sup>40</sup> one, according to the number of substituted hydrogen atoms replacing by fluorines.

The features of all the other possible adducts having PYR as a chemical partner either have been previously described in this thesis (PYR- CH<sub>4</sub>, PYR- CH<sub>3</sub>F) or have been already reported in literature (PYR- CF<sub>4</sub>, PYR- CHF<sub>3</sub>).

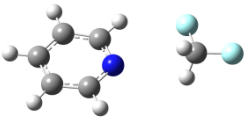
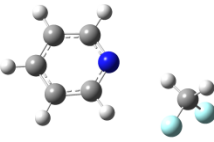

Hence, the PYR-CH<sub>2</sub>F<sub>2</sub> complex rotational study comes full circle for a complete understanding of the effects of the fluorine substitution with respect to the shape of molecular adduct between freons and pyridine.

### Theoretical Calculations

The *ab initio* calculations, at the MP2/6-311++G(d,p), of the 62 structures resulting by Molecular Mechanics<sup>17</sup> exploration of the possible isomers for the PYR-CH<sub>2</sub>F<sub>2</sub> complex, have been found to converge towards three real minima (all positive calculated frequencies) isomers with relative energies below 5 kJ·mol<sup>-1</sup>.

The resulting rotational parameters necessary for the rotational spectrum assignment are reported in Table 36 together with the equilibrium and the dissociation energies, these latter evaluated taking into the account the BSSE corrections. The isomer I is the most stable one, showing a bifurcated C-

H $\cdots$ N interaction together with a C-H $\cdots$ F contact, while for the remaining ones, they are linked by one C-H $\cdots$ N WHB and either a C-H $\cdots$ F (isomer II) or a C-H $\cdots$  $\pi$  (isomer III) contact.

	I	II	II
			
A/MHz	4407	3799	2383
B/MHz	587	590	891
C/MHz	520	532	838
$\chi_{aa}$ /MHz	-4.34	-3.65	3.07
$\chi_{bb}-\chi_{cc}$	-2.34	-2.32	6.09
$\mu_a$ /D	-4.2	-3.4	2.6
$\mu_b$ /D	-0.7	-0.4	-0.4
$\mu_c$ /D	0.0	-0.9	-1.5
$\Delta E$ /kJ $\cdot$ mol $^{-1}$	0.0 <sup>a</sup>	0.5	1.1
$E_D$ /kJ $\cdot$ mol $^{-1}$	11.8 <sup>b</sup>	10.5	3.8

<sup>a</sup>Absolute energy is -486.151117 E<sub>h</sub>. <sup>b</sup>Dissociation energy.

**Table 36.** *Ab initio* rotational and quadrupole constants together with the dipole moment components, the equilibrium and dissociation energies for three isomers of PYR-CH<sub>2</sub>F<sub>2</sub>. (Reprinted from Chemical Physics Letters, 591, Montserrat Vallejo-López, Lorenzo Spada, Qian Gou, Alberto Lesarri, Emilio J. Cocinero, Walther Caminati, Interactions between freons and aromatic molecules: The rotational spectrum of pyridine-difluoromethane, 216-219, Copyright (2014), with permission from Elsevier).

## Experimental Section

A 5% of CH<sub>2</sub>F<sub>2</sub> mixture with Helium at stagnation pressure of 3 bars was flown on PYR and later on (<sup>15</sup>N)PYR, kept at 273 K using ice and expanded into the cavity of the Bologna PJ-FTMW spectrometer.

The rotational spectrum search started with the scan for the  $\mu_a$ -type *R*-branch transitions of isomer I, the most stable according to the *ab initio* calculations, whose this dipole moment component is predicted be the strongest. Three component lines, due to the <sup>14</sup>N atom (*I* = 1) presence, around 8701.7 MHz have been first observed, corresponding to the 8<sub>08</sub> $\leftarrow$ 7<sub>07</sub> transition.

Later on, several other  $\mu_a$ -type and  $\mu_b$ -type transitions have been measured and fitted using SPFIT Pickett's program within the Watson's *S* reduction in the *I'* representation. No  $\mu_c$ -type lines have been observed in agreement with the C<sub>s</sub> symmetry of isomer I.

The results are reported in Table 37 together with those ones for the ( $^{15}\text{N}$ )PYR-  $\text{CH}_2\text{F}_2$  isotopologue ( $I(^{15}\text{N}) = 1/2$ ) for which the same described procedure has been performed.

	PYR- $\text{CH}_2\text{F}_2$	( $^{15}\text{N}$ )PYR- $\text{CH}_2\text{F}_2$
$A/\text{MHz}$	4393.207(2) <sup>a</sup>	4385.178(3)
$B/\text{MHz}$	580.9088(3)	580.6661(5)
$C/\text{MHz}$	515.4690(2)	515.1720(3)
$\chi_{aa}/\text{MHz}$	-4.16(3)	-
$\chi_{bb}-\chi_{cc}/\text{MHz}$	-2.4(2)	-
$q/\text{MHz}$	3.29(2)	-
$D_J/\text{kHz}$	0.1458(9)	0.137(2)
$D_{JK}/\text{kHz}$	2.166(6)	2.17(2)
$d_1/\text{Hz}$	-8.0(9)	-8(1)
$d_2/\text{Hz}$	-1.9(2)	-1.8(3)
$N^b$	113	36
$\sigma^c/\text{kHz}$	0.6	0.7

<sup>a</sup>Error in units of the last digit. <sup>b</sup>Number of lines in the fit. <sup>c</sup>Root-mean-square deviation of the fit.

**Table 37.** The fitted parameters of isomer I of the PYR- $\text{CH}_2\text{F}_2$  complex. (Reprinted from Chemical Physics Letters, 591, Montserrat Vallejo-López, Lorenzo Spada, Qian Gou, Alberto Lesarri, Emilio J. Cocinero, Walther Caminati, Interactions between freons and aromatic molecules: The rotational spectrum of pyridine-difluoromethane, 216-219, Copyright (2014), with permission from Elsevier).

## Structural Information

The nitrogen position along the principal axes of inertia of the most abundant isopologue has been determined using the Kraitchmann's method ( $r_s$ ). The substitution coordinates are compared in Table 38 with those ones from *ab initio* calculations ( $r_e$ ). Their respectively values are a further confirmation, with also the matching of the rotational and quadrupolar constants, of the corrected isomer assignment.

	$a$	$b$
$r_s$	$\pm 0.602(3)$	$\pm 0.456(3)$
$r_e$	-0.590	-0.437

**Table 38.** The  $r_s$  and  $r_e$  nitrogen coordinates along the principal axes of inertia of the most abundant species. (Reprinted from Chemical Physics Letters, 591, Montserrat Vallejo-López, Lorenzo Spada, Qian Gou, Alberto Lesarri, Emilio J. Cocinero, Walther Caminati, Interactions between freons and aromatic molecules: The rotational spectrum of pyridine-difluoromethane, 216-219, Copyright (2014), with permission from Elsevier).

The  $\text{N}\cdots\text{C}$  distance ( $r_{\text{N}\cdots\text{C}}$ ) and the  $\angle\text{F-C}\cdots\text{N}$  angle of the MP2 calculated structure have been fitted, keeping fixed the other ones to their *ab initio* values, to reproduce, within 0.5 MHz error, the experimental rotational constants of the two isopologues. The results are reported in Table 39

together with the derived parameters of the C-H...N and C-H...F distances, which described the WHB interactions, for the PYR-CH<sub>2</sub>F<sub>2</sub>.

Fitted parameters		
	$R_{N...C} / \text{Å}$	$\alpha / ^\circ$
$r_0$	3.151(1)	84.9(1)
$r_e$	3.124	84.3
Derived WHB parameters		
	$R_{C-H...N} / \text{Å}$	$R_{C-H...F} / \text{Å}$
$r_0$	2.873	2.569

**Table 39.** The  $r_0$  and  $r_e$  fitted parameters and the derived parameters involved in the WHBs for PYR-CH<sub>2</sub>F<sub>2</sub>. (Reprinted from Chemical Physics Letters, 591, Montserrat Vallejo-López, Lorenzo Spada, Qian Gou, Alberto Lesarri, Emilio J. Cocinero, Walther Caminati, Interactions between freons and aromatic molecules: The rotational spectrum of pyridine-difluoromethane, 216-219, Copyright (2014), with permission from Elsevier).

### Dissociation Energy

According to equation 1.61 and 1.62 the dissociation energy of the PYR-CH<sub>2</sub>F<sub>2</sub> isomer I complex results be 15.6 kJ·mol<sup>-1</sup>.

## 3.2.6 Indane – Trifluoromethane

### Introduction

Up to now, the molecular adduct which I have described are linked by WHBs of the C-H...Cl-C, C-H...F-C, C-H...N type, for which the geometrical features, the dissociation energies and the observable internal dynamics have been characterized.

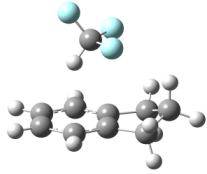
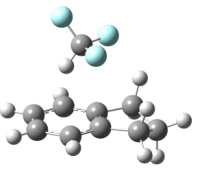
In this study, the features of the C-H... $\pi$  interaction together with the C-H...F contacts, taking place in the Indane- CHF<sub>3</sub> complex<sup>42</sup>, are investigated.

The main goals of the present adduct are the obtaining of information on:

- 1) The isomer preference towards either *Z* or *E* configuration of the Indane with respect to the CHF<sub>3</sub>.
- 2) The  $V_3$  barrier value of the CHF<sub>3</sub> internal rotation, in order to compare with the  $V_3 \approx 0$  and  $V_6 = 0$  internal rotation of CHF<sub>3</sub> in the C-H... $\pi$  linked benzene-CHF<sub>3</sub><sup>43</sup> adduct, since the C-H...F contacts taking place can significantly increase its value.
- 3) The plausible reverse Ubbelohde effect<sup>5</sup> which can take place upon the H→D substitution in the CHF<sub>3</sub> as previously found for the benzene-DCF<sub>3</sub> adduct<sup>44</sup>.

## Theoretical Calculations

The calculations for the  $C_s$  symmetry  $Z$  and  $E$  isomers (according to the  $-CH_2$  apex position, which is located within the  $C_s$  symmetry plane) have been performed at the MP2/6-311++G(d,p) level by using the GAUSSIAN 09 package. Both the isomer are linked by a  $C-H\cdots\pi$  interaction but with a different number of  $C-H\cdots F$  contacts: four in the case of  $Z$  isomer and two in highest energy  $E$  isomer. The rotational parameters, the dipole moment components and the relative energies ( $\Delta E$ ) with also the ones including the zero point corrections ( $\Delta E_0$ ) and the dissociation energies ( $E_D$ ) which are BSSE corrected, are reported in Table 40 for the respectively optimized isomer structures.

	<i>Z</i>	<i>E</i>
		
$A/\text{MHz}$	938	964
$B/\text{MHz}$	674	634
$C/\text{MHz}$	546	527
$ \mu_a /\text{D}$	2.1	2.1
$ \mu_b /\text{D}$	0.6	0.8
$\Delta E/\text{kJmol}^{-1}$	0.0 <sup>a</sup>	1.0
$\Delta E_0/\text{kJmol}^{-1}$	0.0 <sup>b</sup>	0.9
$E_D/\text{kJmol}^{-1}$	11.7	11.4

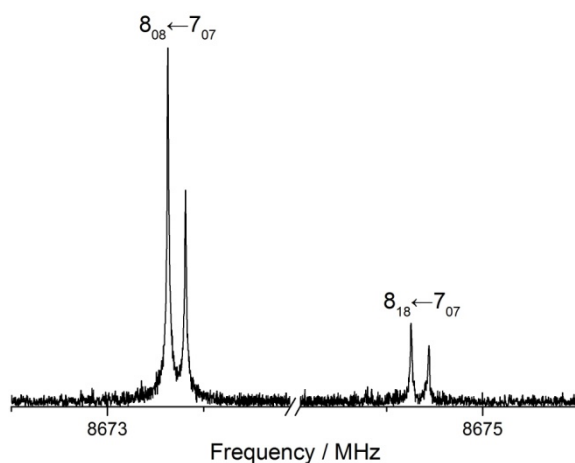
<sup>a</sup>Absolute energy =  $-685.636923 E_h$ . <sup>b</sup>Absolute energy =  $-685.445575 E_h$ .  $\mu_c$  is zero by symmetry.

**Table 40.** The rotational parameters, the dipole moment components and the energies calculated for the two isomers of Indane- $CHF_3$ . (Reused with permission from Laura B. Favero, Weixing Li, Lorenzo Spada, Luca Evangelisti, Giorgio Visentin, Walther Caminati. The Cage Structure of Indan- $CHF_3$  is Based on the Cooperative Effects of  $C-H\cdots\pi$  and  $C-H\cdots F$  Weak Hydrogen Bonds. *Chem. Eur. J.* 2015, 21, 15970 – 15973 © 2015 Wiley-VCH Verlag GmbH & Co. KGaA, Weinheim).

## Experimental Section

The 1:1 complex between Indane and  $CHF_3$  was obtained by flowing a 0.5% gas mixture of  $CHF_3$  and, later on  $CDF_3$ , in Helium at stagnation pressure of 2 bars, over Indane, heated at 323 K, and expanded into the cavity of the Bologna PJ-FTMW spectrometer.

According to Table 40, the rotational spectrum recording started with the search of the  $\mu_a$ -type transitions for isomer *Z* whose  $8_{08} \leftarrow 7_{07}$  line has been found around 8673 MHz. After this first assignment, other  $\mu_a$ -type and, later on,  $\mu_b$ -type transition have been measured and fitted by using the SPFIT Pickett's program within the Watson's S reduction in the  $I'$  representation (see Figure 17).



**Figure 17.** The rotational  $8_{08} \leftarrow 7_{07}$  and  $8_{18} \leftarrow 7_{07}$  transitions of the Indane-  $\text{CHF}_3$  and Indane-  $\text{CDF}_3$ , respectively. (Reused with permission from Laura B. Favero, Weixing Li, Lorenzo Spada, Luca Evangelisti, Giorgio Visentin, Walther Caminati. The Cage Structure of Indan- $\text{CHF}_3$  is Based on the Cooperative Effects of  $\text{C-H}\cdots\pi$  and  $\text{C-H}\cdots\text{F}$  Weak Hydrogen Bonds. *Chem. Eur. J.* 2015, 21, 15970 – 15973 © 2015 Wiley-VCH Verlag GmbH & Co. KGaA, Weinheim).

No line belonging to the  $\mu_c$  dipole moment component have been observed, confirming the  $C_s$  symmetry of the isomer *Z*.

Later on, the same procedure has been followed for the assignment of the rotational spectrum of the Indane- $\text{CDF}_3$  *Z* isomer.

The results from the fittings are reported in Table 41. The comparison between the *ab initio* and the fitted values of the rotational constants and of the ratio  $\mu_a/\mu_b$  deriving from intensity measurements confirm the right assignment. The search of *E* isomer failed plausibly because of the relaxation processes taking place upon supersonic expansion conditions.

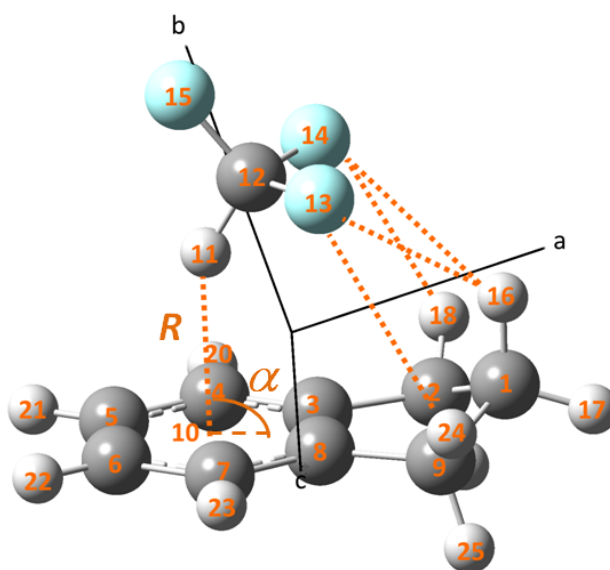
	Indane-CHF <sub>3</sub>	Indane-CDF <sub>3</sub>
<i>A</i> /MHz	940.9516(3) <sup>a</sup>	940.0022(8)
<i>B</i> /MHz	648.7726(2)	648.2286(6)
<i>C</i> /MHz	528.7273(1)	528.0866(4)
<i>D<sub>I</sub></i> /kHz	0.1807(6)	0.180(2)
<i>D<sub>JK</sub></i> /kHz	0.464(5)	0.450(1)
<i>D<sub>K</sub></i> /kHz	-0.598(6)	-0.579(1)
<i>d<sub>1</sub></i> /kHz	-0.0363(4)	-0.037(2)
<i>d<sub>2</sub></i> /kHz	-0.0046(3)	-0.0044(8)
$\sigma^b$ /kHz	1.7	1.3
N <sup>c</sup>	105	45

<sup>a</sup>Errors in units of the last digit. <sup>b</sup>Standard deviation of the fit. <sup>c</sup>Number of fitted transitions.

**Table 41.** The experimental results for the two isotopologues Indane-CHF<sub>3</sub> and Indane-CDF<sub>3</sub> of the *Z* isomer. (Reused with permission from Laura B. Favero, Weixing Li, Lorenzo Spada, Luca Evangelisti, Giorgio Visentin, Walther Caminati. The Cage Structure of Indan-CHF<sub>3</sub> is Based on the Cooperative Effects of C-H $\cdots$  $\pi$  and C-H $\cdots$ F Weak Hydrogen Bonds. *Chem. Eur. J.* 2015, 21, 15970 – 15973 © 2015 Wiley-VCH Verlag GmbH & Co. KGaA, Weinheim).

## Structural Information

A partial  $r_0$  structure has been obtained by fitting the *R* distance and the angle  $\alpha$  (see Figure 18), keeping the other fixed to their *ab initio* values, reproducing the Indane-CHF<sub>3</sub> experimental rotational constants within 0.5 MHz since the much larger error in the Indane-CDF<sub>3</sub> than the 0.5 MHz in the parent species, suggests the occurring of the reverse Ubbelohde effect.



**Figure 18.** The *Z* isomer of the Indane-CHF<sub>3</sub> complex showing the WHB contacts.



The comparison between the  $r_0$  and  $r_e$  results is reported in Table 42.

	$R/\text{\AA}$	$\alpha/^\circ$
$r_0$	2.39(1) <sup>a</sup>	91.8(6)
$r_e$	2.317	90.8

<sup>a</sup>Error in parentheses in units of the last digit.

**Table 42.** Comparison between the  $r_0$  and  $r_e$  results for the  $R$  and the  $\alpha$  angle. The derived distances involved in the C-H...F WHBs are also reported. (Reused with permission from Laura B. Favero, Weixing Li, Lorenzo Spada, Luca Evangelisti, Giorgio Visentin, Walther Caminati. The Cage Structure of Indane-CHF<sub>3</sub> is Based on the Cooperative Effects of C-H... $\pi$  and C-H...F Weak Hydrogen Bonds. *Chem. Eur. J.* 2015, 21, 15970 – 15973 © 2015 Wiley-VCH Verlag GmbH & Co. KGaA, Weinheim).

From the fitting, the values of the four (C)-H...F distances, identical two by two, are 3.31 Å and 3.05 Å.

The reverse Ubbelohde effect has been found occurring upon the H→D substitution in the Indane-CHF<sub>3</sub> complex since a shrinkage of 2.5 mÅ of the  $R$  distance has to be taken into the account to reproduce the differences in the planar moment of inertia ( $P_{gg} = \sum_i m_i g_i^2$ , with  $g = a, b, c$ ) along the  $a$ -axes, resulting from the *ab initio* and from the experimental rotational constants of the Indane-CHF<sub>3</sub> and of the Indane-CDF<sub>3</sub>.

### Dissociation Energy

According to equation 1.61 and 1.62 the dissociation energy of the Indane-CHF<sub>3</sub> has been estimated be 11.2 kJ·mol<sup>-1</sup> ( $k_s = 9.6 \text{ N}\cdot\text{m}^{-1}$ ,  $R_{\text{CM}} = 3.59 \text{ \AA}$ ) whose value is similar to that in the benzene-CHF<sub>3</sub> (8.4 kJ·mol<sup>-1</sup>) which, however undergoes to a free internal rotation motion ( $V_3 \approx 0$  and  $V_6 = 0$ ) with respect to a  $V_3 > 0.70 \text{ kJ}\cdot\text{mol}^{-1}$  for Indane-CHF<sub>3</sub> according to the not observed splitting of the rotational transitions.

### 3.2.7 Conclusions

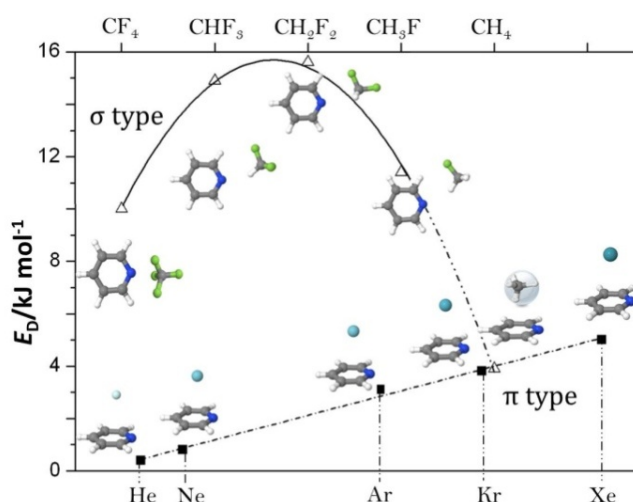
The features of the C-H...F-C and C-H...Cl-C WHBs have been characterized in the CH<sub>2</sub>F<sub>2</sub>-CH<sub>2</sub>ClF and in the CH<sub>2</sub>F<sub>2</sub>-CH<sub>2</sub>Cl<sub>2</sub> adducts, showing that when a competition between the aforementioned types of interactions is possible, the largest number of C-H...Cl-C contacts is observed.

The C---C distance in going from the CH<sub>2</sub>F<sub>2</sub>-CH<sub>2</sub>F<sub>2</sub> to CH<sub>2</sub>F<sub>2</sub>-CH<sub>2</sub>ClF to CH<sub>2</sub>F<sub>2</sub>-CH<sub>2</sub>Cl<sub>2</sub>

increase of about 0.1 Å for each addition of a chlorine atom.

Their typical length ranges are around 3 Å with respect to the 2.5 – 2.9 Å distances usually observed for the C-H...F-C interactions, both showing an estimated WHB energy of about 2 kJ·mol<sup>-1</sup>.

Pyridine adduct series with methane and mono- and di-fluoromethane display that the fluorine substitution causes the changing of shape from the π-type of methane to the σ-type for the mono- and di-fluoromethane. The observed WHBs are of the C-H...N, C-H...π, and C-H...F contacts, determining complex dissociation energies which are plotted in Figure 19 together with those of the pyridine-rare gas ones. According to these estimated values, methane (which is a spherical rotor), displays a simil-rare gas behavior.



**Figure 19.** The dissociation energies of the rare gases, fluoromethane derivatives and methane complexes with pyridine suggesting the simil-rare gas behaviour of methane. (Q. Gou, L. Spada, M. Vallejo-López, A. Lesarri, E. J. Cocinero and W. Caminati, *Phys. Chem. Chem. Phys.*, 2014, 16, 13041 - Reproduced by permission of the PCCP Owner Societies).

In Indane-CHF<sub>3</sub> two WHB types are observed: the C-H...π and the C-H...F ones. The large number of these latter, taking place in isomer *Z* than in isomer *E*, determine the lowest energy of the former isomer. The reverse Ubbelohde effect is also observed upon the H→D substitution in the CHF<sub>3</sub>, consisting in the shrinkage of 2.5 mÅ in the C-H...π distance whose effect has a similar value of that one determined in the benzene-CDF<sub>3</sub> complex (4.4 mÅ)<sup>41</sup>.

## 3.3 HALOGEN BONDING

### 3.3.1 Chlorotrifluoromethane - Fluoromethane

#### Introduction

Halogen bond (HaB), a relatively recent discovered interaction<sup>45</sup>, is involved in many fields such as liquid crystal formation<sup>46</sup>, recognition processes<sup>47</sup>, medicinal chemistry and chemical biology<sup>48</sup> and many others.

In this respect, the rotational spectroscopy studies of single halogen bond connections provide useful information to better understand the behavior of this interaction because of, also, the free environment conditions which the supersonic expansion allow.


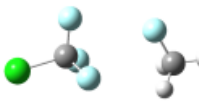
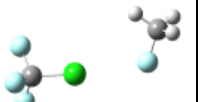
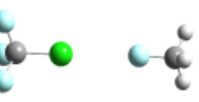
I am describing here, following the previous investigations on the C-Cl...O<sup>49,50</sup> and C-Cl...N<sup>51</sup> HaBs, the CF<sub>3</sub>Cl...FCH<sub>3</sub> complex, showing how the C-Cl...F HaB is preferred to the C-H...F and to the C-H...Cl WHB interactions in forming the molecular adduct, discussing, also, why the predicted (at the MP2/6-311++G(d,p) level) A constant is enormously different from the experimental one<sup>52</sup>.

#### Theoretical Calculations

The C-H...F and C-H...Cl WHB and C-Cl...F HaB contacts are the possible interactions linking the two subunits of the CF<sub>3</sub>Cl...FCH<sub>3</sub>. According to molecular mechanics<sup>17</sup> calculations, about 100 different isomers within 15 kJ mol<sup>-1</sup> relative energy have been found.

The MP2/6-311++G(d,p) optimizations and frequency calculations of these structures determined be four the stable isomers, which are reported in Table 43, together with their respectively rotational parameters necessary to drive the rotational spectrum search as well as the dissociation energies.

A different stability trend is found according to which kind of corrections (BSSE or zero point) is followed: taking into the account the BSSE one, halogen bonded isomer IV is the most stable, while according to the zero point energy correction, isomer I has the lowest energy, involving one C-Cl...F HaB and two weak C-H...F hydrogen bonds.

	I	II	III	IV
				
$A/\text{MHz}$	3028	4708	4788	5512
$B/\text{MHz}$	1256	976	691	611
$C/\text{MHz}$	1058	948	678	611
$\mu_a/\text{D}$	-0.9	0.2	-1.6	-3.2
$\mu_b/\text{D}$	-0.1	-1.2	-1.8	0.0
$\mu_c/\text{D}$	1.2	1.4	1.0	0.0
$\chi_{aa}/\text{MHz}$	37.4	-69.9	-70.2	-74.3
$(\chi_{bb}-\chi_{cc})/\text{MHz}$	-109.9	-0.7	-4.2	0.0
$\chi_{ab}/\text{MHz}$	-10.2	-18.2	20.3	0.0
$\chi_{ac}/\text{MHz}$	0.1	-0.5	-0.4	0.0
$\chi_{bc}/\text{MHz}$	1.7	-0.1	0.0	0.0
$\Delta E/\text{kJ mol}^{-1}$	0.0 <sup>a</sup>	0.9	1.0	1.3
$\Delta E_0/\text{kJ mol}^{-1}$	0.0 <sup>b</sup>	1.2	0.7	0.5
$\Delta E_{\text{BSSE}}/\text{kJ mol}^{-1}$	2.7	3.6	0.3	0.0 <sup>c</sup>
$E_{\text{D}}^{\text{d}}/\text{kJ mol}^{-1}$	1.8	0.8	4.2	4.5

<sup>a</sup>Absolute energy = -936.076714  $E_{\text{h}}$ . <sup>b</sup>Absolute energy zero point corrected = -936.113783  $E_{\text{h}}$ .

<sup>c</sup>Absolute energy BSSE corrected = -936.130914  $E_{\text{h}}$ . <sup>d</sup>Dissociation energy.

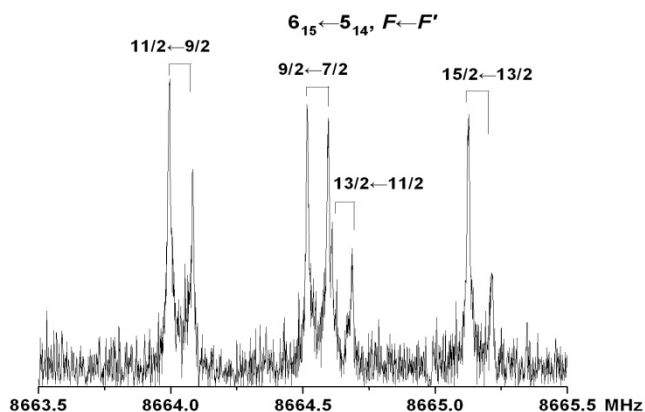
**Table 43.** The *ab initio* values for the four isomers calculated at the MP2/6-311++G(d,p) level for the  $\text{CF}_3\text{Cl}-\text{CH}_3\text{F}$  adduct. (Reprinted with permission from: Gou, Q.; Spada, L.; Cocinero, E. J.; Caminati, W. Halogen–Halogen Links and Internal Dynamics in Adducts of Freons. *J. Phys. Chem. Lett.* 5, 1591 (2014). Copyright {2014} American Chemical Society).

## Experimental Section

The 1:1 gas mixture of  $\text{CF}_3\text{Cl}-\text{CH}_3\text{F}$  and later on of  $\text{CF}_3\text{Cl}-\text{CD}_3\text{F}$  at the 1% in Helium at stagnation pressure of 5 bars has been expanded into the cavity of the Bologna PJ-FTMW spectrometer.

A large scan search for the rotational spectra of  $\text{CF}_3\text{Cl}-\text{CH}_3\text{F}$  isomers has been performed since their relative energy values are really close.

Two lines around 8585.1 and 8586.0 MHz were found, instead of the expected four component transitions typical of the chlorine quadrupole hyperfine structure coupling (both  $^{35}\text{Cl}$  and  $^{37}\text{Cl}$  have  $I = 3/2$ ). The hypothesis of the overlapping between two couples of quadrupole components was confirmed assigning the observed transition to the  $6_{06}\leftarrow 5_{05}$  one of the isomer III of  $\text{CF}_3(^{35}\text{Cl})-\text{CH}_3\text{F}$  and measuring the higher  $J$  transition with  $\Delta K_{-1} = 0$  showing the same pattern. Then, several others  $\mu_a$ -type lines have been measured displaying, as in the case of the  $6_{15}\leftarrow 5_{14}$  transition in Figure 20, four components for the  $\Delta F = 1$ .



**Figure 20.** The  $6_{15} \leftarrow 5_{14}$  rotational transition for isomer III of  $\text{CF}_3\text{Cl-CH}_3\text{F}$  showing four quadrupole coupling components. (Reprinted with permission from: Gou, Q.; Spada, L.; Cocinero, E. J.; Caminati, W. Halogen–Halogen Links and Internal Dynamics in Adducts of Freons. *J. Phys. Chem. Lett.* 5, 1591 (2014). Copyright {2014} American Chemical Society).

Only  $\mu_a$ -type transitions have been measured, instead of the *ab initio* possible  $\mu_b$ - and  $\mu_c$ -type ones because of the really large value of the  $A$  rotational constant coming out from the fitting, performed by using the Pickett's SPFIT program ( $S$  reduction and  $I'$  representation).

Later on, the same procedure has been followed to search the three times weaker transitions (because of the natural abundance with respect to the  $^{35}\text{Cl}$ ) of the  $\text{CF}_3(^{37}\text{Cl})\text{-CH}_3\text{F}$ , and then of the  $\text{CF}_3(^{35}\text{Cl})\text{-CD}_3\text{F}$  and  $\text{CF}_3(^{37}\text{Cl})\text{-CD}_3\text{F}$ .

The results of the respectively fittings of the observed  $\mu_a$ -type transitions are reported in Table 44.

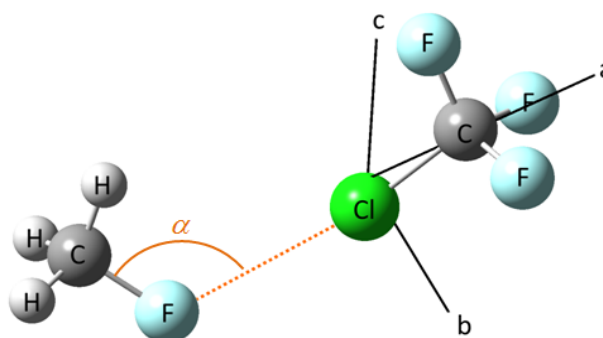
	CF <sub>3</sub> <sup>35</sup> Cl-CH <sub>3</sub> F	CF <sub>3</sub> <sup>37</sup> Cl-CH <sub>3</sub> F	CF <sub>3</sub> <sup>35</sup> Cl-CD <sub>3</sub> F	CF <sub>3</sub> <sup>37</sup> Cl-CD <sub>3</sub> F
A/MHz	21826(28) <sup>a</sup>	21573(64)	17264(35)	17079(39)
B/MHz	728.2164(3)	728.1154(2)	685.7804(4)	685.7554(4)
C/MHz	702.9987(3)	702.7130(3)	658.9718(4)	658.7455(4)
D <sub>J</sub> /kHz	0.9363(8)	0.929(3)	0.961(1)	0.956(2)
D <sub>JK</sub> /MHz	-0.2376(2)	-0.2360(3)	-0.1483(3)	-0.1469(4)
d <sub>1</sub> /kHz	-0.1052(6)	[-0.1052] <sup>b</sup>	-0.1279(9)	[-0.1279] <sup>c</sup>
χ <sub>aa</sub> /MHz	-73.3(1)	-58.1(2)	-72.3(2)	-57.1(2)
χ <sub>bb</sub> -χ <sub>cc</sub> /MHz	-5.2(3)	-4.3(4)	-6.4(4)	-5.2(4)
χ <sub>ab</sub> /MHz	29.0(7)	22(1)	26(1)	18.7(9)
N <sup>d</sup>	80	52	64	56
σ <sup>e</sup> /kHz	2.9	1.7	1.9	2.4

<sup>a</sup>Error in units of the last digit. <sup>b</sup>Fixed at the value of the CF<sub>3</sub><sup>35</sup>Cl-CH<sub>3</sub>F isotopologue. <sup>c</sup>Fixed at the value of the CF<sub>3</sub><sup>35</sup>Cl-CD<sub>3</sub>F isotopologue <sup>d</sup>Number of transitions in the fit. <sup>e</sup>Standard deviation of the fit.

**Table 44.** The obtained rotational parameters from the fittings of four isotopologues of CF<sub>3</sub>Cl-CH<sub>3</sub>F. (Reprinted with permission from: Gou, Q.; Spada, L.; Cocinero, E. J.; Caminati, W. Halogen–Halogen Links and Internal Dynamics in Adducts of Freons. *J. Phys. Chem. Lett.* 5, 1591 (2014). Copyright {2014} American Chemical Society).

### Structural Information and Internal Dynamics

Due to the high error on the A rotational constants, only a partial *r*<sub>0</sub> structure by reproducing the B and C ones for the four isotopologues has been performed, fitting the α valence angle (See Figure 21) (α<sub>0</sub> = 105.7°).



**Figure 21.** The isomer III of the CF<sub>3</sub>Cl-CH<sub>3</sub>F complex along the principal axes of inertia, with atom labels, showing the α valence angle and the Cl···F distance (2.995 Å).

The aforementioned large discrepancy on the A rotational constants is plausibly due to the internal rotation motions taking place in the molecular complex.

The changing in the rotational constants of all the isotopologues due to internal rotation of the two symmetric tops ( $-\text{CH}_3$  and  $-\text{CF}_3$ ) in the isomer III of  $\text{CF}_3\text{Cl}-\text{CH}_3\text{F}$ , is considered by adding a  $W_{00}^{(2)}$   $F\rho_g^2$  (with  $g=a,b$  since the axis  $c$  is perpendicular to the internal rotation axis) term for each of them in the equations 1.52, 1.53, 1.54, neglecting the coupling between the two motions. The respectively  $F\rho_g^2$  term values are reported for all the isotopologues in Table 45, showing that the  $A$  rotational constants are greatly affected by the internal rotation of the  $-\text{CF}_3$  group, since its internal rotation axis is almost parallel to the  $a$  axis.

		$\text{CF}_3^{35}\text{Cl}-\text{CH}_3\text{F}$	$\text{CF}_3^{37}\text{Cl}-\text{CH}_3\text{F}$	$\text{CF}_3^{35}\text{Cl}-\text{CD}_3\text{F}$	$\text{CF}_3^{37}\text{Cl}-\text{CD}_3\text{F}$
$\text{CF}_3$	$F\rho_a^2/\text{MHz}$	17074.0	16932.5	13082.5	12973.4
	$F\rho_b^2/\text{MHz}$	16.7	16.6	14.7	14.6
$\text{CH}_3$	$F\rho_a^2/\text{MHz}$	17.6	17.6	35.7	35.5
	$F\rho_b^2/\text{MHz}$	3.0	3.0	5.2	5.2

**Table 45.** The reported  $F\rho_g^2$  values along  $a$  and  $b$  principal axes for the four observed isotopologues of isomer III of  $\text{CF}_3\text{Cl}-\text{CH}_3\text{F}$ . (Reprinted with permission from: Gou, Q.; Spada, L.; Cocinero, E. J.; Caminati, W. Halogen–Halogen Links and Internal Dynamics in Adducts of Freons. *J. Phys. Chem. Lett.* 5, 1591 (2014). Copyright {2014} American Chemical Society).

Hence, by taking into the account the equation 1.49 ( $A_{00} = A_r + W_{00}^{(2)}F\rho_a^2$ ) for all the isotopologues which is related only to the  $-\text{CF}_3$  top internal rotation along the  $a$  axes, where  $A_r$  are the rotational constants from the previous calculated partial  $r_0$  structure for the respectively isotopologues, and  $A_{00}$  the experimental ones,  $W_{00}^{(2)}$  is determined be 1.0. According to the function plotted in Figure 2 of the Chapter 1, this latter value corresponds to a  $V_3 = 7 \text{ cal}\cdot\text{mol}^{-1}$ .

### 3.3.2 Chlorotrifluoromethane – Formaldehyde

#### Introduction

The previous study has shown that  $\text{CF}_3\text{Cl}$ , having an electrophilic region on the chlorine atom, forms a complex with the  $\text{FCH}_3$  molecule, possessing an nucleophilic zone on the F, through a  $\text{C}\cdots\text{Cl}\cdots\text{F}$  HaB, undergoing to an almost free internal rotation of the  $-\text{CF}_3$  along the  $a$  axes, resulting in about 8 times larger  $A$  experimental constant than the predicted one.

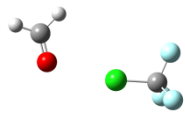
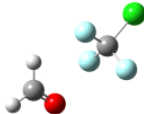
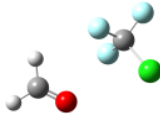
In the present study (the adduct  $\text{CF}_3\text{Cl}-\text{H}_2\text{CO}^{53}$ ) two are the main goals:

- 1) Describe the features of the C-Cl...O HaB which plausibly takes place as suggested by the already observed complexes between CF<sub>3</sub>Cl and water<sup>49</sup> and dimethyether<sup>50</sup>, comparing the respectively results.
- 2) Determine and size the possible internal motions.

## Theoretical Calculations

Three isomers have been optimized at the MP2/6-311++G(d,p) level by using the Gaussian03 package, which are linked by a C-Cl...O HaB (Isomer I), C-H...F WHB and three C-F...O HaBs (Isomer II), C-H...F WHB, two C-F...O HaBs and one C-Cl...O HaB (Isomer III).

The rotational, quadrupole coupling constants as well as the dipole moment components, which are used to perform the predictions for the search of the rotational spectrum, are reported in Table 46 together with the respectively isomer energies ( $\Delta E$ ) and the zero point corrected ones ( $\Delta E_0$ ).

	I	II	III
			
<i>A</i> /MHz	4830	5004	3123
<i>B</i> /MHz	786	997	1297
<i>C</i> /MHz	767	973	1103
$ \mu_a /D$	1.7	0.7	1.5
$ \mu_b /D$	2.0	2.0	0.9
$ \mu_c /D$	0.0	0.0	1.1
$\chi_{aa}$ /MHz	-67.7	-69.9	38.3
$\chi_{bb}-\chi_{cc}$ /MHz	-6.6	-3.1	-109.6
$\chi_{ab}$ /MHz	25.9	17.9	4.3
$\chi_{ac}$ /MHz	0.0	0.3	0.1
$\Delta E/cm^{-1}$	0 <sup>a</sup>	121	181
$\Delta E_0/cm^{-1}$	7	107	0 <sup>b</sup>

<sup>a</sup>Absolute energy = -910.927127  $E_h$ . <sup>b</sup>Absolute energy = -910.884061  $E_h$ .

**Table 46.** *Ab initio* (MP2/6-311++G(d,p) level) rotational parameters and energies for the three calculated isomers of CF<sub>3</sub>Cl-H<sub>2</sub>CO. (Reused with permission from Qian Gou, Gang Feng, Luca Evangelisti, Montserrat Vallejo-López, Lorenzo Spada, Alberto Lesarri, Emilio J. Cocinero, Walther Caminati. Internal Dynamics in Halogen-Bonded Adducts: A Rotational Study of Chlorotrifluoromethane-Formaldehyde. *Chem. Eur. J.* 2015, 21, 4148 – 4152© 2015 Wiley-VCH Verlag GmbH & Co. KGaA, Weinheim).



## Experimental Section

The paraformaldehyde is a polymer at room temperature which has to be heated to produce an enough gas phase concentration of formaldehyde to be used in the experiment.

Hence, the. 2%  $\text{CF}_3\text{Cl}$  / He mixture at stagnation pressure of 5 bars was streamed over the paraformaldehyde kept at 350 K by an heating system and then expanded into the cavity of the Bologna PJ-FTMW spectrometer.

According to the *ab initio* calculations, the rotational spectrum recording started with the search of the  $\mu_a$ -type transitions, which are predicted be quite strong for all the isomers.

In the 7754 – 7761 MHz range, 8 separately lines, showing the typical Doppler splitting, have been observed. These lines have been assigned to the  $5_{05} \leftarrow 4_{04}$  transition of the isomer I of the  $\text{CF}_3^{35}\text{Cl}-\text{H}_2\text{CO}$  and  $\text{CF}_3^{37}\text{Cl}-\text{H}_2\text{CO}$  isotopologues (relative intensity 1:3), showing also the doubling due to the internal rotation of the  $\text{H}_2\text{CO}$  group around its  $C_{2v}$  symmetry axis, exchanging a pair of fermions.

Within the same isotopologue for the same quadrupole coupling component, in fact, a 1:3 relative intensity between the ground state ( $O^+$ ) and the excited torsional state ( $O^-$ ) transition, is observed.

After this first assignment, several other  $\mu_a$ -type transition for the isomer I has been measured for both the isotopologues.

All the transitions have been fitted by using the Pickett's SPFIT program ( $S$  reduction and  $I'$  representation). No  $\mu_b$ -type,  $\mu_c$ -type and the possible  $E$  state transitions, these latter relative to the –  $\text{CF}_3$  internal rotation, have been observed. The results, together with the ones for the  $^{37}\text{Cl}$  isotopologue, are reported in Table 47, showing a really large value of the  $D_{JK}$  centrifugal distortion constant.

	CF <sub>3</sub> <sup>35</sup> Cl-H <sub>2</sub> CO		CF <sub>3</sub> <sup>37</sup> Cl-H <sub>2</sub> CO	
	<i>O</i> <sup>+</sup>	<i>O</i> <sup>-</sup>	<i>O</i> <sup>+</sup>	<i>O</i> <sup>-</sup>
<i>A</i> /MHz	27295(1) <sup>a</sup>	27103(4)	27112(5)	27071(5)
<i>B</i> /MHz	787.4896(3)	787.6476(1)	787.2248(1)	787.3801(1)
<i>C</i> /MHz	764.3730(2)	764.6223(1)	763.8978(2)	764.1432(1)
<i>D</i> <sub>J</sub> /kHz	1.0362(8)	1.0201(4)	1.034(1)	1.015(1)
<i>D</i> <sub>JK</sub> /kHz	-335.59(9)	-308.90(9)	-332.30(9)	-306.59(8)
<i>d</i> <sub>1</sub> /kHz	-0.100(1)	-0.1062(3)	[-0.100] <sup>b</sup>	[-0.1062]
<i>H</i> <sub>JK</sub> /kHz	0.0202(5)	0.0170(4)	[0.0202]	[0.0170]
<i>χ</i> <sub>aa</sub> /MHz	-73.91(5)		-58.20(5)	
<i>χ</i> <sub>bb</sub> - <i>χ</i> <sub>cc</sub> /MHz	-4.52(2)		-3.9(1)	
<i>χ</i> <sub>ab</sub> /MHz	22.96(5)		15.1(3)	
<i>N</i> <sup>c</sup>	136		87	
<i>σ</i> <sup>d</sup> [kHz]	2.6		2.6	

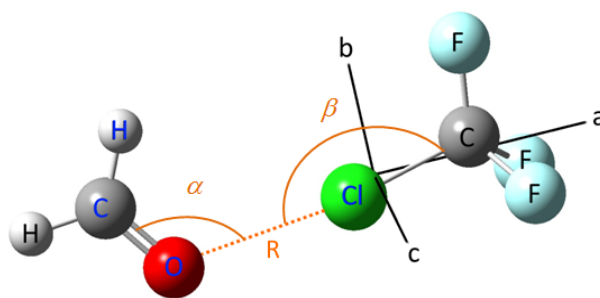
<sup>a</sup>Uncertainties are expressed in units of the last digit. <sup>b</sup>Values in brackets are fixed at the corresponding ones of parent species. <sup>c</sup>Number of transitions in the fit. <sup>d</sup>Standard deviation of the fit.

**Table 47.** Rotational parameters obtained from the fitting of the transitions for the CF<sub>3</sub><sup>35</sup>Cl-H<sub>2</sub>CO and CF<sub>3</sub><sup>37</sup>Cl-H<sub>2</sub>CO isotopologues. (Reused with permission from Qian Gou, Gang Feng, Luca Evangelisti, Montserrat Vallejo-López, Lorenzo Spada, Alberto Lesarri, Emilio J. Cocinero, Walther Caminati. Internal Dynamics in Halogen-Bonded Adducts: A Rotational Study of Chlorotrifluoromethane–Formaldehyde. *Chem. Eur. J.* 2015, 21, 4148 – 4152© 2015 Wiley-VCH Verlag GmbH & Co. KGaA, Weinheim).

As in the case of CF<sub>3</sub>Cl-FCH<sub>3</sub> complex, a large value of the *A* rotational constant is fitted, suggesting the occurring of the internal rotation of the -CF<sub>3</sub>, which, as one can see in Figure 22, takes place almost parallel to the *a* axes.

### Structural Information and Internal Dynamics

The comparison between the experimental *B* and *C* rotational constants with those ones from the *ab initio* calculations suggests that the calculated geometry along *b* and *c* axes matches almost exactly the observed isomer I experimental structure. Hence, no further partial *r*<sub>0</sub> structure fittings are necessary.



**Figure 22.** Image of the observed isomer for the  $\text{CF}_3\text{Cl-H}_2\text{CO}$  along the principal axes whose  $\text{Cl}\cdots\text{O}$  distance ( $R$ ) is 3.048 Å.

Following the same procedure as in the case of  $\text{CF}_3\text{Cl-FCH}_3$ , the calculated values for the  $F\rho_g^2$  ( $g = a$  and  $b$ , since the axis  $c$  is perpendicular to the internal rotation axis) of both the isotopologues show that, the internal rotation of the  $-\text{CF}_3$  provides a 500 times larger contribution on the  $A$  constant (19610.7 MHz and 19321.8 MHz for  $F\rho_a^2$  with respect to the 33.6 MHz and 33.1 MHz for  $F\rho_b^2$  for  $\text{CF}_3^{35}\text{Cl-H}_2\text{CO}$  and  $\text{CF}_3^{37}\text{Cl-H}_2\text{CO}$ , respectively) than on the  $B$  one.

Applying the equation 1.49 in the same way as for the  $\text{CF}_3\text{Cl-FCH}_3$  study, the  $W_{00}^{(2)}$  has been determined to be 1.1, which corresponds to a barrier  $V_3 \sim 7 \text{ cal}\cdot\text{mol}^{-1}$ .

The splitting due to the internal rotation of the  $\text{CH}_2\text{O}$  around its symmetry axis allows us to determine the  $V_2$  barrier.

In fact, applying the one dimensional Meyer's flexible model<sup>36</sup> in order to reproduce the differences of the planar moments of inertia between the two torsional states ( $\Delta M_{aa}$ ,  $\Delta M_{bb}$  and  $\Delta M_{cc}$ ), assuming to be affected in the same way by the internal rotation of the  $-\text{CF}_3$  top, the barrier  $V_2 = 28(5) \text{ cm}^{-1}$  is calculated.<sup>53</sup>

This result is obtained by taking into account a double minima potential as function of the blue  $\text{H-C=O}\cdots\text{Cl}$  dihedral angle in Figure 22, and the structural relaxation of the  $R$ ,  $\alpha$  and  $\beta$  parameters<sup>53</sup>.

### 3.3.3 Conclusions

The two  $\text{C-Cl}\cdots\text{F}$  and  $\text{C-Cl}\cdots\text{O}$  HaB linked molecular systems show that these interactions are favoured with respect to the WHB ones when a competition between them is possible. The two contacts have similar interaction distances ( $\text{Cl}\cdots\text{F}$ : 2.995 Å<sup>52</sup>,  $\text{Cl}\cdots\text{O}$ : 3.048 Å<sup>53</sup>), also in comparison with the ones determined for the  $\text{C-Cl}\cdots\text{O}$  HaB in  $\text{CF}_3\text{Cl-H}_2\text{O}$  (3.028 Å)<sup>49</sup> and for the  $\text{C-Cl}\cdots\text{N}$  HaB in  $\text{CF}_3\text{Cl-NH}_3$  (3.080 Å)<sup>51</sup>.

The C=O...Cl and C-F...Cl valence angles within the CF<sub>3</sub>Cl-CH<sub>2</sub>O and CF<sub>3</sub>Cl-FCH<sub>3</sub> complexes are found to be 105.7° and 118.4°, respectively.

The V<sub>3</sub> barriers relative to the -CF<sub>3</sub> internal rotation motions, taking place along the *a*-axis within both the CF<sub>3</sub>Cl-FCH<sub>3</sub> and the CF<sub>3</sub>Cl-CH<sub>2</sub>O adducts have been determined to be almost free (~7 cal·mol<sup>-1</sup> for both), largely affecting the *A* rotational constants of both the complexes.

Furthermore, applying the one-dimensional flexible model<sup>36</sup> to the internal rotation of water around its C<sub>2v</sub> axis, the V<sub>2</sub> barrier has been determined (V<sub>2</sub>=28(5) cm<sup>-1</sup>).

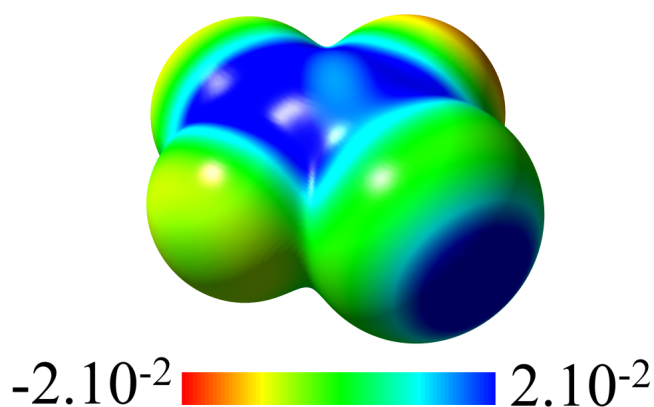
## 3.4 LONE PAIR $\cdots$ $\pi$ INTERACTION

### 3.4.1 Chlorotrifluoroethylene – Ammonia

#### Introduction

The competition between lone-pair $\cdots\pi$  (Lp) and halogen bonding (HaB) interactions is describing in the study of Chlorotrifluoroethylene ( $C_2F_3Cl$ )-Ammonia ( $NH_3$ ) molecular system.

The former molecule is a perhalogenated Freon which has two regions where the electrostatic potential is positive (see Figure 23 with displays the potential range from  $-2.10^{-2}$  V to  $2.10^{-2}$  V): one located on the external side of chlorine and the other one just on the carbon which is bonded to two fluorine atoms.



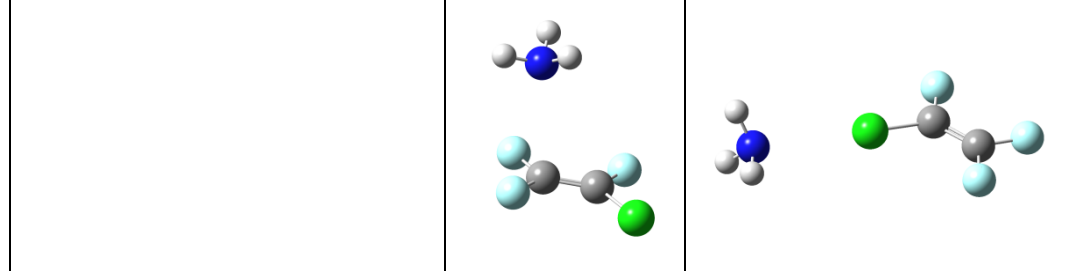
**Figure 23.** The plotting of the electrostatic potential on the molecular surface of the  $C_2F_3Cl$ . (Reprinted with permission from Lorenzo Spada, Qian Gou, Yannick Geboes, Wouter A. Herrebout, Sonia Melandri, Walther Caminati. Rotational Study of Dimethyl Ether–Chlorotrifluoroethylene: Lone Pair $\cdots\pi$  Interaction Links the Two Subunits. *J. Chem. Phys. A*, Article ASAP, Publication Date (Web): January 26, 2016. DOI: 10.1021/acs.jpca.5b12571. Copyright (2016) American Chemical Society).

Because of this, the isomeric preference (which involves different kind of interactions) of  $NH_3$  (it has the N-lone pair) with respect to the  $C_2F_3Cl$  was investigated thanks, also, to the unambiguously isomeric rotational spectrum assignment, allowed by rotational and quadrupole coupling constants comparison between *ab initio* and experimental values.

#### Theoretical Calculations

*Ab initio* calculations for the Lp and HaB structures have been run at the MP2(full)/aug-cc-pVDZ level using the Gaussian09. For both the optimized isomer geometries, the rotational and quadrupole coupling constants (for  $^{35}Cl$  and  $^{14}N$ ) together with the relative energies ( $\Delta E$ ), including

the zero point corrected ones ( $\Delta E_0$ ) are reported in Table 48. The BSSE corrections have been taking into the account to estimate the dissociation energy values ( $E_D$ ) of the two isomers.

		Lone pair $\cdots\pi$	Halogen Bond
			
A/MHz		2191	3839
B/MHz		1281	862
C/MHz		1192	706
Chlorine	$\chi_{aa}, \chi_{bb}-\chi_{cc}$ /MHz	-20.9,-45.2	-65.9,-2.7
	$\chi_{ab}, \chi_{bc}, \chi_{ac}$ /MHz	-50.3,6.3,5.7	-18.1,0.0,0.0
Nitrogen	$\chi_{aa}, \chi_{bb}-\chi_{cc}$ (N)/MHz	-0.3,0.3	-3.3,-0.2
	$\chi_{ab}, \chi_{bc}, \chi_{ac}$ /MHz	1.8,1.9,-1.6	-0.9,0.0,0.0
$ \mu_a ,  \mu_b ,  \mu_c $ /D		1.1,1.4,0.8	2.7,0.6,0.0
$\Delta E, \Delta E_0$ /cm <sup>-1</sup>		0 <sup>a</sup> ,0 <sup>b</sup>	330,331
$E_D$ /kJ mol <sup>-1</sup>		7.5 <sup>c</sup>	7.0

<sup>a</sup>Absolute energy = -890.979805 E<sub>h</sub>. <sup>b</sup>Absolute energy zero point corrected = -890.926933 E<sub>h</sub>. <sup>c</sup>Dissociation energy.

**Table 48.** The *ab initio* rotational parameters for the Lone pair $\cdots\pi$  and Halogen bonding isomers of C<sub>2</sub>F<sub>3</sub>Cl-NH<sub>3</sub>. (Qian Gou, Lorenzo Spada, Yannick Geboes, Wouter A. Herrebout, Sonia Melandri and Walther Caminati. *Phys. Chem. Chem. Phys.*, 2015,17, 7694-7698 - Reproduced by permission of the PCCP Owner Societies).

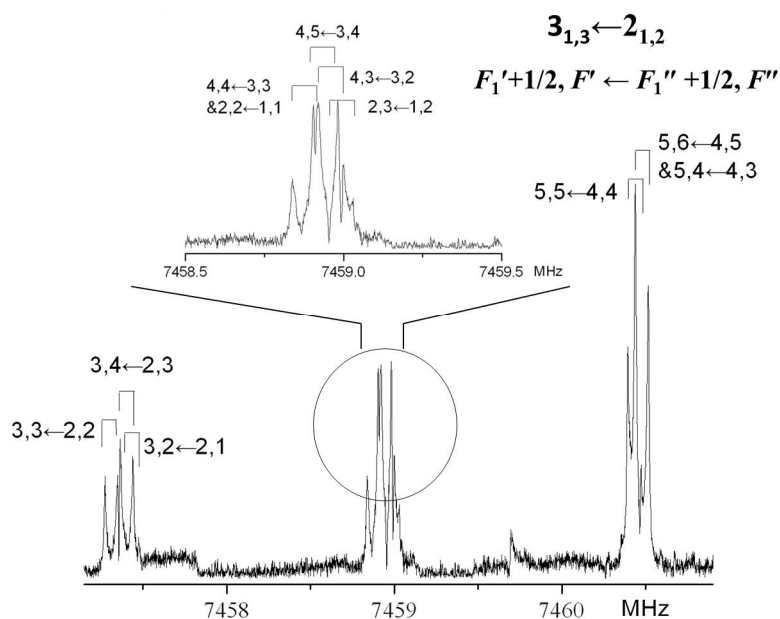
An *ab initio* evaluation of the internal rotation barrier of the NH<sub>3</sub> has been calculated be 2 cm<sup>-1</sup>.

## Experimental Section

The 1:1 sample mixture at 1 % of the C<sub>2</sub>F<sub>3</sub>Cl and NH<sub>3</sub> and, later on, of C<sub>2</sub>F<sub>3</sub>Cl and ND<sub>3</sub> (commercial sample), C<sub>2</sub>F<sub>3</sub>Cl and <sup>15</sup>NH<sub>3</sub> (commercial sample) in Helium at stagnation pressure of 5 bars have been prepared in a sample holder and successively expanded into the cavity of the Bologna PJ-FTMW spectrometer.

According to the predicted values of Table 48, the search for the  $\mu_a$ -type lines of the Lp most stable isomer were first set up. At the beginning, eleven components have been observed in a 2 MHz range around 7580.6, and successively assigned to the 3<sub>03</sub>←2<sub>02</sub> transition of the C<sub>2</sub>F<sub>3</sub><sup>35</sup>Cl - <sup>14</sup>NH<sub>3</sub>

species because of the splitting (see in Figure 24 the  $3_{13} \leftarrow 2_{12}$  transition) carrying out by the presence of the  $^{35}\text{Cl}$  and  $^{14}\text{N}$  nuclei.



**Figure 24.** The component lines of the  $3_{13} \leftarrow 2_{12}$  rotational transition for the Lp  $\text{C}_2\text{F}_3^{35}\text{Cl}-^{14}\text{NH}_3$  adduct. (Qian Gou, Lorenzo Spada, Yannick Geboes, Wouter A. Herrebout, Sonia Melandri and Walther Caminati. *Phys. Chem. Chem. Phys.*, 2015, 17, 7694-7698 - Reproduced by permission of the PCCP Owner Societies).

After this first assignment, several other  $\mu_a$ -type lines and, later on, the  $\mu_b$ -type and some  $\mu_c$ -type transitions have been measured and fitted by using the Pickett's SPFIT program (using the  $S$  reduction and  $I'$  representation).

The results, together with those ones for the later on assigned rotational spectra of the  $\text{C}_2\text{F}_3^{37}\text{Cl}-^{14}\text{NH}_3$  (in natural abundance),  $\text{C}_2\text{F}_3^{35}\text{Cl}-^{14}\text{ND}_3$  and  $\text{C}_2\text{F}_3^{35}\text{Cl}-^{15}\text{NH}_3$  isotopologues are reported in Table 49.

	C <sub>2</sub> F <sub>3</sub> <sup>35</sup> Cl- <sup>14</sup> NH <sub>3</sub>	C <sub>2</sub> F <sub>3</sub> <sup>37</sup> Cl- <sup>14</sup> NH <sub>3</sub>	C <sub>2</sub> F <sub>3</sub> <sup>35</sup> Cl- <sup>15</sup> NH <sub>3</sub>	C <sub>2</sub> F <sub>3</sub> <sup>35</sup> Cl- <sup>14</sup> ND <sub>3</sub>
A/MHz	2236.0689(1) <sup>a</sup>	2225.110(1)	2205.243(3)	2129.536(3)
B/MHz	1317.19498(8)	1294.36090(8)	1295.0543(6)	1234.8271(5)
C/MHz	1219.63324(7)	1196.9012(1)	1198.5099(4)	1138.5060(3)
χ <sub>aa</sub> (Cl)/MHz	-21.817(2)	-18.71(1)	-19.85(4)	-14.33(1)
χ <sub>bb</sub> -χ <sub>cc</sub> (Cl)/MHz	-50.762(4)	-38.630(7)	-51.78(3)	-51.82(1)
χ <sub>ab</sub> (Cl)/MHz	55.9(4)	46.1(8)	[55.9] <sup>b</sup>	56.9(9)
χ <sub>bc</sub> (Cl)/MHz	12(2)	-	[12]	[12]
χ <sub>ac</sub> (Cl)/MHz	10.3(3)	6.8(5)	[10.3]	17.8(4)
χ <sub>aa</sub> (N)/MHz	-0.404(2)	[-0.404]	-	-0.936(7)
χ <sub>bb</sub> -χ <sub>cc</sub> (N)/MHz	-0.435(4)	[-0.435]	-	-1.09(1)
χ <sub>ab</sub> (N)/MHz	0.72(6)	[0.7]	-	3.2(5)
χ <sub>ac</sub> (N)/MHz	1.8(4)	[1.8]	-	[1.8]
D <sub>J</sub> /kHz	2.5186(8)	2.416(1)	2.547(5)	2.654(4)
D <sub>JK</sub> /kHz	-6.710(6)	-6.27(7)	-7.4(1)	-9.2(1)
D <sub>K</sub> /kHz	16.926(9)	[16.926]	[16.926]	[16.926]
d <sub>1</sub> /kHz	-0.3695(8)	[-0.3695]	-0.414(5)	-0.589(4)
d <sub>2</sub> /kHz	-0.1151(9)	[-0.1151]	[-0.1151]	[-0.1151]
σ <sup>c</sup> /kHz	2.8	3.5	2.7	3.1
N <sup>d</sup>	475	176	51	120

<sup>a</sup>Error in units of the last digit; <sup>b</sup>Fixed to the value of the C<sub>2</sub>F<sub>3</sub><sup>35</sup>Cl-<sup>14</sup>NH<sub>3</sub> species. <sup>c</sup>Standard deviation of the fit; <sup>d</sup>Number of lines in the fit.

**Table 49.** The experimental rotational parameters for four isotopologues of the Lp C<sub>2</sub>F<sub>3</sub>Cl-NH<sub>3</sub>.

(Qian Gou, Lorenzo Spada, Yannick Geboes, Wouter A. Herrebout, Sonia Melandri and Walther Caminati. *Phys. Chem. Chem. Phys.*, 2015,17, 7694-7698 - Reproduced by permission of the PCCP Owner Societies).

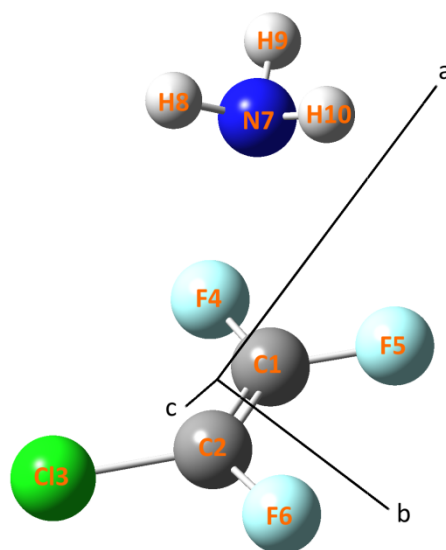
The obtained rotational and quadrupole coupling constants, for the most abundant species, match only the *ab initio* values for the Lp isomer giving the precise indication of the corrected assignment. No lines belonging to the HaB isomer have been observed as well as the *E* state lines deriving from the plausible internal rotation of NH<sub>3</sub>, because of a possible relaxation process (former case), and of the expected far away frequency values (almost zero internal rotation barrier) of those transitions (latter case).

## Structural Information and Internal Dynamics

A partial *r*<sub>0</sub> structure has been calculated by fitting three geometrical parameters (see in Figure 25 the N7-C1 distance (*R*<sub>N7C1</sub>), the N7-C1-C2 valence angle (∠N7-C1-C2) and the N7-C1-C2-Cl3



dihedral angle ( $\angle\text{N7-C1-C2-Cl3}$ )), defining the relative orientation between the  $\text{C}_2\text{F}_3\text{Cl}$  and of the  $\text{NH}_3$  subunits, fixing to their predicted values the other parameters.



**Figure 25.** The  $L_p$  isomer of the  $\text{C}_2\text{F}_3\text{Cl-NH}_3$  adduct along the principal axes of inertia.

The obtained values, reported in Table 50 where are compared with those ones from the *ab initio* calculations, allow to reproduce the experimental rotational constants of all the isotopologues, apart from the  $\text{C}_2\text{F}_3^{35}\text{Cl-}^{14}\text{ND}_3$  ones, within few MHz.

	$R_{\text{N7C2}}/\text{\AA}$	$\angle\text{N7-C2-C1}/^\circ$	$\angle\text{N7-C2-C1-Cl3}/^\circ$
$r_0$	2.987(2) <sup>a</sup>	100.9(1)	88.3(1)
$r_e$	3.103	101.5	89.0

<sup>a</sup>Uncertainties are expressed in units of the last digit.

**Table 50.** The  $r_0$  and  $r_e$  structures comparison of the  $\text{C}_2\text{F}_3\text{Cl-NH}_3$  adduct. (Qian Gou, Lorenzo Spada, Yannick Geboes, Wouter A. Herrebout, Sonia Melandri and Walther Caminati. *Phys. Chem. Chem. Phys.*, 2015,17, 7694-7698 - Reproduced by permission of the PCCP Owner Societies).

The  $r_e/r_0$  structure parameters and the  $r_e/r_0/r_e$  coordinates of the N and Cl positions (see Table 51) comparisons are the further confirmation of the corrected  $L_p$  isomer assignments of the rotational spectra.

		$a/\text{Å}$	$b/\text{Å}$	$c/\text{Å}$
Cl	$r_s^a$	$\pm 1.847(1)$	$\pm 0.766(2)$	$\pm 0.06(3)$
	$r_0^b$	-1.881	-0.724	0.027
	$r_e$	-1.878	-0.759	0.041
N	$r_s^a$	$\pm 2.304(1)$	$\pm 1.400(1)$	$\pm 1.155(1)$
	$r_0^b$	2.156	-1.269	-1.385
	$r_e$	2.307	-1.346	-1.289

<sup>a</sup>Calculated using the Kraitchmann's equations. <sup>b</sup>Derived from the partial  $r_0$  structure.

**Table 51.** The  $r_s/r_0/r_e$  coordinates of the Cl and N atoms in the  $C_2F_3Cl-NH_3$  adduct. (Qian Gou, Lorenzo Spada, Yannick Geboes, Wouter A. Herrebout, Sonia Melandri and Walther Caminati. *Phys. Chem. Chem. Phys.*, 2015, 17, 7694-7698 - Reproduced by permission of the PCCP Owner Societies).

*Ab initio* calculations suggest a barrier for the internal rotation of the  $NH_3$  around its  $C_{3v}$  axis of  $2\text{ cm}^{-1}$ . Following the same procedure applied in the previous studies where a symmetric top rotation was taken into the account, according to the equations 1.52, 1.53, 1.54 and the  $s$  dependence function with respect to  $W_{00}^{(2)}$ , a  $V_3$  barrier zero is calculated, in agreement with the predicted value.

### 3.4.2 Chlorotrifluoroethylene – Dimethylether

#### Introduction

Following the results of the previous study, the features of the O-lone-pair $\cdots\pi$  interaction (Lp) are characterizing for the Chlorotrifluoroethylene ( $C_2F_3Cl$ ) – Dimethylether (DME) adduct.

The O-Lp bonding energy was previously estimated be  $6.6\text{ kJ}\cdot\text{mol}^{-1}$  in the case of the  $C_2F_3Cl-H_2O$  complex<sup>54</sup>, involving an  $O\cdots C(F_2)$  contact, occurring at  $2.947\text{ Å}$ , where water undergoes an almost free internal rotation motion.

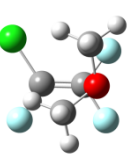
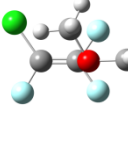
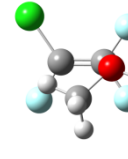
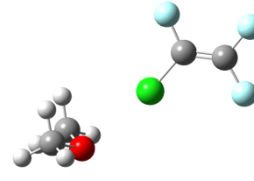
The  $C_2F_3Cl$ -DME adduct is a good candidate to observe if the methyl substitutions in water affect the shape of the complex, in going from the  $C_2F_3Cl-H_2O$  preference towards the O-Lp interaction to the  $C-Cl\cdots O$  halogen bonding. Furthermore, it is interesting to investigate if secondary weak hydrogen bonds can take place, sizing, in that case, their contribution to the molecular adduct stability.

#### Theoretical Calculations

Four isomers have been optimized at the MP2/aug-cc-pVDZ level with Gaussian09: three of them links  $C_2F_3Cl$  and DME through a Lp interaction while the  $C-Cl\cdots O$  halogen bond (HaB) governs the stability of the remaining isomer.

The real minima “Lp-type” isomer structures (isomer I, II, III), according to the frequency calculations in the harmonic approximation also performed for the “HaB-type” one (isomer IV), have been determined by exploring the C8O7-C1C2 (see Figure 27) potential energy surface<sup>55</sup>.

The rotational parameters necessary for the spectroscopic assignment of the rotational spectrum are reported in Table 52, together with the relative energies ( $\Delta E$ ), the zero point corrected ones ( $\Delta E_0$ ) and the estimation of the dissociation energy ( $E_D$ ) taking into the account the BSSE corrections.

	I	II	III	IV
				
$A/\text{MHz}$	1397	1644	1681	2892
$B/\text{MHz}$	900	818	778	455
$C/\text{MHz}$	823	699	731	424
$\mu_a/D$	-0.3	1.1	-1.1	-1.7
$\mu_b/D$	-1.6	-1.2	-0.4	0.7
$\mu_c/D$	0.2	1.0	0.3	0.0
$\chi_{aa}/\text{MHz}$	19.1	12.6	-6.6	-59.6
$\chi_{bb}-\chi_{cc}/\text{MHz}$	-71.0	-64.5	38.4	-8.8
$\chi_{ab}/\text{MHz}$	34.1	-39.1	21.4	-29.5
$\chi_{ac}/\text{MHz}$	11.0	13.1	45.3	-0.2
$\chi_{bc}/\text{MHz}$	-25.1	24.0	-23.8	-0.1
$\Delta E^a/\text{cm}^{-1}$	0	222	180	1000
$\Delta E_0^b/\text{cm}^{-1}$	0	218	168	966
$E_D/\text{kJ}\cdot\text{mol}^{-1}$	12.1	11.5	11.6	9.4

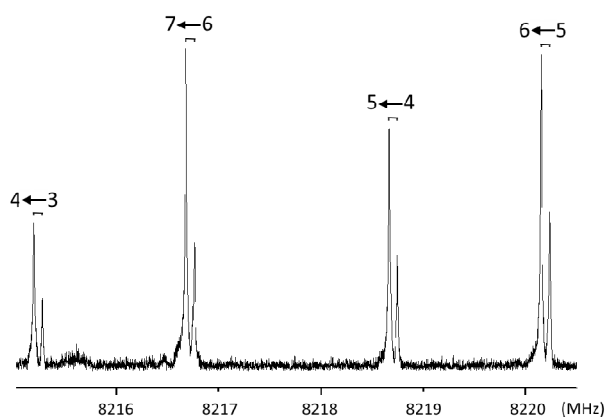
<sup>a</sup>Absolute energy: -989.179788 E<sub>h</sub>, <sup>b</sup>Absolute energy zero point corrected: -989.078983 E<sub>h</sub>,

**Table 52.** The *ab initio* rotational parameters for the four isomers of the C<sub>2</sub>F<sub>3</sub>Cl-DME complex. (Reprinted with permission from Lorenzo Spada, Qian Gou, Yannick Geboes, Wouter A. Herrebout, Sonia Melandri, Walther Caminati. Rotational Study of Dimethyl Ether–Chlorotrifluoroethylene: Lone Pair··· $\pi$  Interaction Links the Two Subunits. *J. Chem. Phys. A*, Article ASAP, Publication Date (Web): January 26, 2016. DOI: 10.1021/acs.jpca.5b12571. Copyright (2016) American Chemical Society).

## Experimental Section

The 1% mixture of  $C_2F_3Cl$  and DME 1:1 in Helium at a stagnation pressure of 6 bars has been supersonically expanded into the cavity of the Bologna PJ-FTMW spectrometer.

According to the relative energies of Table 52, isomer I is the most stable one, having a large  $\mu_b$  dipole moment. Because of this, the detection of the rotational spectrum started from the search of the  $5_{05} \leftarrow 4_{14}$  transition which is expected splitted into four components due to the presence of the chlorine atom. These lines have been found in the frequency range between 8215 MHz and 8221 MHz as shown in Figure 26 and they were assigned to the most abundant isotopologue: the  $C_2F_3^{35}Cl$ -DME one.



**Figure 26.** The  $\Delta F = 1$  components of the  $5_{05} \leftarrow 4_{14}$  transition for the  $C_2F_3^{35}Cl$ -DME isotopologue. (Reprinted with permission from Lorenzo Spada, Qian Gou, Yannick Geboes, Wouter A. Herrebout, Sonia Melandri, Walther Caminati. Rotational Study of Dimethyl Ether–Chlorotrifluoroethylene: Lone Pair $\cdots\pi$  Interaction Links the Two Subunits. *J. Chem. Phys. A*, Article ASAP, Publication Date (Web): January 26, 2016. DOI: 10.1021/acs.jpca.5b12571. Copyright (2016) American Chemical Society).

Several other  $\mu_b$ -type lines have been measured and fitted together with other weaker  $\mu_a$  and  $\mu_c$ -type transitions for the  $C_2F_3^{35}Cl$ -DME isotopologue using Pickett's SPFIT program (Watson's  $S$ -reduction and  $I^r$ -representation) as well as for the  $C_2F_3^{37}Cl$ -DME rotational lines. The results of both the fittings are reported in Table 53.

	C <sub>2</sub> F <sub>3</sub> <sup>35</sup> Cl - DME	C <sub>2</sub> F <sub>3</sub> <sup>37</sup> Cl - DME
<i>A</i> /MHz	1434.4456(2) <sup>a</sup>	1421.3262(2)
<i>B</i> /MHz	903.5197(1)	893.0386(1)
<i>C</i> /MHz	823.4024 (1)	810.43402(9)
<i>D<sub>J</sub></i> /kHz	0.9123(9)	0.9397(7)
<i>D<sub>JK</sub></i> /kHz	7.104(5)	6.334(4)
<i>D<sub>K</sub></i> /kHz	-4.642(6)	-3.577(4)
<i>d<sub>1</sub></i> /kHz	-0.1032(6)	-0.1195(4)
<i>d<sub>2</sub></i> /kHz	0.0129(4)	0.0123(2)
$\chi_{aa}$ /MHz	18.483(5)	13.029(6)
$\chi_{bb}-\chi_{cc}$ /MHz	-81.276(6)	-62.996(7)
$\chi_{ab}$ /MHz	41.5(7)	35(1)
$\chi_{bc}$ /MHz	24.5(5)	18.6(7)
$\chi_{ac}$ /MHz	11.0 <sup>b</sup>	8.8 <sup>b</sup>
$\sigma$ <sup>c</sup> /kHz	2.0	2.3
<i>N</i> <sup>d</sup>	339	330

<sup>a</sup>Error in parentheses in units of the last digit. <sup>b</sup>Undetermined in the fit; fixed to the *ab initio* value.

<sup>c</sup>RMS error of the fit. <sup>d</sup>Number of fitted lines.

**Table 53.** Rotational, quadrupole coupling and quartic distortion constants deriving by fitting the microwave transitions of C<sub>2</sub>F<sub>3</sub><sup>35</sup>Cl-DME and C<sub>2</sub>F<sub>3</sub><sup>37</sup>Cl-DME isotopologues. (Reprinted with permission from Lorenzo Spada, Qian Gou, Yannick Geboes, Wouter A. Herrebout, Sonia Melandri, Walther Caminati. Rotational Study of Dimethyl Ether–Chlorotrifluoroethylene: Lone Pair··· $\pi$  Interaction Links the Two Subunits. *J. Chem. Phys. A*, Article ASAP, Publication Date (Web): January 26, 2016. DOI: 10.1021/acs.jpca.5b12571. Copyright (2016) American Chemical Society).

No lines belonging to the higher energy isomers have been found due to their possible kinetic relaxation upon supersonic expansion conditions towards isomer I.

### Structural Information

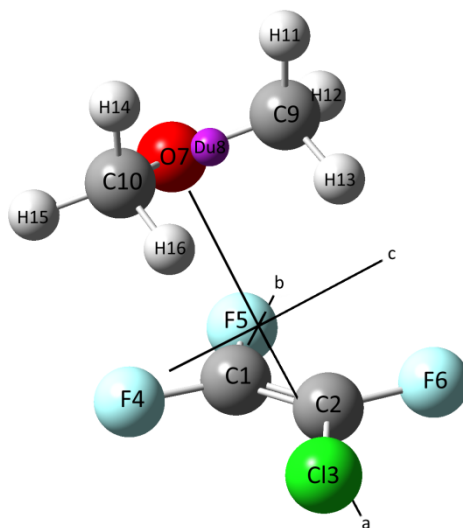
The substitution coordinates (*r<sub>s</sub>*) relative to the chlorine atom position along the principal axes of the most abundant isotopologue have been calculated by means of the Kraitchmann's equations. Their values are compared in Table 54 with the *ab initio* ones, showing their good agreement which confirms that the isomer observed through the analysis of the rotational spectra is isomer I.

	$a/\text{Å}$	$b/\text{Å}$	$c/\text{Å}$
$r_s$	$\pm 1.8102(8)^a$	$\pm 1.305(1)$	$0.0^b$
$r_e$	-1.7676	-1.3480	-0.2175

<sup>a</sup>Error in units of the last digit. <sup>b</sup>Imaginary value, fixed to zero.

**Table 54.** Comparison between the  $r_s$  and the  $r_e$  coordinates relative to the chlorine atom in the  $\text{C}_2\text{F}_3\text{Cl} - \text{DME}$  complex. (Reprinted with permission from Lorenzo Spada, Qian Gou, Yannick Geboes, Wouter A. Herrebout, Sonia Melandri, Walther Caminati. Rotational Study of Dimethyl Ether–Chlorotrifluoroethylene: Lone Pair $\cdots\pi$  Interaction Links the Two Subunits. *J. Chem. Phys. A*, Article ASAP, Publication Date (Web): January 26, 2016. DOI: 10.1021/acs.jpca.5b12571. Copyright (2016) American Chemical Society).

A refinement of the molecular structure has been performed by adjusting two valence ( $\angle\text{O7C1C2}$ ,  $\angle\text{DummyO7C1}$ ) and one dihedral angles ( $\angle\text{O7C1C2Cl3}$ ) which are shown in Figure 27, defining the relative orientation of the two subunits, in a way that the experimental rotational constants have been reproduced, from the *ab initio* geometry of the adduct, within 0.5 MHz.



**Figure 27.** The molecular adduct between  $\text{C}_2\text{F}_3\text{Cl}$  and DME along the principal axes of inertia showing the atom labels. (Reprinted with permission from Lorenzo Spada, Qian Gou, Yannick Geboes, Wouter A. Herrebout, Sonia Melandri, Walther Caminati. Rotational Study of Dimethyl Ether–Chlorotrifluoroethylene: Lone Pair $\cdots\pi$  Interaction Links the Two Subunits. *J. Chem. Phys. A*, Article ASAP, Publication Date (Web): January 26, 2016. DOI: 10.1021/acs.jpca.5b12571. Copyright (2016) American Chemical Society).

The obtained results are reported in Table 55 together with the equilibrium values ( $r_e$ ) indicating the small re-orientation of DME with respect to  $\text{C}_2\text{F}_3\text{C}$ , taken into the account to reproduce the experimental

	$\angle O7C1C2/^\circ$	$\angle O7C1C2C13/^\circ$	$\angle DuO7C1/^\circ$
$r_e$	100.5	88.1	115.3
$r_0$	103.5(1) <sup>a</sup>	87.2(1)	107.7(1)

<sup>a</sup>Uncertainties are expressed in units of the last digit.

**Table 55.** The fitted  $r_0$  structure values of the aforementioned adjust geometrical parameters compared with the corresponding ones deriving from the  $r_e$  structure. (Reprinted with permission from Lorenzo Spada, Qian Gou, Yannick Geboes, Wouter A. Herrebout, Sonia Melandri, Walther Caminati. Rotational Study of Dimethyl Ether–Chlorotrifluoroethylene: Lone Pair $\cdots\pi$  Interaction Links the Two Subunits. *J. Chem. Phys. A*, Article ASAP, Publication Date (Web): January 26, 2016. DOI: 10.1021/acs.jpca.5b12571. Copyright (2016) American Chemical Society).

### 3.4.3 Conclusions

The adducts between  $C_2F_3Cl$  with  $NH_3$  and DME, together with the previous rotational study of that Freon with water, unambiguously suggest that the Lp interaction is favourite with respect to the HaB in perhalogenated alkenes.

As shown in Table 56, the lone-pair donor atom – C-(F<sub>2</sub>) length increase of 40 m Å for each step in going from the DME to  $H_2O$  to  $NH_3$  as counterpart molecule of the  $C_2F_3Cl$  in forming the adduct.

	$r_{X\dots C1}/\text{Å}$	$\angle XC1C2/^\circ$	$\angle XC1C2Cl/^\circ$
DME	2.908	103.5	87.2
$H_2O$	2.947	100.58	88.48
$NH_3$	2.987	100.9	88.3

**Table 56.** The Lp interaction geometrical features for the  $C_2F_3Cl$  adducts with DME,  $H_2O$  and  $NH_3$ . (Reprinted with permission from Lorenzo Spada, Qian Gou, Yannick Geboes, Wouter A. Herrebout, Sonia Melandri, Walther Caminati. Rotational Study of Dimethyl Ether–Chlorotrifluoroethylene: Lone Pair $\cdots\pi$  Interaction Links the Two Subunits. *J. Chem. Phys. A*, Article ASAP, Publication Date (Web): January 26, 2016. DOI: 10.1021/acs.jpca.5b12571. Copyright (2016) American Chemical Society).

If the in the case of the  $C_2F_3Cl-H_2O$  and  $C_2F_3Cl-NH_3$  complexes, the hydrogen atoms which are in the opposite side with respect to the Freon, do not have any effect on the adduct stabilization, while in the case of  $C_2F_3Cl-DME$  a small contribution from the C-H $\cdots$ F contacts can be possible since their distances are close to the typical 2.5 – 2.9 Å range for these WHBs (e. g. H11-F4 distance = 2.989 Å)<sup>55</sup>.

Furthermore, the differences in the calculated *ab initio* energies at the MP2/aug-cc-pVDZ level for  $C_2F_3Cl-H_2O$  (6.1 kJ·mol<sup>-1</sup>) and  $C_2F_3Cl-DME$  (12.1 kJ·mol<sup>-1</sup>) suggest a contribution from WHBs.

## 3.5 ISOLATED MOLECULES

### 3.5.1 Fluoroxene

#### Introduction

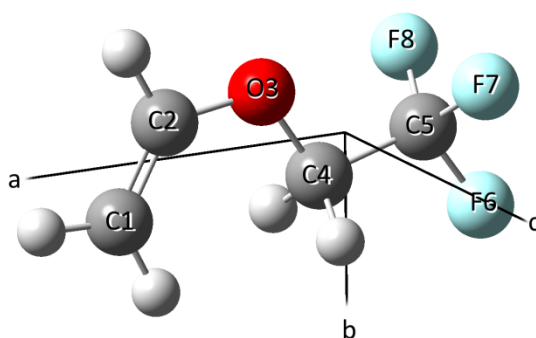
Fluoroxene (2,2,2-trifluoroethylvinyl ether in Figure 28) is a general anesthetic drug for which several conformations are possible. Its different conformational preferences and their relative populations in the gas phase can be determined by means of rotational spectroscopy, although the conformational equilibrium could be broken by a kinetic relaxation of all the isomers towards the most stable conformer in the free-jets.

Furthermore, an instrumental aspect of interest was provided by investigating fluoroxene, since this was the first study performed by using the Bilbao CP-FTMW spectrometer.

One of the most important goals is to observe the performances of the aforementioned spectrometer in determining, in natural abundance, the less abundant isopologues ( $^{13}\text{C}$ ,  $^{18}\text{O}$ ) of the backbone structure, providing the unambiguously proof on the corrected conformational assignment.<sup>56</sup>

#### Theoretical Calculations

The exploration of the conformational structures of the Fluorexene (see Figure 29) has been first performed using Molecular mechanics<sup>17</sup>, followed by the optimization of the conformers within 20  $\text{kJ}\cdot\text{mol}^{-1}$  at the MP2/6-311++G(d,p) level using GAUSSIAN 09 package.



**Figure 28.** The shape of the Fluoroxene, with the backbone atoms numbering along the principal axes system.

The rotational parameters, together with the relative zero point energies ( $\Delta E_0$ ) for the resulting four conformers, are reported in Table 57.

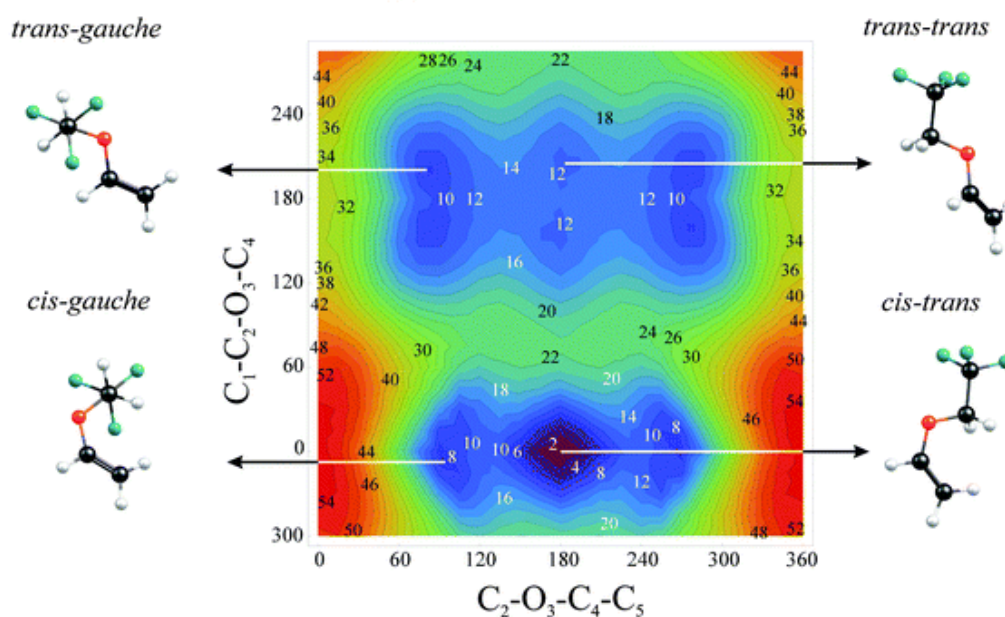
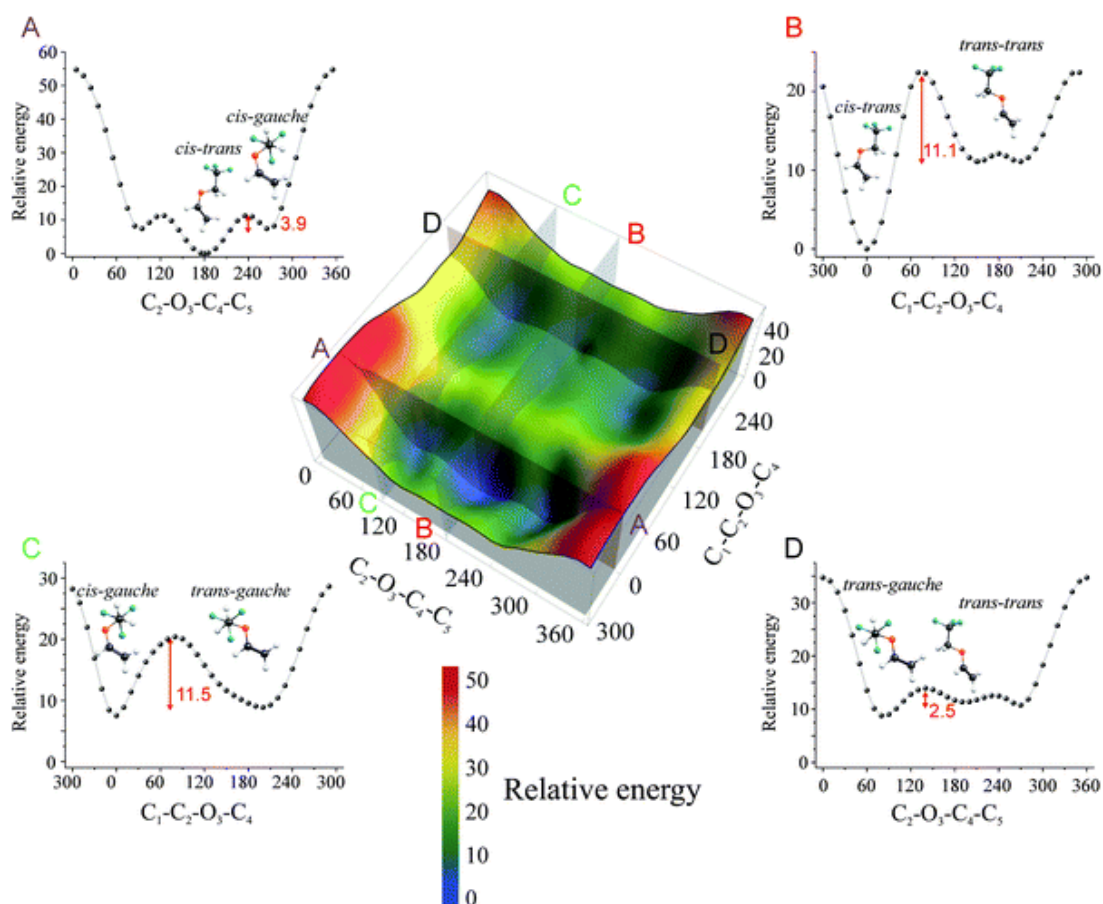


	<i>cis-trans</i>	<i>cis-gauche</i>	<i>trans-gauche</i>	<i>trans-trans</i>
A/MHz	4394	3756	4179	4920
B/MHz	1121	1399	1226	1011
C/MHz	1068	1279	1189	994
$ \mu_a /D$	2.2	1.4	0.7	1.8
$ \mu_b /D$	1.4	0.0	1.0	2.1
$ \mu_c /D$	0.0	1.5	1.7	0.9
$\Delta E_0/kJ mol^{-1}$	0.0 <sup>a</sup>	7.3	7.5	9.6

<sup>a</sup>Absolute Energy-528.974568 E<sub>h</sub>.

**Table 57.** The *ab initio* rotational constants, dipole moment components and zero point energies for the *cis-trans*, *cis-gauche*, *trans-gauche*, *trans-trans* conformers, according to the *vinyl-trifluoroethoxy* conformation. (Uriarte, I.; Écija, P.; Spada, L.; Zabalza, E.; Lesarri, A.; Basterretxea, F. J.; Fernández, J. A.; Caminati, W.; Cocinero, E. J. Potential energy surface of fluoroxene: experiment and theory. *Phys. Chem. Chem. Phys.* **18**, 3966 (2016) - Reproduced by permission of the PCCP Owner Societies).

These conformational structures (see Figure 29) have been found to be real minima according to the frequency calculations, in the harmonic approximation, whose interconversion barrier has been calculated by exploring the bidimensional potential energy surface, in steps of 15°, varying the dihedral angles C1C2-O3C4 and C2O3-C4C5 (see Figure 28) at the MP2/6-311++G(d,p) level.



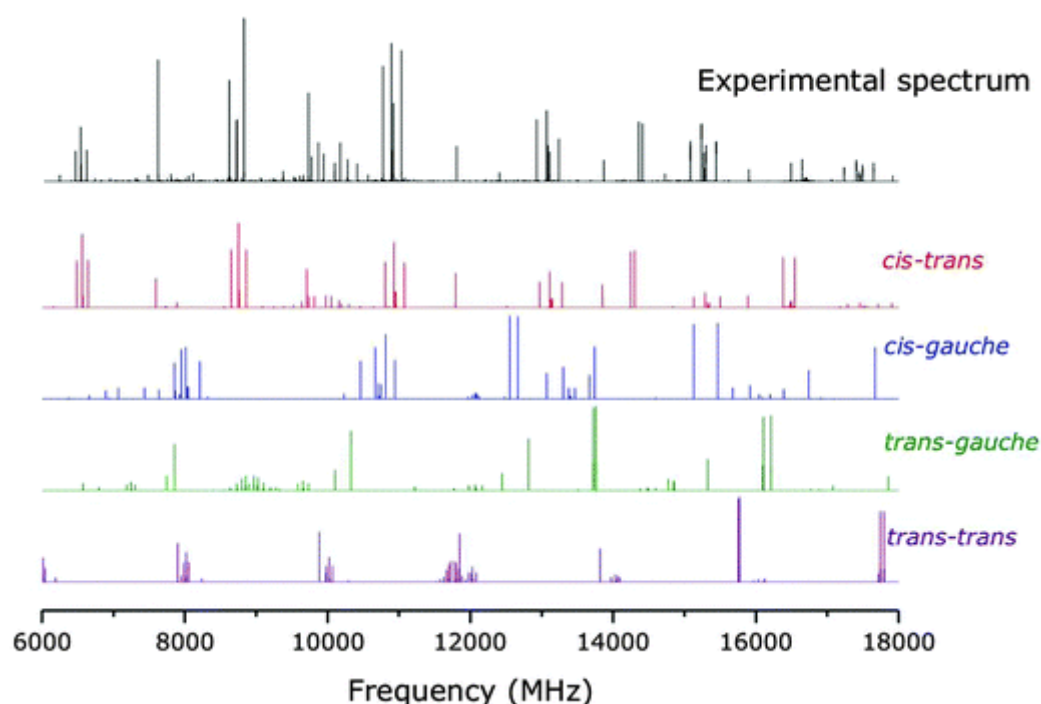
**Figure 29.** Potential energy surface of the Fluoroxene, showing the interconversion barrier between the four calculated most stable conformers at the MP2/6-311++G(d,p) level. The energy and dihedral angle units are  $\text{kJ}\cdot\text{mol}^{-1}$  and degrees, respectively. (Uriarte, I.; Écija, P.; Spada, L.; Zabalza, E.; Lesarri, A.; Basterretxea, F. J.; Fernández, J. A.; Caminati, W.; Cocinero, E. J. Potential energy surface of fluoroxene: experiment and theory. *Phys. Chem. Chem. Phys.* **18**, 3966 (2016) - Reproduced by permission of the PCCP Owner Societies).

The highest interconversion barriers (11.5 and 11.1 kJ·mol<sup>-1</sup>, connecting the *cis-gauche* (or *trans*) to the *trans-gauche*(or *trans*) conformations, respectively, involve the variation of the C1C2-O3C4 dihedral angle. The global minimum is calculated by the *cis-trans* conformer geometry (it has a C<sub>s</sub> symmetry), while the *cis-gauche* is the second most stable isomer as also confirmed by the *ab initio* results of Table 57.

## Experimental Section

A 0.5 % mixture of fluorexene in Neon/Helium (80/20) at stagnation pressure of 2 bars has been expanded into the cavity of the Bilbao CP-FTMW spectrometer.

The collected rotational spectrum in the 6 – 18 GHz range is shown in Figure 30. The lines belonging to the *cis-trans* conformer (190 transitions), with a signal/noise of 13000/1 for the strongest transition after about 1.6 millions of accumulations, have been fitted by using the Pickett's SPFIT program (Watson's *S*-reduction and *I*<sup>r</sup>-representation).



**Figure 30.** The collected rotational spectrum (top) and the *ab initio* predicted ones for the four conformers. (Uriarte, I.; Écija, P.; Spada, L.; Zabalza, E.; Lesarri, A.; Basterretxea, F. J.; Fernández, J. A.; Caminati, W.; Cocinero, E. J. Potential energy surface of fluorexene: experiment and theory. *Phys. Chem. Chem. Phys.* **18**, 3966 (2016) - Reproduced by permission of the PCCP Owner Societies).

Only  $\mu_a$ - and  $\mu_b$ -type transitions have been observed, in agreement with the  $C_s$  symmetry of the *cis-trans* conformer, given a further proof of the corrected conformational assignment together with the comparison between the experimental and *ab initio* rotational constants. The results, together with the ones obtained for the  $^{13}\text{C}$  and  $^{18}\text{O}$  isotopologues are reported in Table 58, which are in really good agreement with those ones obtained from a low resolution study<sup>57</sup>.

<i>cis-trans</i>						
	PARENT	$^{13}\text{C}1$	$^{13}\text{C}2$	$^{13}\text{C}4$	$^{13}\text{C}5$	$^{18}\text{O}3$
$A/\text{MHz}$	4431.8225 (3) <sup>a</sup>	4412.9769(3)	4423.9479(3)	4421.6391(2)	4432.0162(3)	4399.5606 (6)
$B/\text{MHz}$	1116.73685(8)	1092.8743(1)	1101.62935(7)	1116.49153(7)	1113.90780(8)	1110.3711(1)
$C/\text{MHz}$	1065.05889(8)	1042.2833(1)	1050.86580(6)	1064.25378(6)	1062.47436(9)	1057.4200(1)
$D_J/\text{kHz}$	0.0679 (2)	[0.0679] <sup>b</sup>	[0.0679]	[0.0679]	[0.0679]	[0.0679]
$D_{JK}/\text{kHz}$	1.077(1)	[1.077(1)]	[1.077(1)]	[1.077(1)]	[1.077(1)]	[1.077(1)]
$D_K/\text{kHz}$	-0.136(4)	[-0.136(4)]	[-0.136(4)]	[-0.136(4)]	[-0.136(4)]	[-0.136(4)]
$d_1/\text{Hz}$	-3.61(5)	[-3.61(5)]	[-3.61(5)]	[-3.61(5)]	[-3.61(5)]	[-3.61(5)]
$d_2/\text{Hz}$	3.02(1)	[3.02(1)]	[3.02(1)]	[3.02(1)]	[3.02(1)]	[3.02(1)]
$N^c$	190	83	81	67	72	51
$\sigma^d/\text{kHz}$	5.8	5.8	5.1	3.3	4.8	5.4

<sup>a</sup>Errors in units of the last digit. <sup>b</sup>Fixed at the value of the parent species. <sup>c</sup>Number of fitted transitions. <sup>d</sup>rms deviation of the fit.

**Table 58.** Experimental rotational parameters for the most abundant species and other four isotopologues of the only observed *cis-trans* conformer. (Uriarte, I.; Écija, P.; Spada, L.; Zabalza, E.; Lesarri, A.; Basterretxea, F. J.; Fernández, J. A.; Caminati, W.; Cocinero, E. J. Potential energy surface of fluoroxene: experiment and theory. *Phys. Chem. Chem. Phys.* **18**, 3966 (2016) - Reproduced by permission of the PCCP Owner Societies).

No lines belonging to the other conformers have been observed because, according to the data of Figure 29, kinetic relaxations of the *cis-gauche* conformer towards the *cis-trans*, and of the *trans-trans* towards the *trans-gauche* can take place but not the *cis-gauche* (or *trans*)  $\rightarrow$  *trans-gauche* or *trans*) relaxation because their high interconversion barrier values. However, the much higher energy of the *trans-gauche* than the one for the *cis-trans* one results in really low populated states, whose rotational spectrum has not been observed.

## Structural Information

The availability of the most abundant isotopologue and of the four isotopologues of the atoms constituting the backbone structure make it possible to determine the  $r_s$  coordinates<sup>56</sup>. Furthermore,

the  $r_0$  structures has been calculated<sup>56</sup>, allowing to compared the geometrical parameters deriving from the different meaning  $r_s$ ,  $r_0$  and  $r_e$  structures as reported in Table 59.

	$r_s$	$r_0$	$r_e$
$R_{C1-C2} / \text{Å}$	1.335(5) <sup>a</sup>	1.343(5)	1.343
$R_{C2-O3} / \text{Å}$	1.365(3)	1.364(4)	1.362
$R_{O3-C4} / \text{Å}$	1.432(8)	1.419(5)	1.407
$R_{C4-C5} / \text{Å}$	1.482(7)	1.508(7)	1.512
$R_{C5-F6} / \text{Å}$		1.343(12)	1.347
$R_{C5-F7} = R_{C5-F8} / \text{Å}$		1.334(3)	1.339
$\angle (C1-C2-O3) / ^\circ$	127.6(4)	127.2(3)	127.5
$\angle (C2-O3-C4) / ^\circ$	117.1(5)	116.0(3)	115.0
$\angle (O3-C4-C5) / ^\circ$	105.1(4)	106.8(4)	107.4
$\angle (C4-C5-F6) / ^\circ$		108.8(5)	109.0
$\angle (F6-C5-F7) = \angle (F6-C5-F8) / ^\circ$		107.4(4)	107.8
$\tau_1 = \tau (C1-C2-O3-C4) / ^\circ$	[180.0] <sup>b</sup>	[180.0]	180.0
$\tau_2 = \tau (C2-O3-C4-C5) / ^\circ$	[0.0]	[0.0]	0.0

<sup>a</sup>Error in the units of the last digit. <sup>b</sup>Fixed to their *ab initio* values.

**Table 59.** The  $r_s$ ,  $r_0$  and  $r_e$  comparison of the heavy atom geometrical parameters for the observed conformer. (Uriarte, I.; Écija, P.; Spada, L.; Zabalza, E.; Lesarri, A.; Basterretxea, F. J.; Fernández, J. A.; Caminati, W.; Cocinero, E. J. Potential energy surface of fluoroxene: experiment and theory. *Phys. Chem. Chem. Phys.* **18**, 3966 (2016) - Reproduced by permission of the PCCP Owner Societies).

### 3.5.2 Methyl $\beta$ -D-Ribofuranoside

#### Introduction

Rotational spectroscopy is a suitable technique to investigate the gas phase conformational isomerism in chiral molecules such as sugars, as well as the epimerization<sup>58</sup> and the anomeric effects.<sup>59</sup>

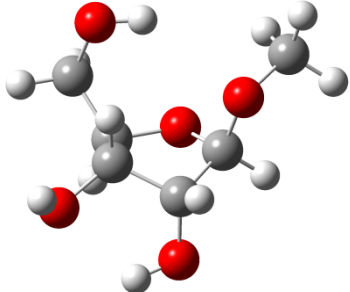
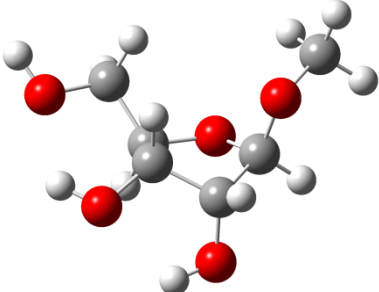
The  $\beta$ -ribofuranoside is the furanositic form of ribose which, together with phosphate group and the nucleobases, constitutes the building blocks of nucleic acids.

In the case of isolated unit of ribose, it has been shown that the pyranose form is favourite with respect to the furanose one and to the highest energy linear shape, taking into the account both the possible  $\alpha$  and  $\beta$  anomers<sup>60</sup>.

The aim of the present study is to investigate the conformation equilibrium relative to an isolated Methyl  $\beta$ -D-Ribofuranoside unit, previously synthesised, which involves different O-H...O hydrogen bonds.

## Theoretical Calculations

The conformational space exploration has been performed by means of Molecular mechanics method and, successively, the obtained structures have been optimized at the MP2/6-311++G(d,p) level using Gaussian 09 package. 28 different conformers<sup>61</sup>, within 23 kJ·mol<sup>-1</sup> have been found, showing a network of O-H···O contacts. The two most stable ones (both have twisted conformation of the five member ring) are reported in Table 60 together with the rotational parameters necessary for the rotational spectrum assignment which include the predicted value of barrier for the internal rotation of the methyl group.

	I	II
		
<i>A</i> / MHz	1295	1439
<i>B</i> / MHz	1101	944
<i>C</i> / MHz	719	675
$\mu_a$ / D	0.02	-0.93
$\mu_b$ / D	-0.30	-3.49
$\mu_c$ / D	-1.16	-0.87
$\Delta E$ / kJ mol <sup>-1</sup>	0.0 <sup>a</sup>	0.7
$V_{3(\text{methyl})}$ / kJ mol <sup>-1</sup>	7.90	8.23

<sup>a</sup>Absolute Energy = -610.541796  $E_h$ .

**Table 60.** The two most stable conformers calculated at the MP2/6-311++G(d,p) level.<sup>61</sup>

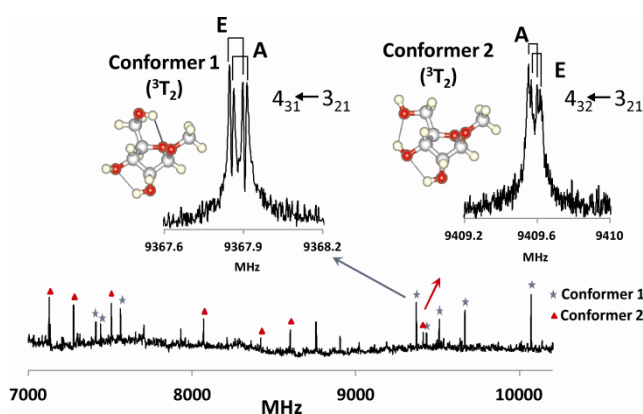
## Experimental Section

Methyl  $\beta$ -D-Ribofuranoside has been synthesized by adding to a D-ribose solution (5.0 g, 33 mmol) in anhydrous methanol in an ice bath, 0.3 mL of concentrated sulfuric acid and stirring for 16h. Then, the obtained solution was neutralized using an ion exchange resin (Amberlite IRA-400(OH)) which, later on, was removed by filtration as well as the remotion of the solvent under vacuum. The remaining mixture was then azeotroped with toluene, giving a yellow oil (4.3g, 79% yield) in which a 4:1  $\beta/\alpha$  anomers ratio is found. The flash chromatography (15% MeOH/EtOAc) repetition

allowed to separate the pure  $\beta$  anomer, later on lyophilized from water, for which:  $[\alpha]_D^{20}$  (c, 1.3 MeOH) = - 55.4  $\{[\alpha]_D^{20}$  (c, 1.0 MeOH) = - 62.4 $\}$ ;  $^{13}\text{C}$  NMR ( $\text{D}_2\text{O}$ )  $\delta$  107.2, 82.0, 73.5, 70.0, 62.1, 54.4.<sup>62</sup>

The sample (solid rod whose preparation has been described in Chapter 2) was vaporized using laser ablation and coexpanded into the cavity of the Bilbao PJ-FTMW spectrometer with Ne at stagnation pressure of 6 bars.

The rotational spectrum of the  $\beta$ -D-Ribofuranoside has been collected in the 6 – 18 GHz, range in which the  $\mu_c$ -type  $R$ -branch and the  $\mu_b$ -type  $R$ -branch transitions have been measured for the conformer I and II, respectively. All the lines are splitted into two components (see Figure 31) because of the internal rotation of the methyl group whose barriers in the conformer has been fitted as well as the rotational and centrifugal distorsion constants, using the XIAM program within the Watson's  $S$  reduced semirigid-rotor Hamiltonian ( $I^f$  representation).



**Figure 31.** The  $4_{31} \leftarrow 3_{21}$  and  $4_{32} \leftarrow 3_{21}$  transitions for the conformer I and II, respectively, showing the splittings due to the internal rotation of the methyl group. (Écija, P., Uriarte, I.; Spada, L.; Davis, B. G.; Caminati, W.; Basterretxea, F. J.; Lesarri, A.; Cocinero, E. J. Furanosic forms of sugars: Conformational equilibrium of methyl  $\beta$ -D-ribofuranoside. *Submitted*).

The obtained values are reported in Table 61.

	I	II
$A/\text{MHz}$	1307.146(55) <sup>a</sup>	1443.5094(14)
$B/\text{MHz}$	1095.47128(50)	924.98477(53)
$C/\text{MHz}$	717.8046(49)	661.97710(32)
$D_J/\text{kHz}$	0.953(81)	0.2752(48)
$D_{JK}/\text{kHz}$	-0.339(88)	-1.264(27)
$D_K/\text{kHz}$		1.702(97)
$d_1/\text{Hz}$	0.723(66)	-0.1004(31)
$d_2/\text{Hz}$	-0.277(24)	
$V_3^b/\text{kJ mol}^{-1}$	7.304(13)	7.503(64)
$\sigma/\text{kHz}^c$	4.7	3.0
$N^d$	46	32

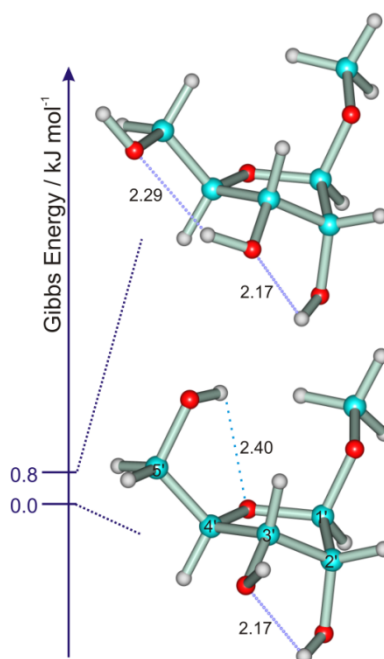
<sup>a</sup>Uncertainties in units of the last digit. <sup>b</sup>Internal rotation barrier. The values of  $I_\alpha$  ( $=3.195 \text{ u}\text{\AA}^2$ ) and  $\langle(i,a), \langle(i,b), \langle(i,c) = 23.1^\circ, 81.3^\circ, 68.8^\circ, 51.4^\circ, 43.9^\circ$  and  $72.3^\circ$ , respectively, for conformers 1 and 2) have been fixed to the ab initio values. <sup>c</sup>Standard deviation of the fit. <sup>d</sup>Number of transitions.

**Table 61.** The results from the fittings for the two observed conformers of  $\beta$ -D-Ribofuranoside. (Écija, P., Uriarte, I.; Spada, L.; Davis, B. G.; Caminati, W.; Basterretxea, F. J.; Lesarri, A.; Cocinero, E. J. Furanosic forms of sugars: Conformational equilibrium of methyl  $\beta$ -D-ribofuranoside. *Submitted.*)

## Structural Information

The O-H...O contact distances as well as the relative Gibbs energies are shown in Figure 32 for the two observed conformers.





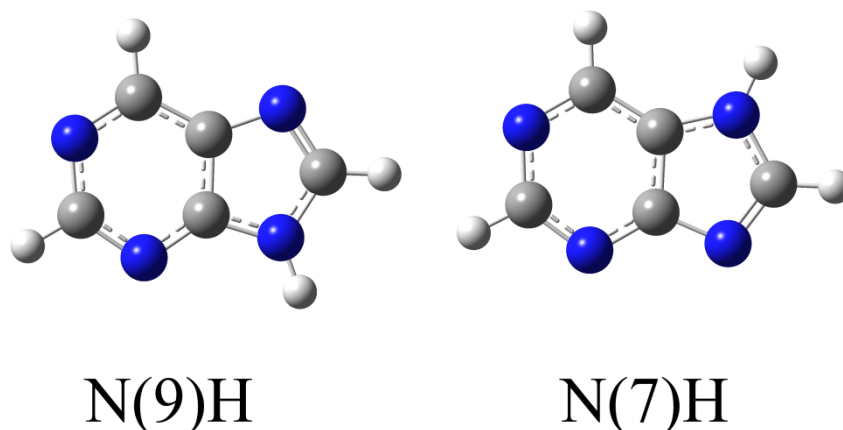
**Figure 32.** The two observed conformation structures of the  $\beta$ -D-Ribofuranoside, showing the O-H $\cdots$ O hydrogen bonds with relative distances (in Å) and the relative Gibbs energy *ab initio* calculated. (Écija, P., Uriarte, I.; Spada, L.; Davis, B. G.; Caminati, W.; Basterretxea, F. J.; Lesarri, A.; Cocinero, E. J. Furanosic forms of sugars: Conformational equilibrium of methyl  $\beta$ -D-ribofuranoside. *Submitted.*)

### 3.5.3 Purine

#### Introduction

Nucleobases are the constituents of RNA and DNA where, in this latter, the coupling between complementary purine and pyrimidine bases provides the stability of the double helix.

In this respect, the purine molecule constitutes the skeleton of two nitrogenous bases (Adenine and Guanine) in which the tautomers interconversion  $\text{N}(9)\text{H} \rightleftharpoons \text{N}(7)\text{H}$  (see Figure 33) takes place (calculated barriers 60-70 kcal/mol)<sup>62</sup>, which can play a role in mutagenesis<sup>63</sup>.



**Figure 33.** The tautomer forms of purine.

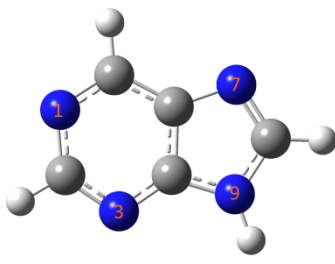
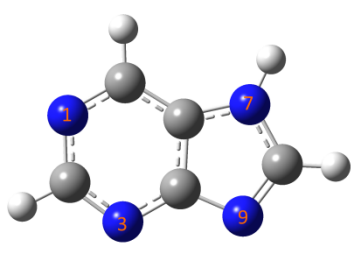
Solid state purine exists as N(7)H tautomer<sup>64</sup> while in solution a mixture of N(7)H and N(9)H tautomers has been found<sup>65</sup>.

In the present study, the rotational study of purine has been performed to estimate the population ratio in the gas phase between the two tautomers providing the difference, in energy, between the vibrational and rotational ground states of the two forms through an unambiguously assignment of their relative spectra.

### Theoretical Calculations

The optimized tautomer structures have been calculated at the MP2/6-311++G(d,p) level by using Gaussian 09 package. The relative rotational constants and the quadrupole coupling constants for the four nitrogen atoms ( $^{14}\text{N } I = 1$ ) are reported in Table 62.

Tautomer N(9)H is found to be the most stable, while the N(7)H tautomer is predicted  $16.9 \text{ kJ}\cdot\text{mol}^{-1}$  higher in energy than the former one, whose energy difference decreases to  $15.9 \text{ kJ}\cdot\text{mol}^{-1}$  if the zero point corrections are considered.

	N(9)H	N(7)H
		
<i>A, B, C</i> /MHz	4099, 1750, 1227	4101, 1745, 1224
N1: $\chi_{aa}, \chi_{bb}, \chi_{cc}, \chi_{ab}$ /MHz	-3.502, 0.381, 3.121, 2.540	-3.553, 0.367, 3.187, -2.478
N3: $\chi_{aa}, \chi_{bb}, \chi_{cc}, \chi_{ab}$ /MHz	1.659, -4.663, 2.630, 0.111	1.427, -4.633, 3.207, -0.098
N7: $\chi_{aa}, \chi_{bb}, \chi_{cc}, \chi_{ab}$ /MHz	1.567, -3.171, 1.605, -1.690	1.680, 1.488, -3.168, -0.138
N9: $\chi_{aa}, \chi_{bb}, \chi_{cc}, \chi_{ab}$ /MHz	1.432, 1.508, -2.940, -0.118	1.373, -3.379, 2.005, -1.570
$ \mu_a ,  \mu_b /D^a$	3.0, 2.3	3.1, 5.0
$\Delta E, \Delta E_0/kJ \cdot mol^{-1}$	0.0, <sup>b</sup> 0.0 <sup>c</sup>	16.9, 15.9

<sup>a</sup> $\mu_c =$  zero due to the planarity. <sup>b</sup>Absolute energy = -410.922989 E<sub>h</sub>. <sup>c</sup>Zero point corrected absolute energy = -410.829145 E<sub>h</sub>.

**Table 62.** The *ab initio* rotational parameters for the N(9)H and N(7)H tautomers of purine. (Reprinted with permission from Favero, L. B.; Uriarte, I.; Spada, L.; Écija, P.; Calabrese, C.; Caminati, W.; Cocinero, E. J. Solving the Tautomeric Equilibrium of Purine through Analysis of the Complex Hyperfine Structure of the Four <sup>14</sup>N Nuclei. *J. Phys. Chem. Lett.*, 2016, 7, pp 1187-1191, DOI: 10.1021/acs.jpcclett.6b00374. Copyright (2016) American Chemical Society).

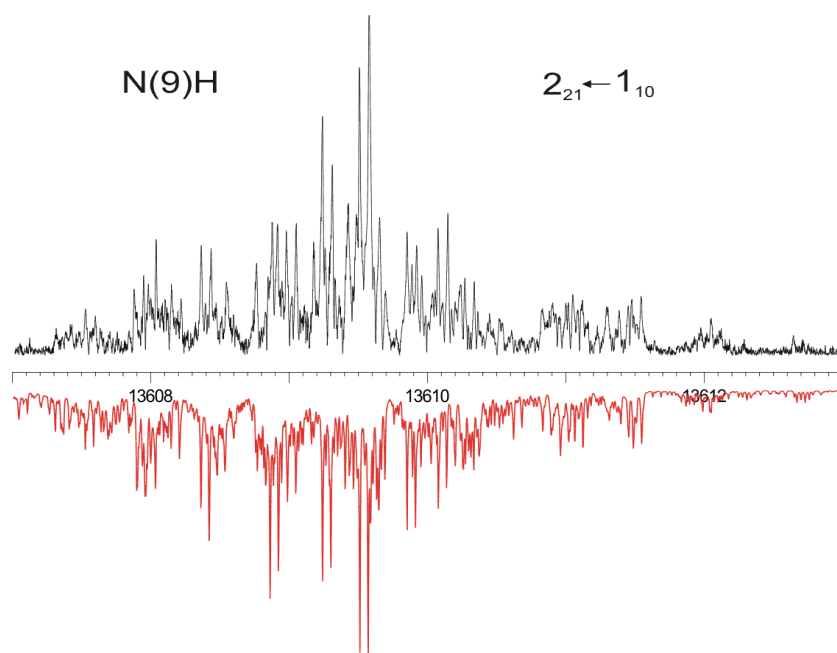
## Experimental Section

The laser ablated purine and a Ne:He 80:20 gas carrier mixture at stagnation pressure of 6 bars have been expanded into the Bilbao PJ-FTMW spectrometer.

The first transition searched was the  $3_{03} \leftarrow 2_{02}$  of N(9)H tautomer, according to the dipole moment component along *a*-axis and the availability of the rotational constants from a previous rotational study<sup>66</sup>. Later on, several other  $\mu_a$ -type and weaker  $\mu_b$ -type transitions have been measured.

After empirical corrections of the predicted rotational constants of the N(7)H, the  $4_{04} \leftarrow 3_{03}$  has been found, followed by another  $\mu_a$ -type and several stronger  $\mu_b$ -type transitions.

All the transitions (see in Figure 34 the  $2_{21} \leftarrow 1_{10}$  transition for the N(9)H tautomer) show a complex hyperfine structure due to the presence of four <sup>14</sup>N atoms.



**Figure 34.** The observed (black) and simulated (red)  $2_{21} \leftarrow 1_{10}$  transition for the N(9)H tautomer. (Reprinted with permission from Favero, L. B.; Uriarte, I.; Spada, L.; Écija, P.; Calabrese, C.; Caminati, W.; Cocinero, E. J. Solving the Tautomeric Equilibrium of Purine through Analysis of the Complex Hyperfine Structure of the Four  $^{14}\text{N}$  Nuclei. *J. Phys. Chem. Lett.*, 2016, 7, pp 1187-1191, DOI: 10.1021/acs.jpcllett.6b00374. Copyright (2016) American Chemical Society).

The observed lines have been fitted using the Pickett's SPFIT program and the results are summarized in Table 63.

	N(9)H	N(7)H
A/MHz	4125.8895(2) <sup>a</sup>	4127.3813(3)
B/MHz	1755.1720(1)	1749.7594(3)
C/MHz	1231.55819(6)	1229.42760(7)
[N1] $\chi_{aa}$ /MHz <sup>b</sup>	-3.343(5)	-3.560(15)
$\chi_{bb}$ /MHz	0.440(6)	0.566(17)
$\chi_{cc}$ /MHz	2.904(6)	2.994(17)
[N3] $\chi_{aa}$ /MHz	1.673(7)	0.695(11)
$\chi_{bb}$ /MHz	-4.229(9)	-2.744(20)
$\chi_{cc}$ /MHz	2.555(9)	2.049(20)
[N7] $\chi_{aa}$ /MHz	1.547(7)	1.254(11)
$\chi_{bb}$ /MHz	-3.379(9)	1.532(16)
$\chi_{cc}$ /MHz	1.833(9)	-2.786(16)
[N9] $\chi_{aa}$ /MHz	1.489(5)	1.541(11)
$\chi_{bb}$ /MHz	1.495(7)	-3.239(18)
$\chi_{cc}$ /MHz	-2.985(7)	1.699(18)
$\Delta_c/u\text{\AA}^2$	-0.0693(3)	-0.2046(4)
$\sigma$ /kHz <sup>c</sup>	4.8	4.9
N <sup>d</sup>	292	113

<sup>a</sup>Error in units of the last digit. <sup>b</sup>Out diagonal  $\chi_{ab}$  quadrupole coupling constants are undetermined from the fit and have been fixed to the *ab initio* values (Table 1). <sup>c</sup>RMS error of the fit. <sup>d</sup>Number of lines in the fit.

**Table 63.** The rotational and quadrupole coupling constants values from the fittings of the two tautomers. (Reprinted with permission from Favero, L. B.; Uriarte, I.; Spada, L.; Écija, P.; Calabrese, C.; Caminati, W.; Cocinero, E. J. Solving the Tautomeric Equilibrium of Purine through Analysis of the Complex Hyperfine Structure of the Four <sup>14</sup>N Nuclei. *J. Phys. Chem. Lett.*, 2016, 7, pp 1187-1191, DOI: 10.1021/acs.jpcclett.6b00374. Copyright (2016) American Chemical Society).

## Quadrupole Analysis

The four nitrogen atoms show a really complex pattern to be analysis but, due to the planarity of both structures, the comparison of the  $\chi_{cc}$  values of purine with those ones of pyrrole, pyrimidine and imidazole (see Table 64), provides an unambiguously assignment of the two tautomer spectra, together with the comparison between the *ab initio* and the experimental values of the rotational constants.

	N(9)H	N(7)H	$\chi_{cc}$ values (MHz) of $^{14}\text{N}$ nuclei in isolated molecule
$\chi_{cc}[\text{N1}]/\text{MHz}$	2.904(6)	2.994(17)	Pyrimidine N: 3.5584(7) <sup>67</sup>
$\chi_{cc}[\text{N3}]/\text{MHz}$	2.555(9)	2.049(20)	Pyrrole N: -2.704(4) <sup>68</sup>
$\chi_{cc}[\text{N7}]/\text{MHz}$	1.833(9)	-2.786(16)	Imidazole N1 (pyrrole-like): -2.559(9) <sup>69</sup>
$\chi_{cc}[\text{N9}]/\text{MHz}$	-2.985(7)	1.699(18)	Imidazole N3 (pyrimidine-like): 2.228(8) <sup>69</sup>

**Table 64.** The comparison between the  $\chi_{cc}$  values of the various nitrogen atoms in the two tautomers with those ones in pyrimidine, pyrrole and imidazole. (Reprinted with permission from Favero, L. B.; Uriarte, I.; Spada, L.; Écija, P.; Calabrese, C.; Caminati, W.; Cocinero, E. J. Solving the Tautomeric Equilibrium of Purine through Analysis of the Complex Hyperfine Structure of the Four  $^{14}\text{N}$  Nuclei. *J. Phys. Chem. Lett.*, 2016, 7, pp 1187-1191, DOI: 10.1021/acs.jpcclett.6b00374. Copyright (2016) American Chemical Society).

One can see in fact that, apart from the N1 and N3 which are similar pyrimidine nuclei, the  $\chi_{cc}$  values of the N7 and the N9 atom become similar to that in the pyrrole when the proton is bound to those nitrogen atoms and to pyrimidine when they are free from hydrogens.

### Population Ratio

The population ratio between the two tautomers has been estimated from relative intensity measurements of pairs of nearby transitions, which results be:  $N_{\text{N(9)H}}/N_{\text{N(7)H}} \approx 40/1$ . According to equation 1.60, this value corresponds to a difference between the vibrational and rotational ground states of the two tautomers of 9(1)  $\text{kJ}\cdot\text{mol}^{-1}$ .

### 3.5.4 Conclusions

The conformational and the tautomeric preferences of isolated fluoroxene,  $\beta$ -D-Ribofuranoside and purine, respectively, have been described, showing that if in the case of the anesthetic a single conformation is observed, the sugar and the purine undergoing to an equilibrium.

For the chiral  $\beta$ -D-Ribofuranoside two conformers, which establish internal O-H $\cdots$ O hydrogen bonds, have been found in the gas phase where the internal rotation of the methyl group generates a small splitting of the rotational transitions.

On the other hand, purine shows a really complex rotational spectrum (fully resolved), due to the simultaneous presence of four  $^{14}\text{N}$  atoms. The population ratio between the two tautomers has been estimated be 40/1 in favor of the N(9)H one showing as well as it was found in solution, the presence of both the tautomers.

### 3.6 References

- 1) Cooke, S. A.; Corlett, G. K.; Legon, A. C. The rotational spectrum of the pyridine-hydrogen fluoride complex. *J. Mol. Struct.* **448**, 107 (1998).
- 2) Cooke, S. A.; Corlett, G. K.; Lister, D. G.; Legon, A. C. Is pyridinium hydrochloride a simple hydrogen-bonded complex  $C_5H_5N \cdots HCl$  or an ion pair  $C_5H_5NH^+ \cdots Cl^-$  in the gas phase? An answer from its rotational spectrum. *J. Chem. Soc., Faraday Trans.* **94(7)**, 837 (1998).
- 3) Cole, G. C.; Legon, A. C. The nature of the complex formed between pyridine and hydrogen bromide in the gas phase: An experimental approach using rotational spectroscopy. *J. Chem. Phys.* **121**, 10467 (2004).
- 4) Ubbelohde, A. R.; Gallagher, K. J. Acid-base Effects in Hydrogen Bonds in Crystals. *Acta Crystallogr.* **8**, 71 (1955).
- 5) See for example, Tang, S.; Majerz, I.; Caminati, W. Sizing the Ubbelohde Effect: The Rotational Spectrum of *tert*-Butylalcohol Dimer. *Phys. Chem. Chem. Phys.* **13**, 9137 (2011).
- 6) Fernandez-Berridi, M. J.; Iruin, J. J.; Irusta, L.; Mercero, J. M.; Ugalde, J. M. Hydrogen-Bonding Interactions between Formic Acid and Pyridine. *J. Phys. Chem. A* **106**, 4187 (2002).
- 7) X.- Z. Li; Walker, B.; Michaelides, A. Quantum nature of the hydrogen bond. *PNAS* **108**, 6369 (2011).
- 8) Smirnov, S. N.; Golubev, N. S.; Denisov, G. S.; Benedict, H.; Schah-Mohammedi, P.; Limbach, H.-H. Hydrogen/Deuterium Isotope Effects on the NMR Chemical Shifts and Geometries of Intermolecular Low-Barrier Hydrogen-Bonded Complexes. *J. Am. Chem. Soc.* **118**, 4094 (1996).
- 9) Evangelisti, L.; Caminati, W. Internal dynamics in complexes of water with organic molecules. Details of the internal motions in *tert*-butylalcohol–water. *Phys. Chem. Chem. Phys.* **12**, 14433 (2010).
- 10) Evangelisti, L.; Feng, G.; Écija, P.; Cocinero, E. J.; Castaño, F.; Caminati, W. The Halogen Bond and Internal Dynamics in the Molecular Complex of  $CF_3Cl$  and  $H_2O$ . *Angew. Chem. Int. Ed.* **50**, 7807 (2011).

- 11) Suzuki, S.; Green, P. G.; Bumgarner, R. E.; Dasgupta, S.; Goddard III, W. A.; Blake, G. A. Benzene Forms Hydrogen Bonds with Water. *Science* **257**, 942 (1992).
- 12) Priem, D.; Ha, T. - K.; Bauder, A. Rotational spectra and structures of three hydrogen-bonded complexes between formic acid and water. *J. Chem. Phys.* **113**, 169 (2000).
- 13) Alonso, J. L.; Cocinero, E. J.; Lesarri, A.; Sanz, M. E.; López, J. C. The Glycine–Water Complex. *Angew. Chem. Int. Ed.* **45**, 3471 (2006).
- 14) Mata, S.; Cortijo, V.; Caminati, W.; Alonso, J. L.; Sanz, M. E.; López, J. C.; Blanco, S. Tautomerism and Microsolvation in 2-Hydroxypyridine/2-Pyridone. *J. Phys. Chem. A* **114**, 11393 (2010).
- 15) Tubergen, M. J.; Andrews, A. M.; Kuczkowski, R. L. Microwave spectrum and structure of a hydrogen-bonded pyrrole-water complex. *J. Phys. Chem.* **97**, 7451 (1993).
- 16) Blanco, S.; López, J. C.; Alonso, J. L.; Ottaviani, P.; Caminati, W. Pure rotational spectrum and model calculations of indole–water. *J. Chem. Phys.* **119**, 880 (2003).
- 17) MASTRO, version 9.2, Schrödinger, LLC, New York, NY, 2012.
- 18) Van Dijk, C. W.; Sun, M.; Van Wijngaarden, J. Microwave Rotational Spectra and Structures of 2-Fluoropyridine and 3-Fluoropyridine. *J. Phys. Chem. A* **116**, 4082 (2012).
- 19) Boopalachandran, P.; Laane, J. Vibrational Spectra, Structure, and Theoretical Calculations of 2-Fluoro and 3-Fluoropyridine. *Spectrochimica Acta A* **79**, 1191 (2011).
- 20) Caminati, W.; Favero, L. B.; Favero, P. G.; Maris, A.; Melandri, S. Intermolecular Hydrogen Bonding between Water and Pyrazine. *Angew. Chem. Int. Ed.* **37**, 792 (1998).
- 21) Melandri, S.; Sanz, M. E.; Caminati, W.; Favero, P. G.; Kisiel, Z. The Hydrogen Bond between Water and Aromatic Bases of Biological Interest: An Experimental and Theoretical Study of the 1:1 Complex of Pyrimidine with Water. *J. Am. Chem. Soc.* **120**, 11504 (1998).
- 22) Caminati, W.; Moreschini, P.; Favero, P. G. The Hydrogen Bond between Water and Aromatic Bases of Biological Interest: Rotational Spectrum of Pyridazine-Water. *J. Phys. Chem. A* **102**, 8097 (1998).
- 23) Onda, M.; Toda, A.; Mori, S.; Yamaguchi, I. Microwave Spectrum of Anisole. *J. Mol. Struct.* **144**, 47 (1986).
- 24) Federdel, D.; Herrmann, A.; Christen, D.; Sander, S.; Willner, H.; Oberhammer, H. Structure and Conformation of  $\alpha,\alpha,\alpha$ -Trifluoroanisole,  $C_6H_5OCF_3$ . *J. Mol. Struct.* **567-568**, 127 (2001).
- 25) Giuliano, B. M.; Caminati, W. Isotopomeric Conformational Change in Anisole–Water. *Angew. Chem. Int. Ed.* **44**, 603 (2005).



- 26) Caminati, W.; Melandri, S.; Moreschini, P.; Favero, P. G. The C-F...H-C “Anti-Hydrogen Bond” in the Gas Phase: Microwave Structure of the Difluoromethane Dimer. *Angew. Chem. Int. Ed.* **38**, 2924 (1999).
- 27) Blanco, S.; Melandri, S.; Ottaviani, P.; Caminati, W. Shapes and Noncovalent Interactions of Oligomers: The Rotational Spectrum of the Difluoromethane Trimer. *J. Am. Chem. Soc.* **129**, 2700 (2007).
- 28) Feng, G.; Evangelisti, L.; Cacelli, I.; Carbonaro, L.; Prampolini, G.; Caminati, W. Oligomers based on weak hydrogen bond networks: a rotational study of the tetramer of difluoromethane. *Chem. Commun.* **50**, 171 (2014).
- 29) Caminati, W.; López, J. C.; Alonso, J. L.; Grabow, J.- U. Weak CH...F Bridges and Internal Dynamics in the CH<sub>3</sub>F·CHF<sub>3</sub> Molecular Complex. *Angew. Chem. Int. Ed.* **44**, 3840 (2005).
- 30) Feng, G.; Gou, Q.; Evangelisti, L.; Vallejo-López, M.; Lesarri, A.; Cocinero, E. J.; Caminati, W. Competition between weak hydrogen bonds: C–H...Cl is preferred to C–H...F in CH<sub>2</sub>ClF–H<sub>2</sub>CO, as revealed by rotational spectroscopy. *Phys. Chem. Chem. Phys.* **16**, 12261 (2014).
- 31) Christenholz, C. L.; Obenchain, D. A.; Peebles, S. A.; Peebles, R. A. Reduced bandwidth chirped-pulse microwave spectroscopy for analysis of weakly bound dimers: Rotational spectrum and structural analysis of CH<sub>2</sub>ClF...FHC=CH<sub>2</sub>. *J. Mol. Spectrosc.* **280**, 61 (2012).
- 32) Gou, Q.; Spada, L.; Vallejo-López, M.; Kisiel, Z.; Caminati, W. Interactions between Freons: A Rotational Study of CH<sub>2</sub>F<sub>2</sub>–CH<sub>2</sub>Cl<sub>2</sub>. *Chem. Asian J.* **9**, 1032 (2014).
- 33) Kisiel, Z.; Kosarzewski, J.; Pszczółkowski, L. Nuclear Quadrupole Coupling Tensor of CH<sub>2</sub>Cl<sub>2</sub>: Comparison of Quadrupolar and Structural Angles in Methylene Halides. *Acta Phys. Polon. A* **92**, 507 (1997).
- 34) Suenram, R. D.; Fraser, G. T.; Lovas, F. J.; Kawashima, Y. The microwave spectrum of CH<sub>4</sub>–H<sub>2</sub>O. *J. Chem. Phys.* **101**, 7230 (1994).
- 35) Hearn, J. P. I.; Howard, B. J. Microwave and infrared spectroscopy of the CH<sub>4</sub>–OCS complex. *Mol. Phys.* **100**, 2679 (2002).
- 36) Caminati, W.; Melandri, S.; Favero, P. G.; Meyer, R. Free jet absorption millimeter wave spectrum of the pyrimidine–argon molecular complex. *Chem. Phys. Lett.* **268**, 393 (1997).
- 37) Meyer, R. Flexible models for intramolecular motion, a versatile treatment and its application to glyoxal. *J. Mol. Spectrosc.* **76**, 266 (1979).
- 38) Gou, Q.; Spada, L.; Vallejo-López, M.; Lesarri, A.; Cocinero, E. J.; Caminati, W. Interactions between alkanes and aromatic molecules: a rotational study of pyridine–methane. *Phys. Chem. Chem. Phys.* **16**, 13041 (2014).

- 39) Favero, L. B.; Giuliano, B. M.; Maris, A.; Melandri, S.; Ottaviani, P.; Velino, B.; Caminati, W. Features of the C-H $\cdots$ N Weak Hydrogen Bond and Internal Dynamics in Pyridine-CHF<sub>3</sub>. *Chem. Eur. J.* **16**, 1761 (2010).
- 40) Maris, A.; Favero, L. B.; Velino, B.; Caminati, W. Pyridine-CF<sub>4</sub>: A Molecule with a Rotating Cap. *J. Phys. Chem. A* **117**, 11289 (2013).
- 41) Murray, J. S.; Lane, P.; Clark, T.; Riley, K. E.; Politzer, P.  $\sigma$ -Holes,  $\pi$ -Holes and Electrostatically - Driven Interactions. *J. Mol. Model.* **18**, 541 (2012).
- 42) Favero, L. B.; Li, W.; Spada, L.; Evangelisti, L.; Visentin, G.; Caminati, W. The Cage Structure of Indan-CHF<sub>3</sub> is Based on the Cooperative Effects of C-H $\cdots$ p and C-H $\cdots$ F Weak Hydrogen Bonds. *Chem. Eur. J.* **21**, 15970 (2015).
- 43) López, J. C.; Caminati, W.; Alonso, J. L. The C-H $\cdots$  $\pi$  Hydrogen Bond in the Benzene-Trifluoromethane Adduct: A Rotational Study. *Angew. Chem., Int. Ed.* **45**, 290 (2006).
- 44) Gou, Q.; Feng, G.; Evangelisti, L.; Loru, D.; Alonso, J. L.; J. C. López, Caminati, W. Ubbelohde Effect within Weak C-H $\cdots$  $\pi$  Hydrogen Bonds: The Rotational Spectrum of Benzene-DCF<sub>3</sub>. *J. Phys. Chem. A* **117**, 13531 (2013).
- 45) Legon, A. C. The halogen bond: an interim perspective. *Phys. Chem. Chem. Phys.* **12**, 77 (2010).
- 46) Nguyen, H. L.; Horton, P. N.; Hursthouse, M. B.; Legon, A. C.; Bruce, D. W. Halogen Bonding: A New Interaction for Liquid Crystal Formation. *J. Am. Chem. Soc.* **126**, 16 (2004).
- 47) Metrangolo, P.; Neukirch, H.; Pilati, T.; Resnati, G. Halogen Bonding Based Recognition Processes: A World Parallel to Hydrogen Bonding. *Acc. Chem. Res.* **38**, 386 (2005).
- 48) Wilcken, R.; Zimmermann, M. O.; Lange, A.; Joerger, A. C.; Boeckler, F. M. Principles and Applications of Halogen Bonding in Medicinal Chemistry and Chemical Biology. *J. Med. Chem.* **56**, 1363 (2013).
- 49) Evangelisti, L.; Feng, G.; Écija, P.; Cocinero, E. J.; Castaño, F.; Caminati, W. The Halogen Bond and Internal Dynamics in the Molecular Complex of CF<sub>3</sub>Cl and H<sub>2</sub>O. *Angew. Chem. Int. Ed.* **50**, 7807 (2011).
- 50) Evangelisti, L.; Feng, G.; Gou, Q.; Grabow, J.-U.; Caminati, W. Halogen Bond and Free Internal Rotation: The Microwave Spectrum of CF<sub>3</sub>Cl-Dimethyl Ether. *J. Phys. Chem. A* **118**, 579 (2014).
- 51) Feng, G.; Evangelisti, L.; Gasparini, N.; Caminati, W. On the Cl $\cdots$ N Halogen Bond: A Rotational Study of CF<sub>3</sub>Cl $\cdots$ NH<sub>3</sub>. *Chem. Eur. J.* **18**, 1364 (2012).

- 52) Gou, Q.; Spada, L.; Cocinero, E. J.; Caminati, W. Halogen–Halogen Links and Internal Dynamics in Adducts of Freons. *J. Phys. Chem. Lett.* **5**, 1591 (2014).
- 53) Gou, Q.; Feng, G.; Evangelisti, L.; Vallejo-López, M.; Spada, L.; Lesarri, A.; Cocinero, E. J.; Caminati, W. Internal Dynamics in Halogen-Bonded Adducts: A Rotational Study of Chlorotrifluoromethane–Formaldehyde. *Chem. Eur. J.* **21**, 4148 (2015).
- 54) Gou, Q.; Feng, G.; Evangelisti, L.; Caminati, W. Lone-Pair··· $\pi$  Interaction: A Rotational Study of the Chlorotrifluoroethylene–Water Adduct. *Angew. Chem. Int. Ed.* **52**, 11888 (2013).
- 55) Spada, L.; Gou, Q.; Geboes, Y.; Herrebout, W. A.; Melandri, S.; Caminati, W. Rotational Study of Dimethyl Ether–Chlorotrifluoroethylene: Lone Pair··· $\pi$  Interaction Links the Two Subunits. *J. Chem. Phys. A*, Article ASAP, Publication Date (Web): January 26, 2016. DOI: 10.1021/acs.jpca.5b12571.
- 56) Uriarte, I.; Écija, P.; Spada, L.; Zabalza, E.; Lesarri, A.; Basterretxea, F. J.; Fernández, J. A.; Caminati, W.; Cocinero, E. J. Potential energy surface of fluoroxene: experiment and theory. *Phys. Chem. Chem. Phys.* **18**, 3966 (2016).
- 57) Dennison, F. T.; Gillies, C. W.; Borchert, S. J. Characteristics of low resolution Q-branch microwave bands: Applications to 2,2,2-trifluoroethyl vinyl ether and 7-methylbicyclo[2.2.1]-hept-2-ene-5-one. *J. Chem. Phys.* **75**, 3238 (1981).
- 58) Peña, I.; Cabezas, C.; Alonso, J. L. Unveiling epimerization effects: a rotational study of  $\alpha$ -D-galactose. *Chem. Commun.* **51**, 10115 (2015).
- 59) Alonso, E. R.; Peña, I.; Cabezas, C.; Alonso, J. L. Structural Expression of Exo-Anomeric Effect. *J. Phys. Chem. Lett.* **7**, 845 (2016).
- 60) Cocinero, E. J.; Lesarri, A.; Écija, P.; Basterretxea, F. J.; Grabow, J.-U.; Fernández, J. A.; Castaño, F. Ribose Found in the Gas Phase. *Angew. Chem. Int. Ed.* **51**, 3119 (2012).
- 61) Écija, P., Uriarte, I.; Spada, L.; Davis, B. G.; Caminati, W.; Basterretxea, F. J.; Lesarri, A.; Cocinero, E. J. Furanosic forms of sugars: Conformational equilibrium of methyl  $\beta$ -D-ribofuranoside. *Submitted*.
- 62) Doo-Sik, A.; Sungyul, L.; Bongsoo, K. Solvent-mediated tautomerization of purine: single to quadruple proton transfer. *Chem. Phys. Lett.* **390**, 384 (2004).
- 63) Stolarski, R.; Kierdaszuk, B.; Hagberg C.E.; Shugar, D. Hydroxylamine and methoxyamine mutagenesis: displacement of the tautomeric equilibrium of the promutagen N6-methoxyadenosine by complementary base pairing. *Biochemistry* **23**, 2906 (1984).
- 64) Watson, D. G.; Sweet, R. M.; Marsh, R. E. The Crystal and Molecular Structure of Purine. *Acta Crystallogr.* **19**, 573 (1965).

- 65) Gonella, N. C.; Roberts, J. D. Studies of the Tautomerism of Purine and the Protonation of Purine and Its 7- and 9-Methyl Derivatives by Nitrogen-15 Nuclear Magnetic Resonance Spectroscopy. *J. Am. Chem. Soc.* **104**, 3162 (1982).
- 66) Caminati, W.; Maccaferri, G.; Favero, P. G.; Favero, L. B. Free Jet Absorption Millimeterwave Spectrum of Purine. *Chem. Phys. Lett.* **251**, 189 (1996).
- 67) Kisiel, Z.; Pszczółkowski, L.; López, J. C.; Alonso, J. L.; Maris, A.; Caminati, W. Investigation of the Rotational Spectrum of Pyrimidine from 3 to 337 GHz: Molecular Structure, Nuclear Quadrupole Coupling, and Vibrational Satellites. *J. Mol. Spectrosc.* **195**, 332 (1999).
- 68) Bohn, R. K.; Hillig, K. W., II; Kuczkowski, R. L. Pyrrole-Argon: Microwave Spectrum, Structure, Dipole Moment, and  $^{14}\text{N}$  Quadrupole Coupling Constants. *J. Phys. Chem.* **93**, 3456 (1989).
- 69) Stolze, M.; Sutter, D. H. The Rotational Zeeman Effect of Pyrazole and Imidazole. *Z. Naturforsch.* **42a**, 49 (1987).

# ACKNOWLEDGEMENTS

I would like to express my gratitude to all those who have made this thesis possible.

First of all, my heartfelt thanks go to my parents and to my supervisor, Prof. Walther Caminati for their patience, availability and wisdom.

Thanks, in a special way to Dr. Luca Evangelisti, to Dr. Qian Gou, to Mr. Weixing Li, to Dr. Assimo Maris, to Prof. Sonia Melandri, to Dr. Laura Favero, to Dr. Biagio Velino, to Dr. Camilla Calabrese, to Ms. Annalisa Vigorito, to Dr. Gang Feng, to Dr. Montserrat Vallejo-López, to Ms. Donatella Loru, to Mr. Yannick Geboes, and to all the students who spent some time in our group.

Furthermore, my gratitude goes to Prof. Brooks H. Pate and to Dr. Nathan Seifert as well as to Dr. Emilio J. Cocinero, to Dr. Patricia Écija, to Ms. Iciar Uriarte and to all the people in the Bilbao spectroscopy group.

Many thanks go to Prof. J.-U. Grabow, to Prof. Juan Carlos Lopez, to Prof. Susana Blanco, to Prof. Zbigniew Kisiel and to Prof. W. A. Herrebout.

Thanks to all my relatives and my friends because without them nothing is possible.